

5-26-1961

# Absorbance of the OH Radical in a Specific Wavelength Interval Near 309A

Paul F. Bird

Follow this and additional works at: [https://digitalrepository.unm.edu/phyc\\_etds](https://digitalrepository.unm.edu/phyc_etds)



Part of the [Astrophysics and Astronomy Commons](#), and the [Physics Commons](#)

---

## Recommended Citation

Bird, Paul F.. "Absorbance of the OH Radical in a Specific Wavelength Interval Near 309A." (1961).  
[https://digitalrepository.unm.edu/phyc\\_etds/90](https://digitalrepository.unm.edu/phyc_etds/90)

This Thesis is brought to you for free and open access by the Electronic Theses and Dissertations at UNM Digital Repository. It has been accepted for inclusion in Physics & Astronomy ETDs by an authorized administrator of UNM Digital Repository. For more information, please contact [disc@unm.edu](mailto:disc@unm.edu).



UNIVERSITY OF NEW MEXICO-GENERAL LIBRARY



A14425 250453

378.789

Un30bi

1961

cop. 2



ASSOCIATION OF THEOLOGICAL STUDENTS  
MEMBER 3090A



THE LIBRARY  
UNIVERSITY OF NEW MEXICO



Call No.

378.789

Un30bi


1961

cop.2

Accession  
Number

273889





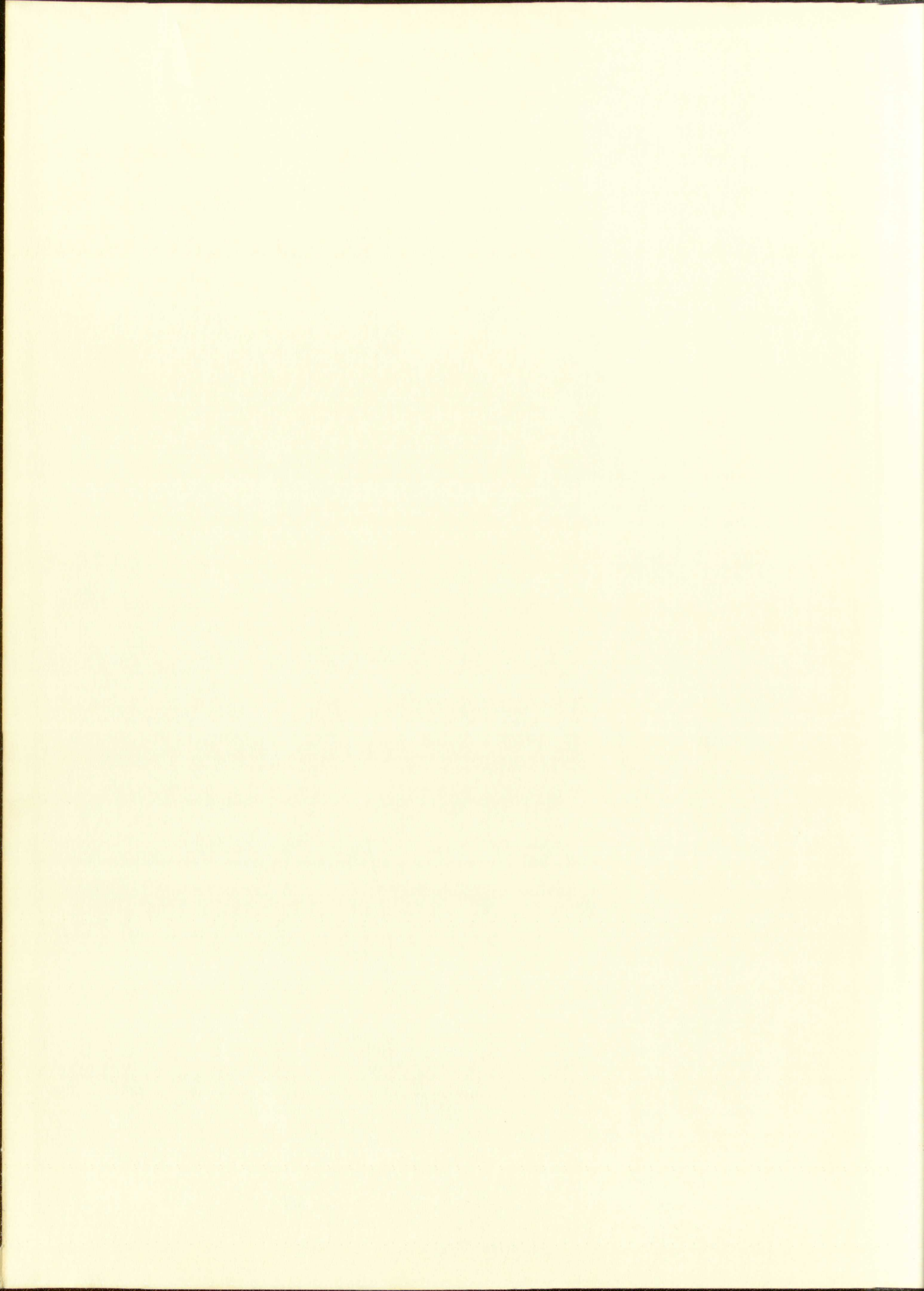
Each reader is required  
to read the regulations  
and sign his name on the  
sheet provided in the front  
of this thesis.





18





COLTON CONTENT  
EZEKIEL  
MILLERS FALLS



WILLIAM WALKER  
1850



UNIVERSITY OF NEW MEXICO LIBRARY

MANUSCRIPT THESES

Unpublished theses submitted for the Master's and Doctor's degrees and deposited in the University of New Mexico Library are open for inspection, but are to be used only with due regard to the rights of the authors. Bibliographical references may be noted, but passages may be copied only with the permission of the authors, and proper credit must be given in subsequent written or published work. Extensive copying or publication of the thesis in whole or in part requires also the consent of the Dean of the Graduate School of the University of New Mexico.

This thesis by Paul F. Bird.....  
has been used by the following persons, whose signatures attest their acceptance of the above restrictions.

A Library which borrows this thesis for use by its patrons is expected to secure the signature of each user.

NAME AND ADDRESS	DATE
<i>Daniel J. Seery</i> <i>United Aircraft Research Labs.</i>	<i>3/16/66</i>
<i>William M. Houghton</i> <i>NASA WANGLEY RES CEN</i>	<i>2-21-68</i>



UNIVERSITY OF NEW MEXICO LIBRARY

MANUSCRIPT THESES

Unpublished theses submitted for the Master's and Doctor's degrees and deposited in the University of New Mexico Library are open for inspection, but are to be used only with due regard to the rights of the authors. Bibliographical references may be noted, but passages may be copied only with the permission of the authors, and proper credit must be given in subsequent written or published work. Extensive copying or publication of the thesis in whole or in part requires also the consent of the Dean of the Graduate School of the University of New Mexico.

This thesis by Paul E. Bird  
has been used by the following persons, whose signatures attest their acceptance of the above restrictions.

A library which borrows this thesis for use by its patrons is expected to secure the signature of each user.

NAME AND ADDRESS DATE

Paul E. Bird	3/10/50
United Aircraft Research Lab.	
William M. Johnston	
NASA Wallops R-2 Club	5-21-58

ABSORBANCE OF THE OH RADICAL IN A  
SPECIFIC WAVELENGTH INTERVAL NEAR 3090A

By

Paul F. Bird

A Thesis

Submitted in Partial Fulfillment of the  
Requirements for the Degree of  
Master of Science in Physics

The University of New Mexico

1961





This thesis, directed and approved by the candidate's committee, has been accepted by the Graduate Committee of the University of New Mexico in partial fulfillment of the requirements for the degree of

MASTER OF SCIENCE

*E. H. Castetter*  
Dean

May 26, 1961  
Date

Thesis committee

*Russell E. Duff*  
Chairman

*Walter M. Esano*

*Donald K. Ketchum*



This thesis, directed and approved by the candidate's advisor, has been accepted by the Graduate Committee of the University of New Mexico in partial fulfillment of the requirements for the degree of

MASTER OF SCIENCE

[Signature]  
Date

[Signature]  
Date

Thesis committee

[Signature]  
Chairman

[Signature]

[Signature]

378.789  
Un306i  
1961  
cop. 2

#### ABSTRACT

The absorbance of the OH radical as a function of optical density was studied by computing the absorbance for an incident radiation in the wavelength interval 3089A-3097A. The absorbance was studied for 3 different temperatures and various values of the parameters specifying the line shapes and the magnitude of the spectral absorption coefficient. The integrated absorption was assumed independent of line shape, pressure, or other perturbations. The absorption line shapes considered were pure Doppler and a combination of natural, Doppler, and collision (Lorentz) broadened shapes. The emission spectrum of a water vapor filled flash lamp used in a series of shock tube calibrations for studies of the OH radical was measured. Absorbance was computed for several different incident radiation spectra. Different line shapes were used for different spectra but the lines of a particular spectrum all had the same shape. The measured relative intensities were used for all the spectra.

The absorbance for the range of optical densities studied was found to increase with increase in the assumed f-number; to decrease with increased width of the lines of the incident radiation spectrum. The dependence of absorbance as a function of optical density upon temperature and the line shapes of the spectral absorption coefficient is not simple. For the particular region of the spectrum used, the behavior of the absorbance can be discussed in terms of the predominating low-energy level, strongly absorbing states. For a particular band f-number and low optical densities in the range covered, the absorbance varies in the same



The results of the 1947 election in the United States were a surprise to many observers. The Democratic Party, led by Harry Truman, won a narrow victory over the Republican Party, led by Dwight D. Eisenhower. This was the first time since the end of World War II that a Republican had been elected President.

The election was held on November 4, 1947. Truman received 302 electoral votes, while Eisenhower received 224. The margin of victory was 78 electoral votes. In the popular vote, Truman received 48.3%, while Eisenhower received 47.8%. The remaining 1.9% of the vote went to various third-party candidates.

The election was a reflection of the public's desire for change after the war. Truman had been in office since 1945, and his administration had been marked by the end of World War II, the beginning of the Cold War, and the Korean War. Many Americans were looking for a new direction for the country.

Eisenhower, a military hero, represented a new generation of leaders. He was seen as a man of peace and stability. His victory was a sign that the American people were looking for a change in leadership and a new direction for the country.

The election was also a reflection of the public's desire for a strong executive. Eisenhower was seen as a strong leader who would be able to handle the challenges of the Cold War. His victory was a sign that the American people were looking for a strong leader to guide the country through these difficult times.

The election was a turning point in American history. It marked the beginning of the Eisenhower era, a time of relative peace and stability. It also marked the beginning of the end of the Truman administration, which had been marked by the end of World War II and the beginning of the Cold War.

direction as the peak spectral absorption coefficient. At high optical densities the width of the lines is the predominating feature and absorbance varies in the same direction as the width of the lines of the absorption coefficient.

The computed absorbance versus optical density curves were compared with those obtained in the calibration experiments. The values of the parameters best describing the absorption coefficient of the OH radical were determined by attempting to superimpose the computed and experimental curves. Relatively good agreement was obtained but distinct differences were noted. Values obtained for the parameters agree well with those reported in the literature. The differences cannot be explained by errors in the widths of the line used to generate the incident radiation spectrum. Errors in the width of the lines of the incident spectrum affect the f-number and line shape used to obtain agreement between the measured and computed curves but cannot account for the noted differences. The best value of the constant F in the expression for the f-number is  $3.32 \cdot 10^{-4}$ ; the best expression for the collision broadening factor is  $a = \frac{450p}{T}$  (p in atmospheres and T in degrees Kelvin).

The computation of absorbance with the aid of a high speed computer is practical and provides a method for advancing understanding of the complex dependence on temperature, line shape, and f-number of the absorbance of a species characterized by line absorption. This method, in conjunction with experimental measurements, provides an additional technique for determining the parameters describing an absorption coefficient composed of distinct and overlapping lines.



The first part of the paper is devoted to a general discussion of the problem. It is shown that the problem is well-posed in the sense of Hadamard. The second part is devoted to the construction of the solution. The third part is devoted to the numerical solution of the problem. The fourth part is devoted to the results of the numerical solution. The fifth part is devoted to the conclusions. The sixth part is devoted to the references.

## ACKNOWLEDGEMENTS

I wish to express my great appreciation to Dr. Garry Schott for the opportunity to use this work as a thesis and for permission to use the results of his calibration experiments. I am also grateful for the many helpful discussions with him which served to clarify the interpretation of the computed results and the significance of the uncertainties in the absorption coefficient and the calibration experiments. He has unstintingly given of time from his own work for which I am also thankful.

I am indebted to Dr. Russell Duff for his instructions and advice in computer programming, his assistance in the mathematics of this problem, and his guidance as a thesis advisor. I express my thanks to him for permitting almost complete freedom in pursuing these studies and ready willingness to offer advice and help when so requested.

I also wish to express my thanks to Dr. D. W. Steinhaus for the use of his spectrograph and for his assistance and much helpful advice in making the spectrograms; Dr. Robert T. Phelps and his co-workers for the use of their densitometer; Walter Gould for the neutral density filters and their calibration; John Williamson for assistance in taking the spectrograms; and Aurelia Madrid for assistance in preparation of the final manuscript.

I express my thanks to my wife, June, for much patience and very much assistance in typing.

I extend my appreciation to the administration of the Los Alamos Scientific Laboratory for the opportunity to work toward a Master's Degree. And thanks to the United States Atomic Energy Commission under the auspices of which this work was performed.



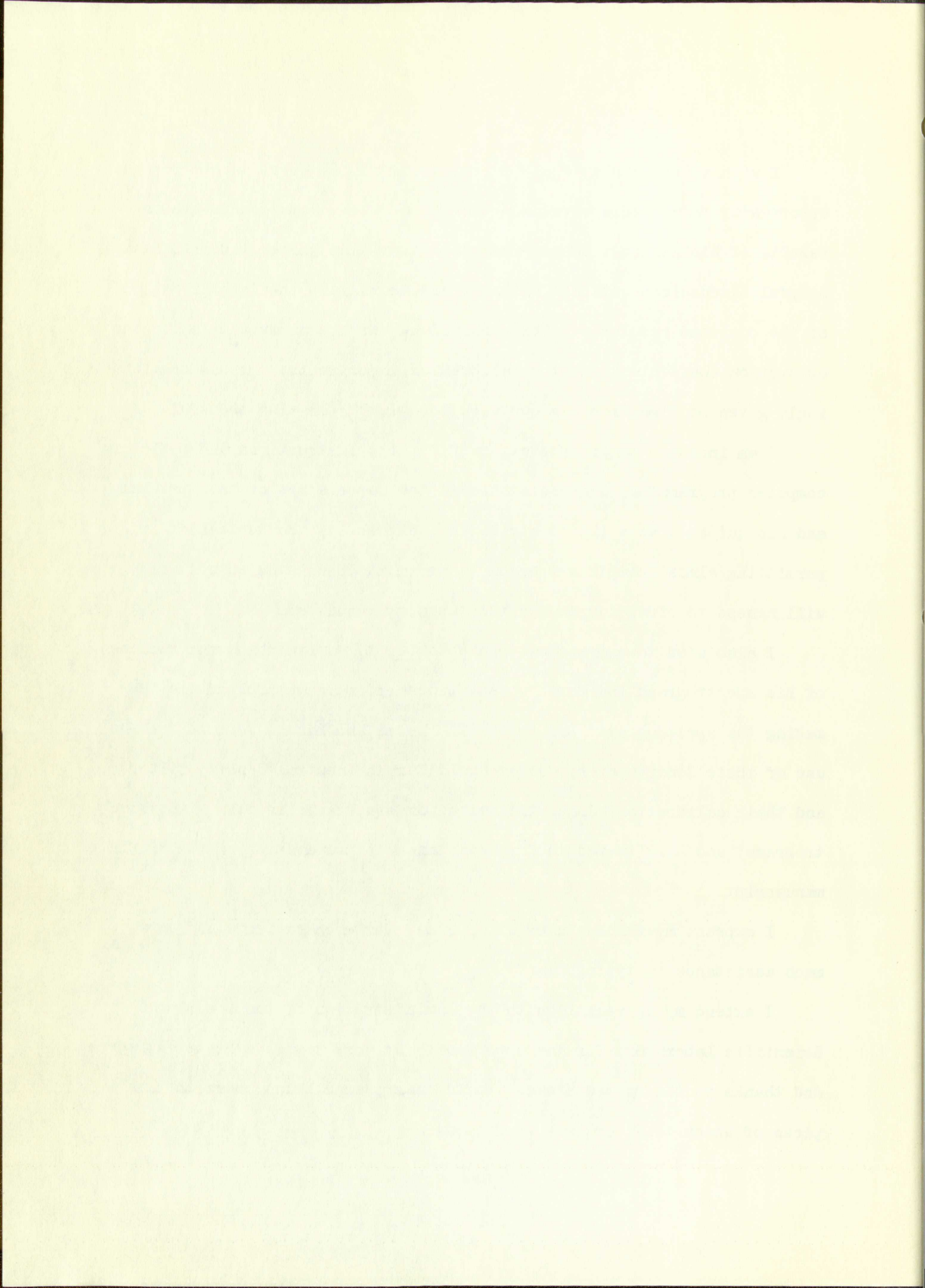
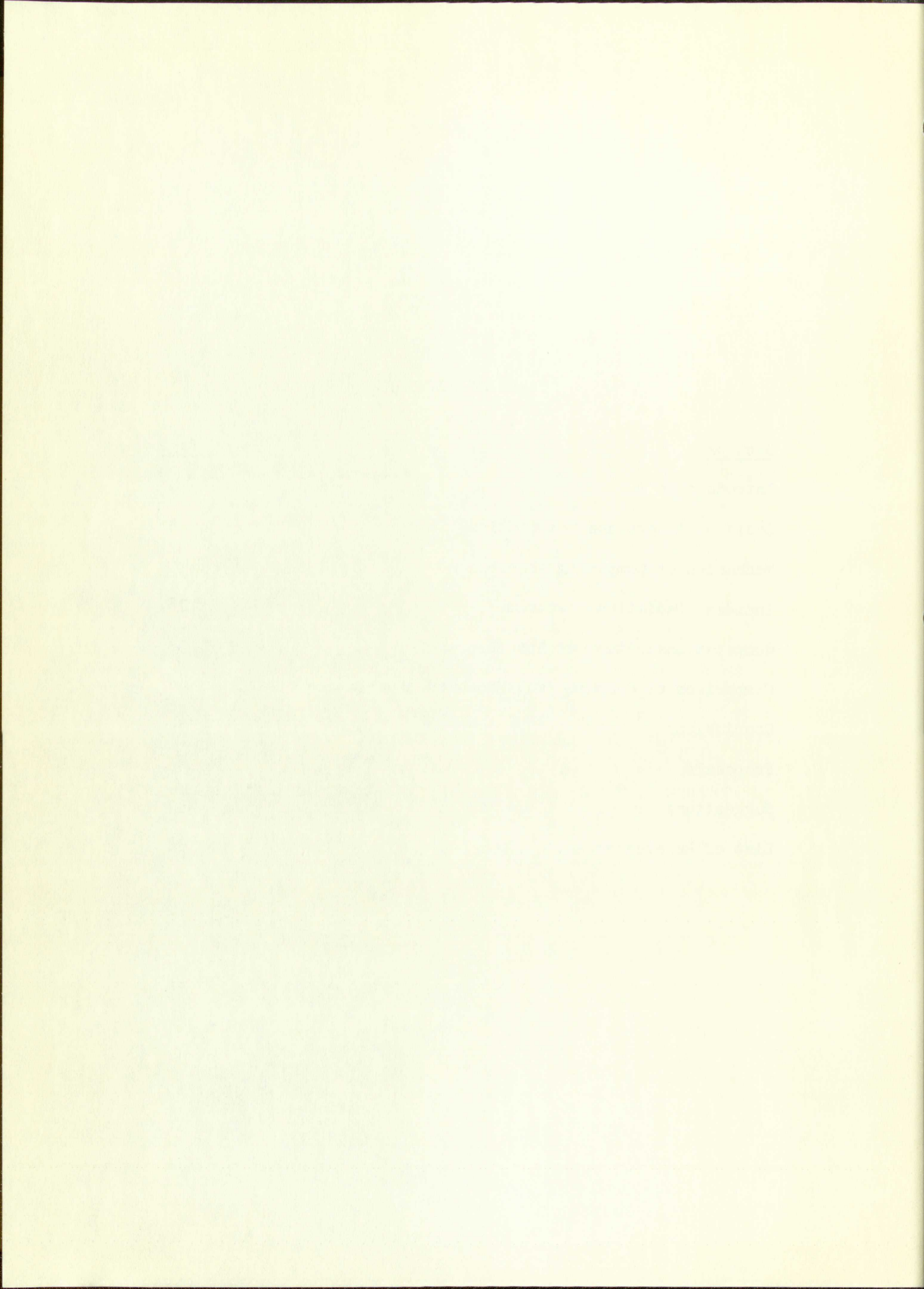


TABLE OF CONTENTS

<u>Section</u>	<u>Page</u>
Introduction . . . . .	1
Basis of Absorbance Computations . . . . .	3
Mechanics of Computing Absorbance. . . . .	9
Incident Radiation Spectrum . . . . .	18
Computational Study of Absorbance. . . . .	33
Comparison of Computed and Measured Absorbance . . . . .	44
Conclusions . . . . .	54
Proposals. . . . .	56
Suggestions . . . . .	57
List of References . . . . .	58



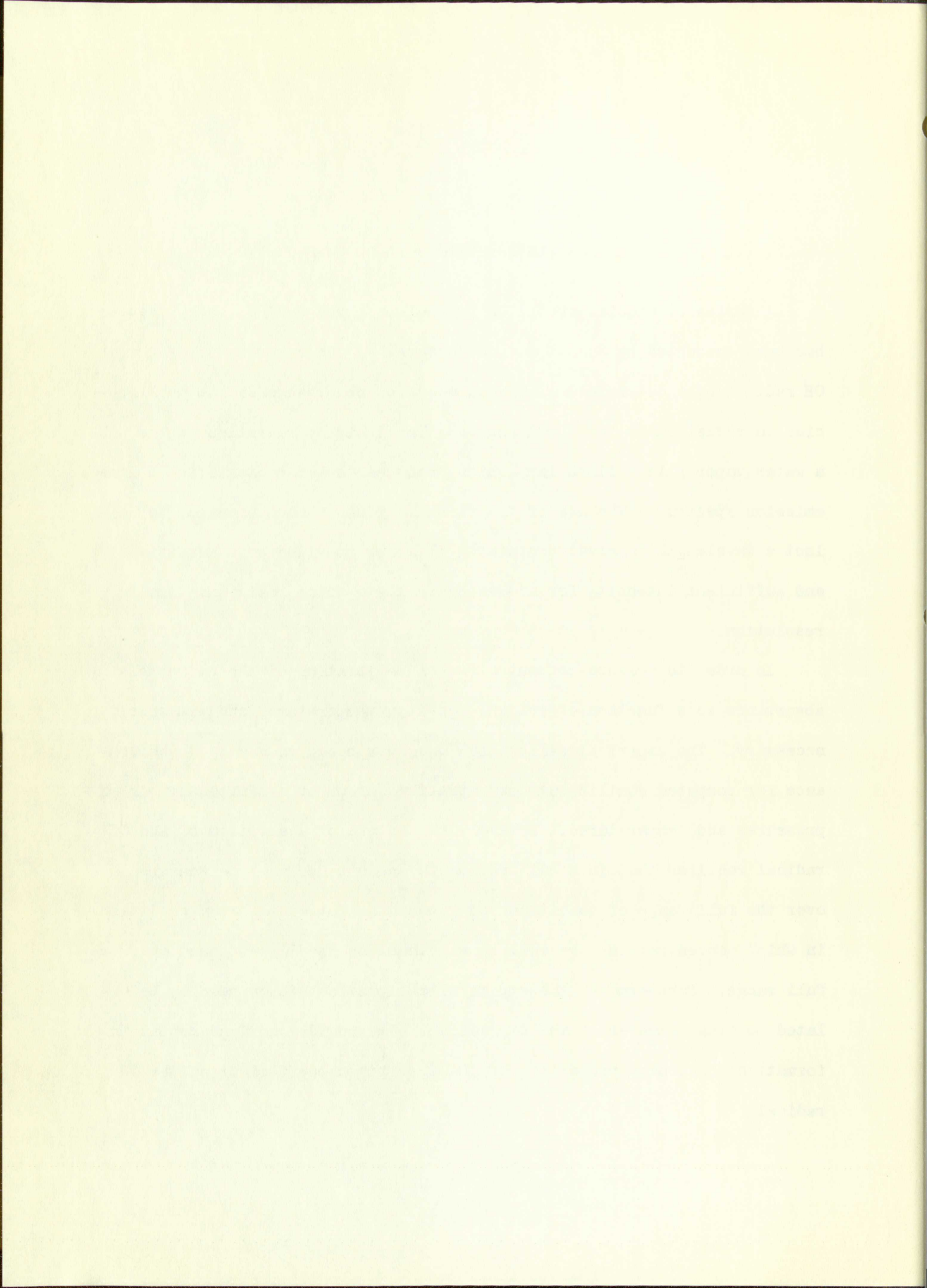


## INTRODUCTION

A series of studies of the OH radical observed behind shock waves has been conducted by Schott and co-workers.<sup>1-3</sup> Concentrations of the OH radical were determined using the measured absorbance due to this species to radiation in the 3090A region. The incident radiation source was a water vapor filled flash lamp which produces the characteristic OH line emission spectrum. The use of the flash lamp and a monochromator to select a wavelength interval containing 31 lines provided good sensitivity and sufficient intensity for adequate signal-to-noise ratio and time resolution.

In order to measure concentrations a calibration of the system giving absorbance as a function of optical density, temperature, and pressure is necessary. The empirical calibration used was based on measured absorbance for computed equilibrium concentrations of OH at a limited number of pressures and temperatures. However, the nature of absorption of the OH radical requires that in a calibration the absorbance must be measured over the full range of conditions of interest. But equilibrium conditions in which concentrations are well known cannot be readily attained over the full range. Furthermore, the empirical calibration cannot readily be related to other studies of the OH radical. It provides no fundamental information concerning properties of the absorption coefficient of the OH radical.

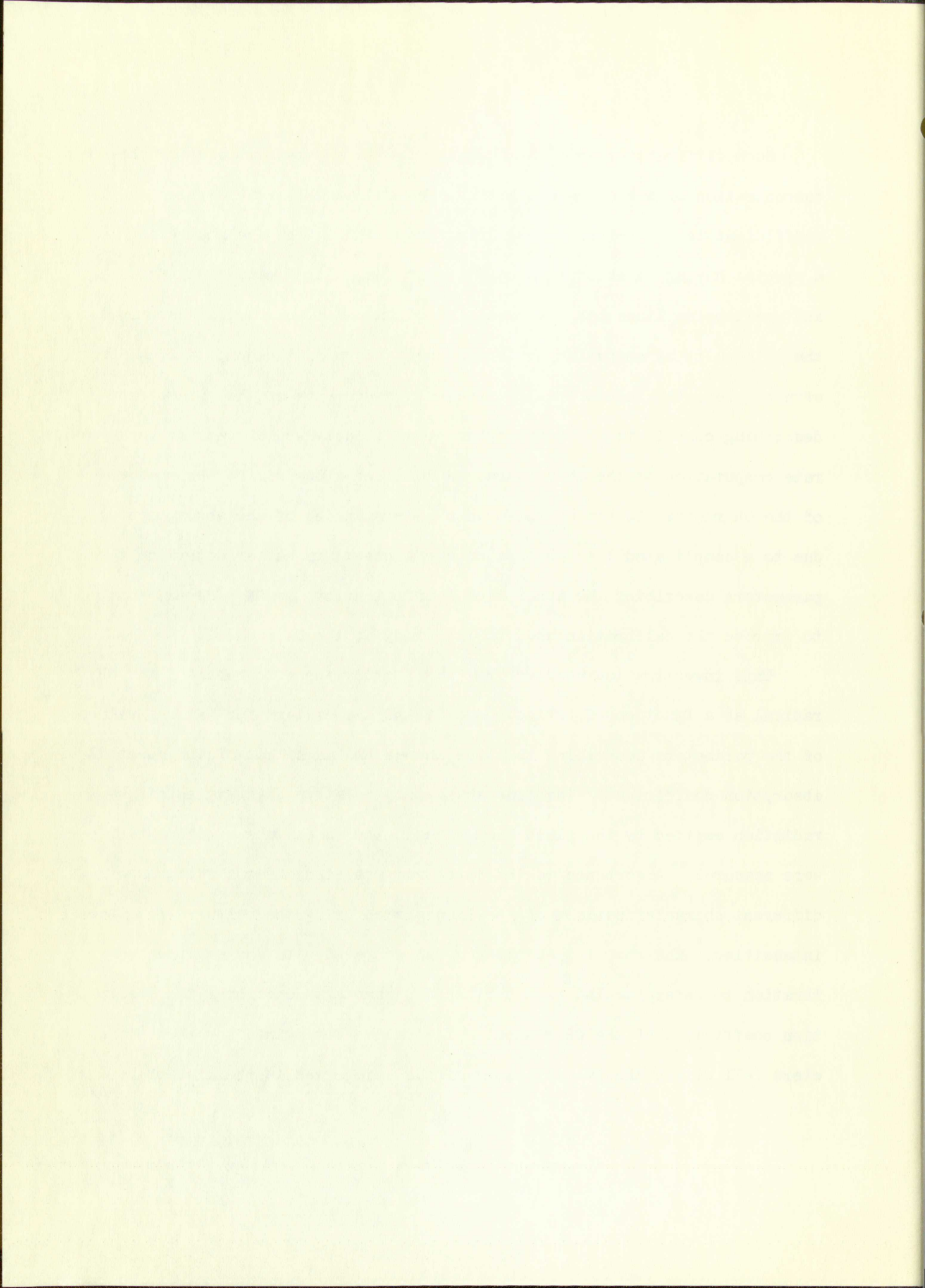




Such difficulties would be associated with any system in which the concentration of a species exhibiting a complicated line absorption coefficient is determined by measuring absorbance. The absorbance of a species having an absorption coefficient composed of many distinct and overlapping lines has not been studied in detail previously due to the difficulty of computing the absorbance. Even if the computations were simpler, the lack of really precise measurements of the parameters describing complicated line absorption coefficients would preclude accurate computation of the absorbance. A detailed study of the absorbance of the OH radical is needed to further understanding of the absorption due to a complicated line absorption coefficient, to better determine the parameters describing the absorption coefficient of the OH radical, and to improve the calibration used in the study of the OH radical.

This investigation used an IBM 704 to study the absorbance of the OH radical as a function of optical density and temperature for various values of the parameters describing the line shapes and magnitude of the spectral absorption coefficient. The line shapes and relative intensities of the radiation emitted by the flash lamp used in the shock tube experiments were measured. Absorbance to this spectrum was studied as a function of different characterizations of the line shapes using the measured relative intensities. The computed absorbance was compared with the empirical calibration to determine the best choice of parameters describing the absorption coefficient of the OH radical. The values determined for these parameters fell within the overall range of those reported in the literature.<sup>4-7</sup>





## BASIS OF ABSORBANCE COMPUTATIONS

### Absorbance

The quantitative absorption of radiation in a particular wavelength interval by an absorbing medium may be expressed by the absorbance, given by

$$A = -\log_{10} T_R = -\log_{10} \frac{I}{I^{\circ}}, \quad (1)$$

where  $A \equiv$  absorbance,

$T_R \equiv$  fractional transmissivity,<sup>8</sup>

$I^{\circ} \equiv$  integrated intensity of radiation incident upon the absorbing medium,

$I \equiv$  integrated intensity of radiation transmitted by the absorbing medium.

The transmitted intensity at some wavelength  $\lambda$  is given by the expression

$$I_{\lambda} = I_{\lambda}^{\circ} e^{-P_{\lambda} X}, \quad (2)$$

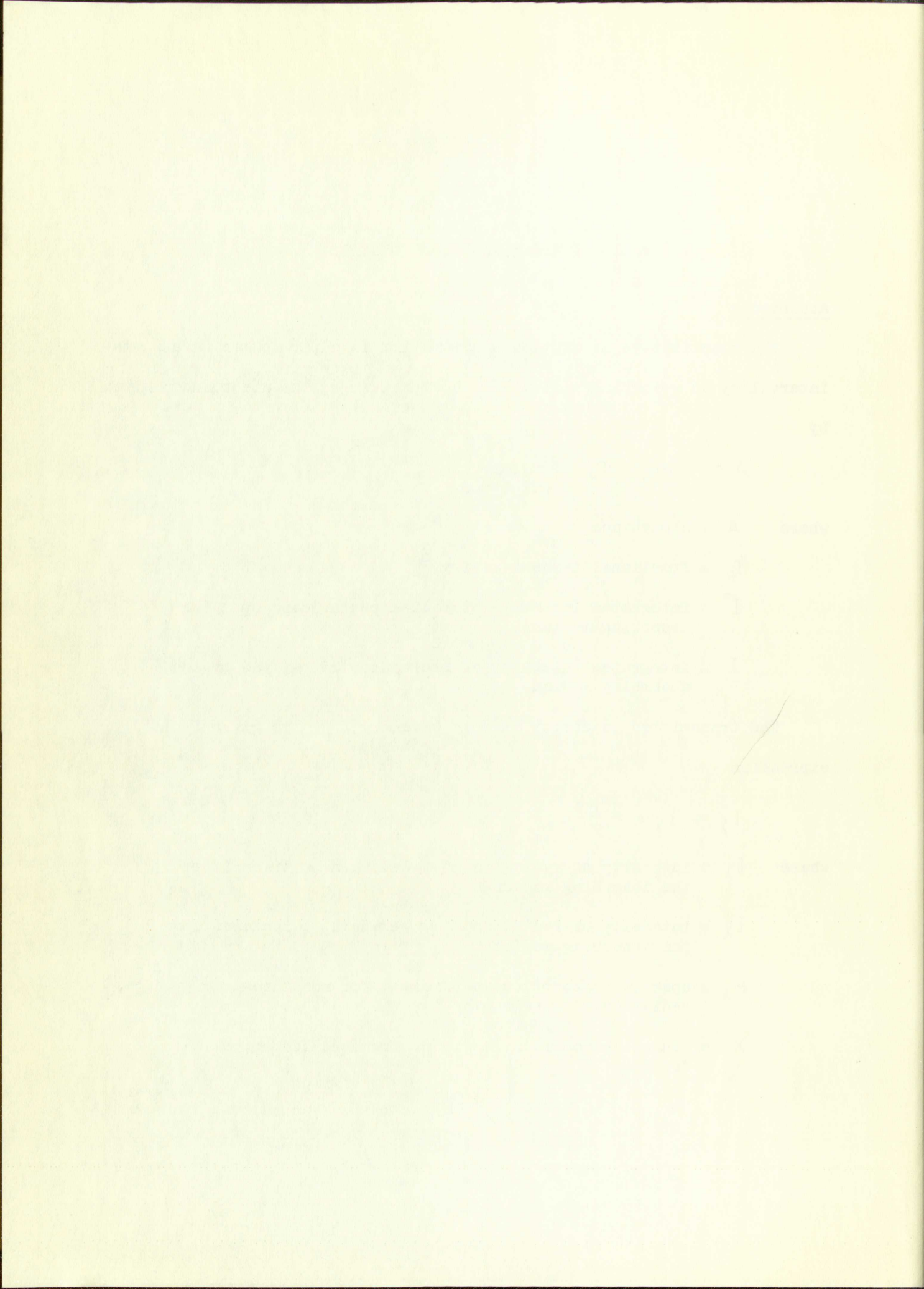
where  $I_{\lambda} \equiv$  intensity of radiation at wavelength  $\lambda$  transmitted by the absorbing medium,

$I_{\lambda}^{\circ} \equiv$  intensity of radiation at wavelength  $\lambda$  incident upon the absorbing medium,

$P_{\lambda} \equiv$  spectral absorption coefficient for monochromatic radiation of wavelength  $\lambda$ ,

$X \equiv$  concentration-path length product, called optical density.





The integrated incident and transmitted radiation intensities are then given by the expressions

$$I = \int_{\lambda_1}^{\lambda_2} I_{\lambda} d\lambda = \int_{\lambda_1}^{\lambda_2} I_{\lambda}^{\circ} \epsilon^{-P_{\lambda} X} d\lambda , \quad (3)$$

$$I^{\circ} = \int_{\lambda_1}^{\lambda_2} I_{\lambda}^{\circ} d\lambda , \quad (4)$$

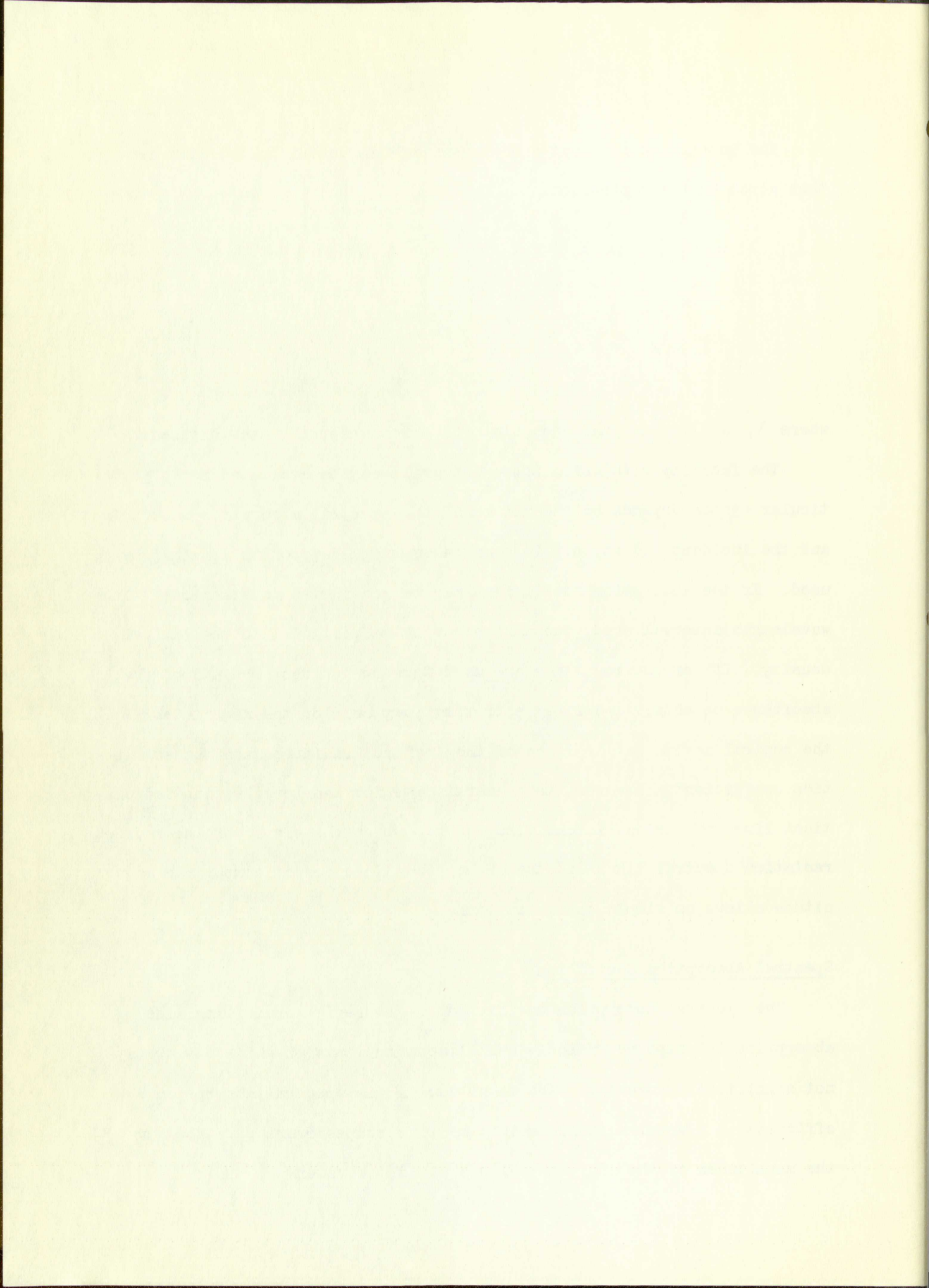
where  $\lambda_1$  and  $\lambda_2$  are the end points of the wavelength interval used.

The facility with which these integrals may be evaluated for a particular system depends on the nature of the spectral absorption coefficient and the incident radiation. In some cases simple approximations may be used. If the absorption coefficient may be considered constant over the wavelength interval used, the absorbance is proportional to the optical density. If very narrow lines are used for the incident radiation, the absorbance depends, to a first approximation, only on the magnitudes at the central maxima of the lines of the incident radiation and the absorption coefficient. However, the general case for many overlapping and distinct lines of various intensities and for which the widths of the incident radiation spectral lines and the absorption lines are of comparable magnitude allows no simple approximations.

### Spectral Absorption Coefficient

The spectral absorption coefficient of a species exhibiting line absorption is composed of individual lines the wings of which may or may not significantly overlap. The magnitude of the spectral absorption coefficient at a wavelength for which the line shapes overlap is the sum of the magnitudes of the individual lines at that wavelength. Thus the





spectral absorption coefficient can be synthesized from a knowledge of the shapes of the absorption lines and their wavelengths at the central maximum. This investigation considers only absorption lines which have a pure Doppler shape or which are a combination of natural, Doppler, and collision broadened shapes.

Computation of the shape of each line is based on the assumption that the integrated absorption for that line is independent of the line shape and the total pressure for any specified temperature. Classical electron dispersion theory gives for the integrated absorption of a line,<sup>9,10</sup> neglecting the negligible induced emission term,

$$S = \int_0^{\infty} P_{\lambda} d\lambda = \frac{\pi e^2}{mc} N_1 f_1 \left( \frac{\lambda_0^2}{c N_0} \right) , \quad (5)$$

where  $S$   $\equiv$  vacuum wavelength integrated absorption,

$e$   $\equiv$  electronic charge,

$m$   $\equiv$  mass of the electron,

$c$   $\equiv$  speed of light,

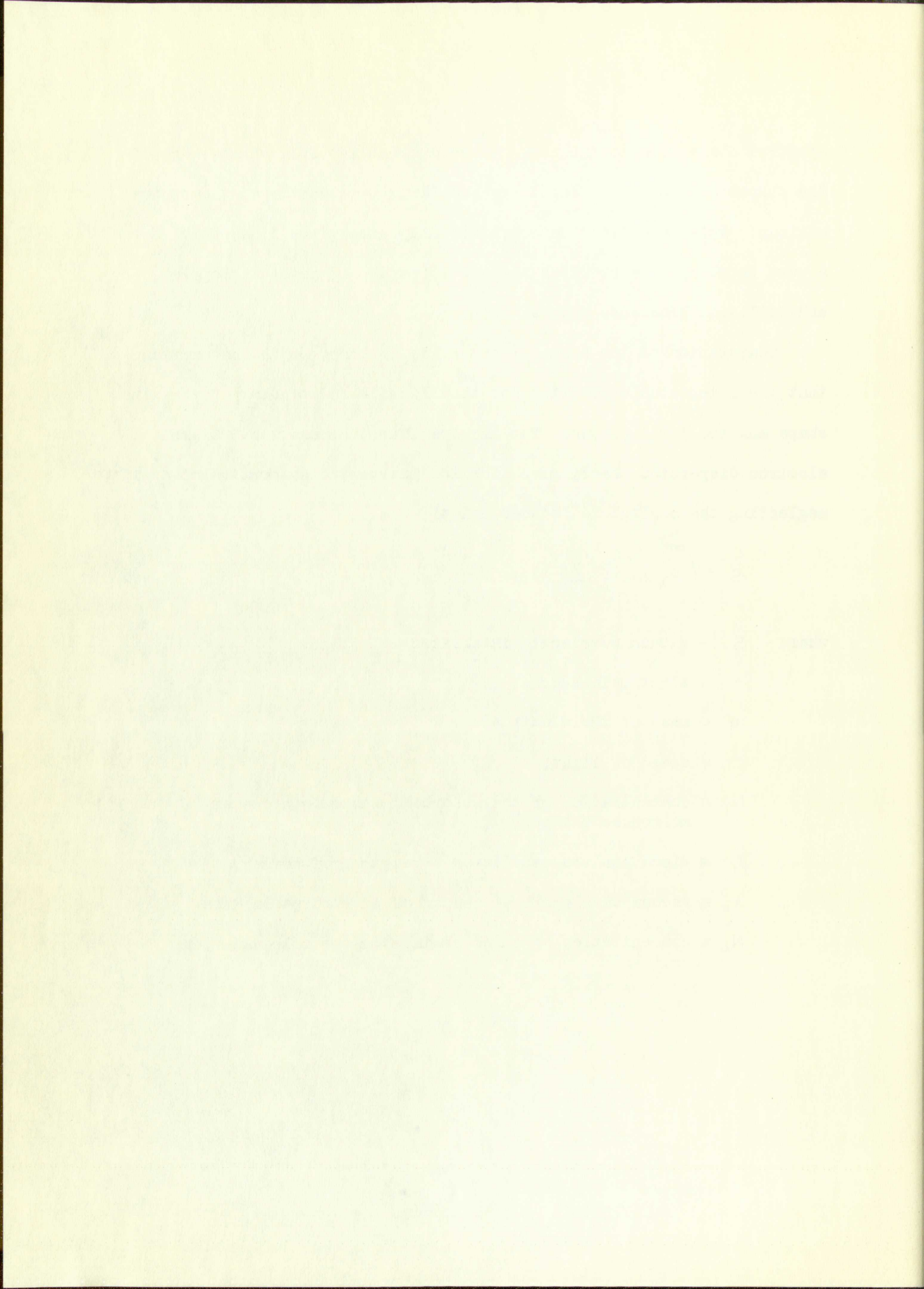
$N_1$   $\equiv$  concentration of the absorbing state in atoms or molecules per cc,

$f_1$   $\equiv$  dimensionless oscillator strength or f-number,

$\lambda_0$   $\equiv$  vacuum wavelength at center of an absorption line,

$N_0$   $\equiv$  concentration of absorber in atoms or molecules per cc.





The shape of a pure Doppler absorption line may be expressed by<sup>11</sup>

$$P_{\lambda} = P' e^{-\omega^2}, \quad (6)$$

$$\omega = \frac{2(\lambda - \lambda_0)}{\Delta\lambda_D} \sqrt{\ln 2},$$

$$\Delta\lambda_D = \frac{2\sqrt{2R \ln 2}}{c} \lambda_0 \sqrt{\frac{T}{M}},$$

where  $P'$   $\equiv$  peak absorption coefficient for a Doppler line,

$\Delta\lambda_D \equiv$  half-width of a Doppler line (full width at  $\frac{1}{2}$  of the peak absorption coefficient for the line),

$R \equiv$  universal gas constant,

$T \equiv$  temperature of absorbing gas,

$M \equiv$  molecular weight of absorber.

Integrating the spectral absorption coefficient over the line and solving for  $P'$  gives

$$P' = \frac{2\sqrt{\ln 2}}{\Delta\lambda_D} \frac{e^2 \sqrt{\pi}}{mc^2} \lambda_0^2 \frac{N_l f_l}{N_0}. \quad (7)$$

The  $f$ -number for a line may be expressed by

$$f_l = \frac{F S_l}{g_l}, \quad (8)$$

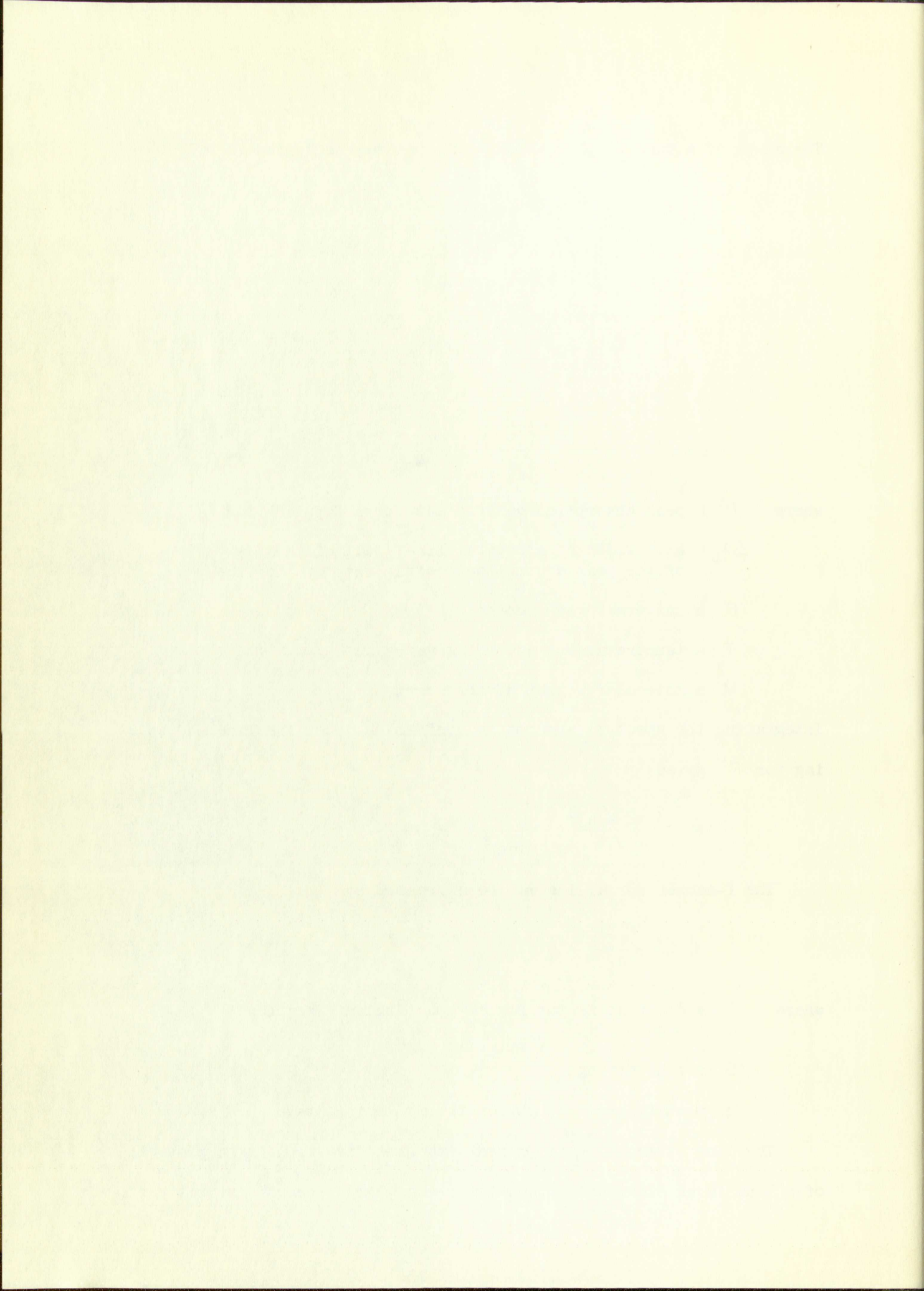
where  $F \equiv$  constant factor for any particular vibration band,

$S_l \equiv$  line strength,

$g_l \equiv$  statistical weight of the absorbing state.

The line strength  $S_l$  represents the relative transition probability of a line in an electronic transition. The line strength is that part,





a multiplicative factor, of the square of the matrix element of the electric dipole moment which is a function of  $J$ , the angular momentum quantum number. A comparison of the quantum mechanical expression for the integrated absorption and that given here shows that  $F$  is given by

$$F = \frac{8 \pi^2 m c}{3 \lambda_0 h e^2} \frac{g_u |R_{ul}|^2}{S_l}, \quad (9)$$

where  $h \equiv$  Planck's constant,

$g_u \equiv$  statistical weight of upper state,

$|R_{ul}|^2 \equiv$  square of matrix element of the electric dipole moment.

For a thermal population of rotational states the Maxwell-Boltzmann statistics apply and

$$N_l = \frac{g_l N_0 \epsilon^{-\frac{f(J'')}{kT}}}{Q_{int}}, \quad (10)$$

where  $f(J'') \equiv$  energy level of absorbing state in  $\text{cm}^{-1}$ ,

$k \equiv$  Boltzmann's constant,

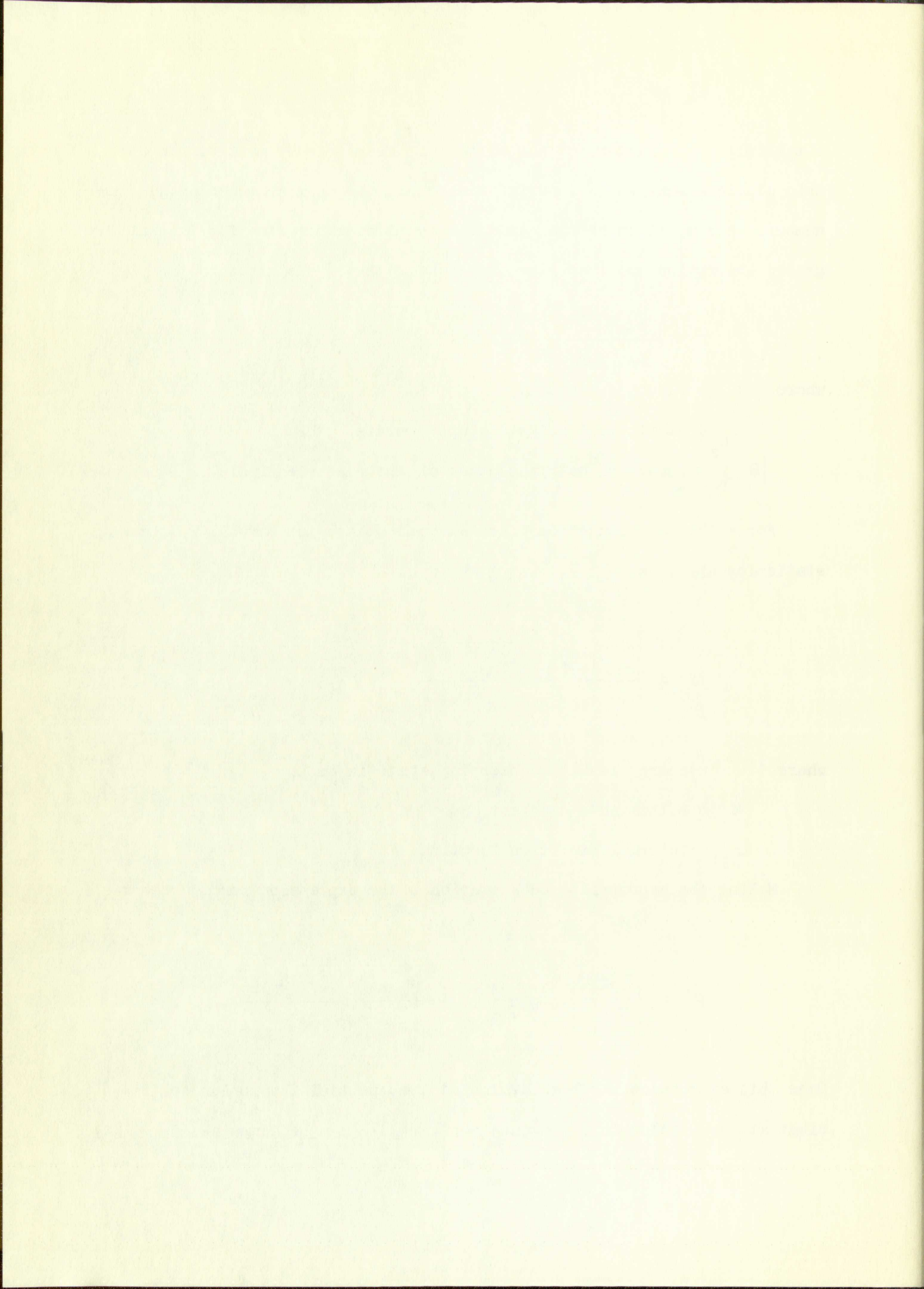
$Q_{int} \equiv$  internal partition function.

Making the appropriate substitutions, the expression for  $P'$  becomes

$$P' = \frac{e^2 \sqrt{\pi}}{m c} \lambda_0 \sqrt{\frac{M}{2RT}} \frac{\epsilon^{-\frac{f(J'')}{kT}} F S_l}{Q_{int}}. \quad (11)$$

Once this expression has been evaluated the spectral absorption coefficient at any wavelength for a pure Doppler line can be computed.





For lines which are a combination of natural, Doppler, and collision broadened shapes the absorption coefficient may be expressed by the Reiche formula<sup>12</sup>

$$P_{\lambda} = \frac{P'}{\sqrt{\pi}} \int_0^{\infty} e^{-ax - \frac{x^2}{4}} \cos \omega x \, dx, \quad (12)$$

$$a = \frac{\Delta\lambda_N + \Delta\lambda_L}{\Delta\lambda_D} \sqrt{\ln 2}, \quad (13)$$

where  $x \equiv$  dummy variable,

$a \equiv$  quantity specifying the line shape (called the collision broadening factor),

$\Delta\lambda_N \equiv$  natural half-width,

$\Delta\lambda_L \equiv$  collision half-width (Lorentz).

This integral cannot be evaluated in closed form. With the aid of the IBM 704 good approximations to it are possible for each value of  $\lambda$ .

Inherent in the use of the above method of generating the absorption lines for combined natural, Doppler, and collision broadening is the assumption that asymmetry of the absorption lines is negligible. Possible effects of asymmetry have not been considered in detail in this investigation.

It should be noted that a given value of  $a$  completely specifies the line shape for any temperature. If  $a = 0$ , the above integral may be evaluated in closed form and reduces to the expression for the Doppler line shape.



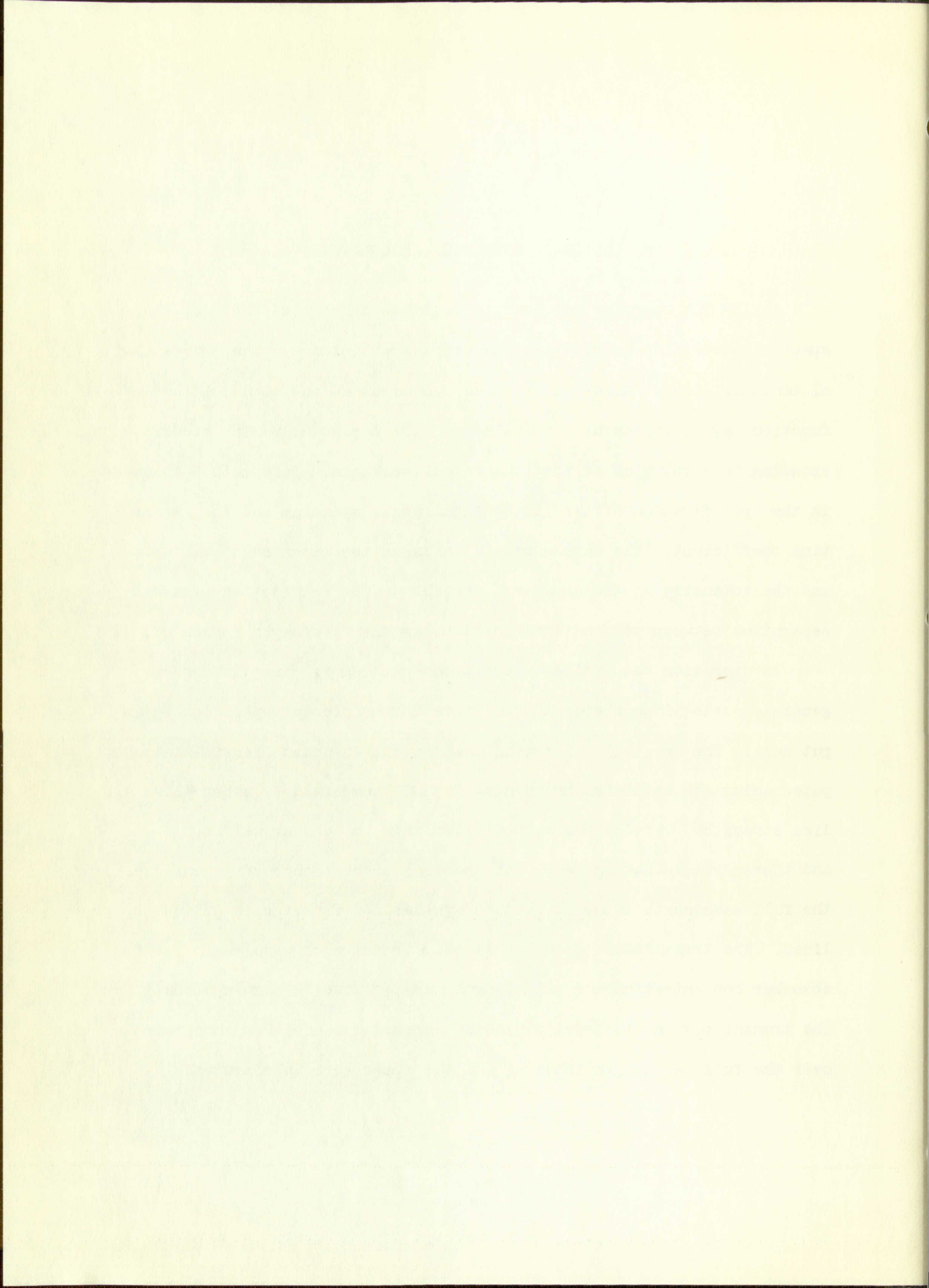


## MECHANICS OF COMPUTING ABSORBANCE

An IBM 704 computer was used to evaluate the expressions for the spectral absorption coefficient and compute absorbance. The 704, a digital computer, cannot handle continuous functions as such. A continuous function may be represented by values of the dependent variable corresponding to each value of the independent variable. This method is used in the specification of the incident radiation spectrum and the absorption coefficient. The wavelength is taken as the independent variable and the intensity as the dependent variable. The constant wavelength separation between points is referred to as the wavelength increment.

In operation the incident radiation spectrum is first loaded or generated using line shapes and relative intensities as specified by input data. The spectral absorption coefficient for each line is then computed using the collision broadening factor, temperature, energy levels, line strengths, wavelengths at central maxima, molecular weight,  $F$ , and thermodynamic data given. The spectral absorption coefficient over the full wavelength interval is then synthesized from the individual lines. The transmitted intensity is computed at each wavelength for the absorber concentration and path length as specified in the input data. The transmitted and incident radiation intensities are then integrated over the full wavelength interval and the absorbance is computed.



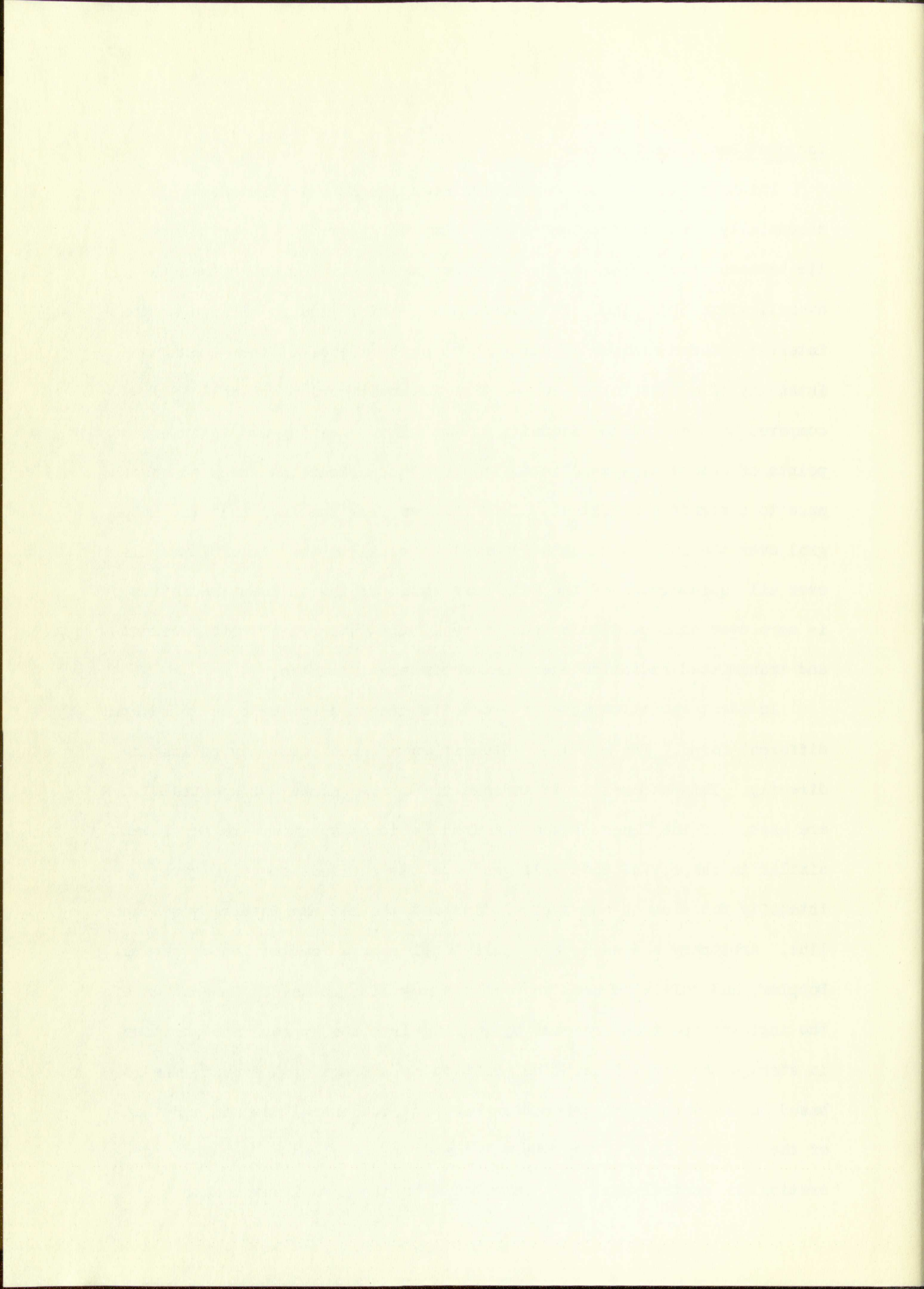


### Incident Radiation Spectrum

Points of the incident radiation spectrum at which intensity is essentially zero are not loaded into computer storage. These points lie between lines separated by a wavelength interval greater than the overall width of a line. The overall width of a line is defined as the interval between minimum intensities at each side of a line. Minimum intensity of a line is defined as that intensity which is small ( $\leq 1\%$ ) compared to the maximum intensity of the line. Leaving out intermediate points of essentially zero intensity does not affect the computed absorbance to a significant extent. This follows from the fact that the integral over the full wavelength interval is equal to the sum of integrals over all subintervals of the full interval. If the incident radiation is zero over some particular subinterval, the integral of both incident and transmitted radiation over that subinterval is zero.

Incident radiation intensity data is accepted by the code in several different forms. The measured intensities at each point may be loaded directly. This becomes quite tedious if a large number of spectral lines are used. If the lines of the measured incident spectrum are sufficiently similar in shape, the code will generate the incident spectrum given the intensity function of one typical line and the maximum intensity of each line. Arbitrary shapes such as pure Doppler or a combination of natural, Doppler, and collision broadened shapes may also be used. Generation of the incident spectrum proceeds by loading into the appropriate position in storage the first line. The position in storage of the next line is based on the wavelength separation between its central maximum and that of the previous line. The integral number of wavelength increments separating the central maxima is computed from the actual wavelength





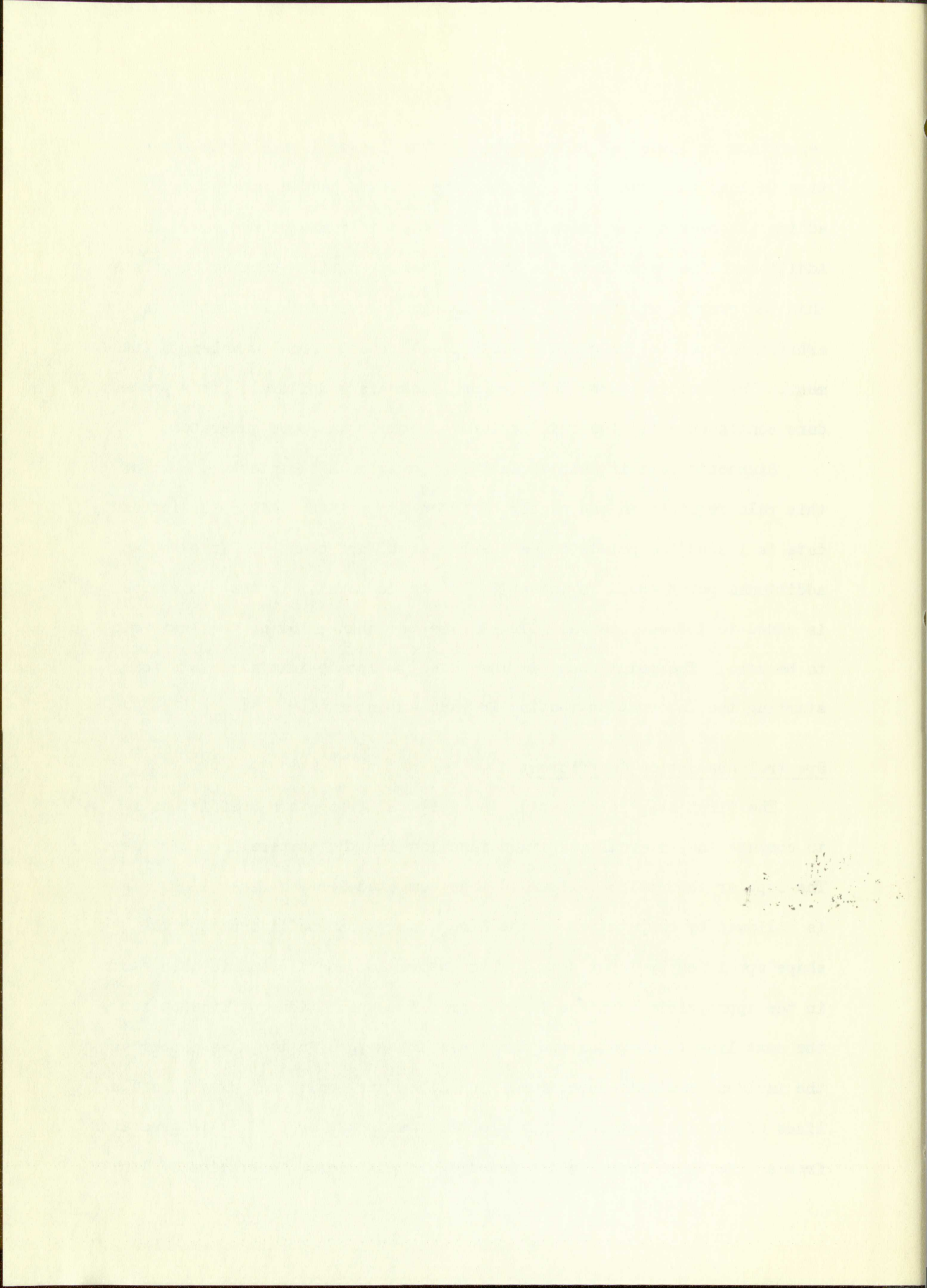
separation or loaded as input data. If the integral wavelength separation is less than the overall width, the line is loaded into storage, adding its overlapping intensities to intensities of the previous line. Additional lines are loaded in the same manner until a separation greater than the overall width occurs. The integral wavelength separation is then arbitrarily set to the overall width plus one additional wavelength increment. The line is stored and further lines are considered. This procedure continues until the full incident spectrum has been generated.

Simpson's rule is used to integrate over each subinterval. Use of this rule requires an odd number of intensity points. After the intensity data is loaded the points in each subinterval are counted. If even, an additional point equal in intensity to the last point in the subinterval is added to the subinterval. This is better than allowing the last point to be zero. The point count is then used to locate initial points for starting the integration routine in each subinterval.

#### Spectral Absorption Coefficient

The first step in computing the spectral absorption coefficient is to compute the internal partition function for the temperature specified. The Doppler absorption maximum is then computed for the first line. This is followed by computation of the line absorption coefficient for the shape specified by input data. This absorption coefficient is then stored in the appropriate position in storage. The absorption coefficient for the next line is computed and the lines are merged in the same manner as the incident radiation spectrum. The lines are positioned exactly as the lines of the incident radiation spectrum are positioned if it is generated from a line shape function and measured intensities. Generation of line





absorption coefficients and merging of the lines continues until the complete spectral absorption coefficient is synthesized.

### Internal Partition Function

Direct evaluation of the internal partition function for a particular temperature is a difficult spectroscopic and computational effort. Fortunately, for many species tables of the free energy function are available. The internal partition function may be computed with the aid of these tables. For an ideal gas the logarithm of the internal partition function may be expressed<sup>13</sup>

$$\ln Q_{\text{int}} = - \frac{(F^\circ - E_0^\circ)}{RT} + \frac{5}{2} - \frac{S_{\text{tr}}^\circ}{R}, \quad (14)$$

where  $F^\circ \equiv$  standard free energy,

$E_0^\circ \equiv$  heat of formation at absolute zero,

$S_{\text{tr}}^\circ \equiv$  entropy of translational motion.

$\frac{S_{\text{tr}}}{R}$  for an ideal gas is given by

$$\frac{S_{\text{tr}}}{R} = \frac{5}{2} + \ln \left[ \left( \frac{2\pi M}{N} \right)^{\frac{3}{2}} \frac{(kT)^{\frac{5}{2}}}{p h^3} \right], \quad (15)$$

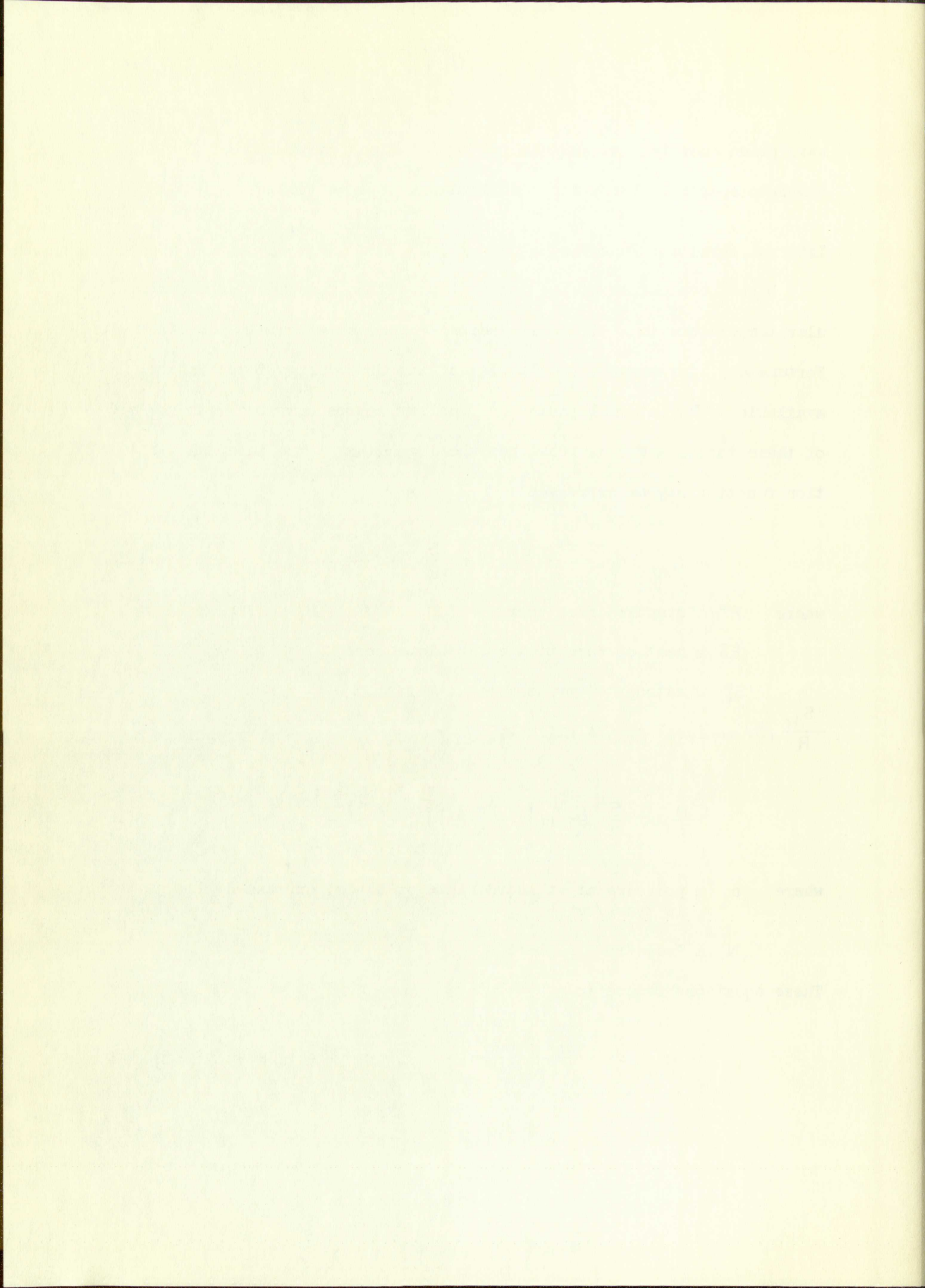
where  $p \equiv$  pressure at standard state of 1 atm. expressed in dynes/cm<sup>2</sup>,

$N \equiv$  Avogadro's number.

These equations reduce to<sup>14</sup>

$$\ln Q_{\text{int}} = - \frac{(F^\circ - E_0^\circ)}{RT} - \frac{3}{2} \ln M - \frac{5}{2} \ln T + 3.6651. \quad (16)$$





Rather than store a table of data and then interpolate for temperatures not listed, the free energy function is computed from an expression derived from the table. The expression which has been found adequate for this purpose is

$$-\frac{(F^\circ - E^\circ)}{RT} = A + B \ln T + CT + DT^2 + ET^3 + FT^4, \quad (17)$$

where the constants A through F were derived from the tabulated data.<sup>15</sup>

#### Generation of Line Shapes

The line shape for a pure Doppler line is computed directly from equation 6. Evaluation of the improper integral, equation 12, for a line which is a combination of natural, Doppler, and collision broadened shapes is accomplished in several ways depending on the value of  $\underline{a}$ . The following series is used for  $0 < \underline{a} \leq 0.8$ :

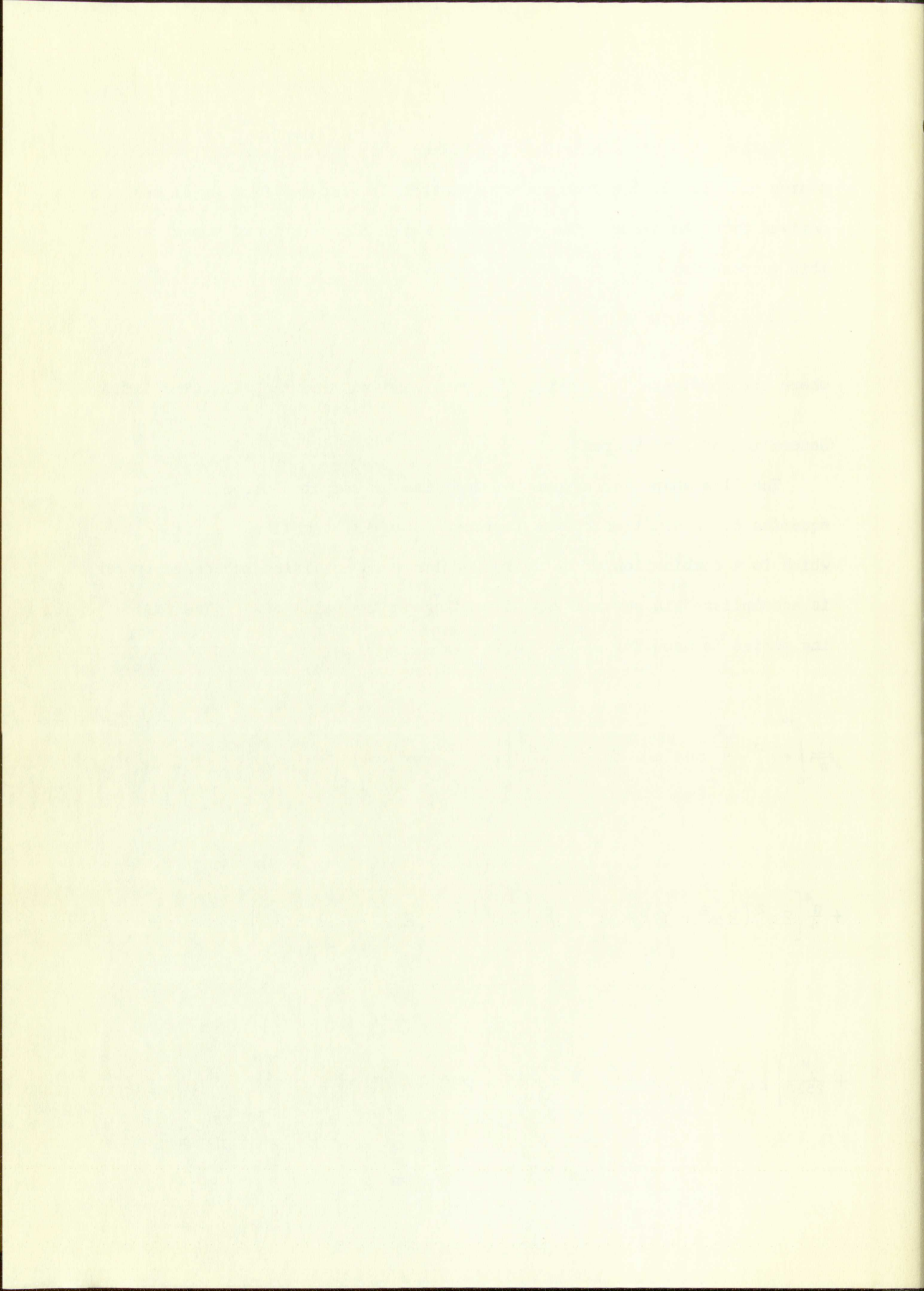
$$\frac{1}{\sqrt{\pi}} \int_0^\infty \epsilon^{-ax - \frac{x^2}{4}} \cos \omega x \, dx = \epsilon^{-\omega^2} \left\{ 1 - a^2(2\omega^2 - 1) \right.$$

$$+ \frac{a^4}{6} \left[ 2\omega^2(2\omega^2 - 6) + 3 \right] - \frac{a^6}{90} \left[ 2\omega^2 \left\{ 2\omega^2(2\omega^2 - 15) + 45 \right\} - 15 \right]$$

$$+ \frac{a^8}{2520} \left[ 2\omega^2 \left\{ 2\omega^2 \left[ 2\omega^2(2\omega^2 - 28) + 210 \right] - 420 \right\} + 105 \right]$$

(continued on next page)





$$\begin{aligned}
& -\frac{1}{\sqrt{\pi}} \left\{ 2\alpha\beta - \frac{2\alpha^3}{3} \left[ 2\omega^2\beta - (3\beta-1) \right] + \frac{\alpha^5}{15} \left[ 2\omega^2 \left\{ 2\omega^2\beta - (10\beta-1) \right\} + (15\beta-7) \right] \right. \\
& - \frac{\alpha^7}{315} \left[ 2\omega^2 \left\{ 2\omega^2 \left[ 2\omega^2\beta - (21\beta-1) \right] + (105\beta-18) \right\} - (105\beta-57) \right] \\
& + \frac{\alpha^9}{11340} \left[ 2\omega^2 \left\{ 2\omega^2 \left[ 2\omega^2 \left\{ 2\omega^2\beta - (36\beta-1) \right\} + (378\beta-33) \right] \right. \right. \\
& \left. \left. - (1260\beta-285) \right\} + (945\beta-561) \right] \left. \right\}, \tag{18}
\end{aligned}$$

$$\beta = 1 - 2\omega F(\omega),$$

$$F(\omega) = e^{-\omega^2} \int_0^{\omega} e^{x^2} dx.$$

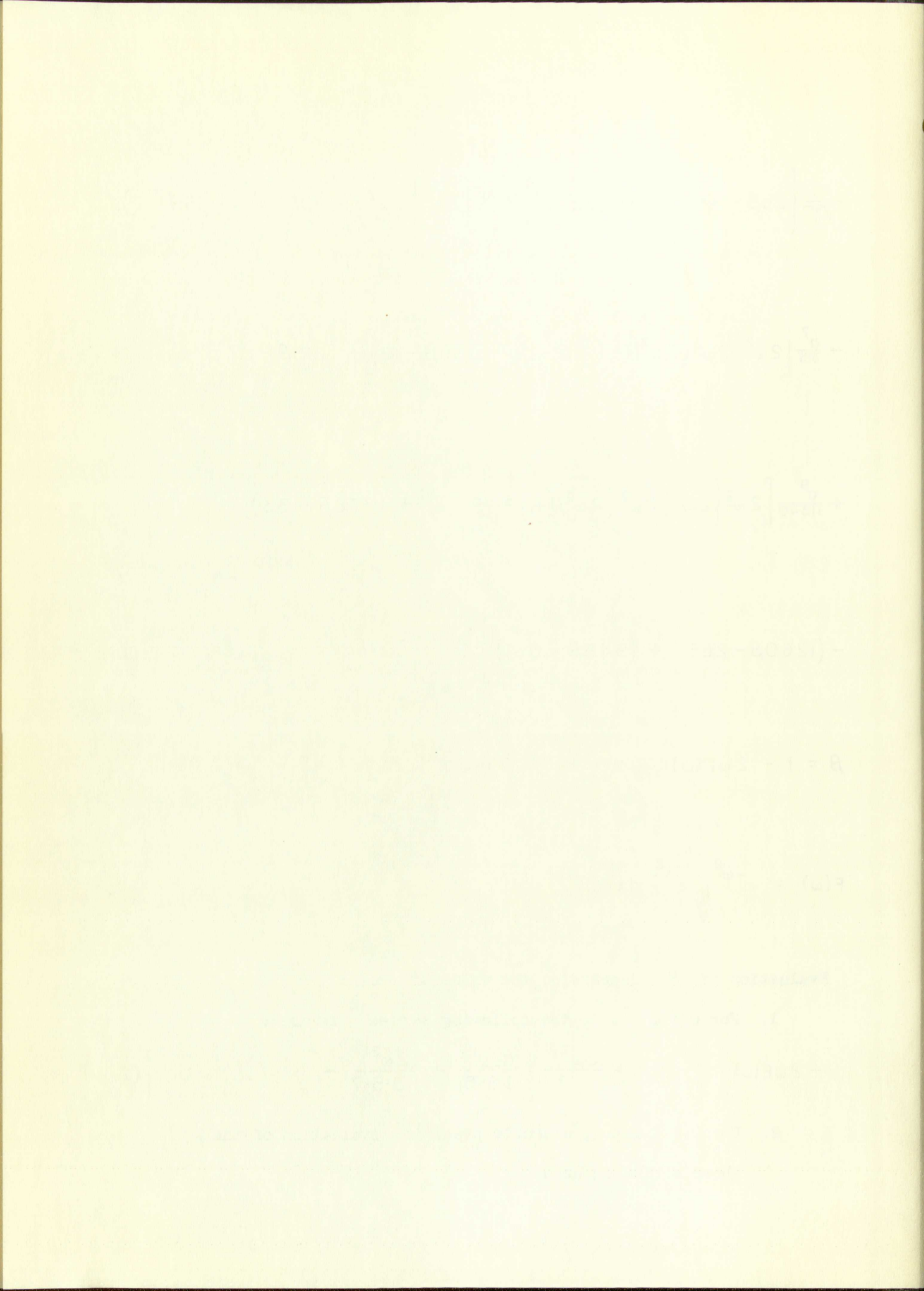
Evaluation of  $\beta$  depends on the value of  $\omega$  :

1. For  $0 \leq \omega < 0.7$ , the following series<sup>16</sup> is used:

$$1 - 2\omega F(\omega) = 1 - 2\omega^2 + \frac{(2\omega^2)^2}{1 \cdot 3} - \frac{(2\omega^2)^3}{1 \cdot 3 \cdot 5} + \frac{(2\omega^2)^4}{1 \cdot 3 \cdot 5 \cdot 7} - \dots \tag{19}$$

2. For  $0.7 \leq \omega \leq 2$ , a double precision evaluation of the above series is used.





3. For  $2 < \omega < 6$ , an expression given by Miller & Gordon<sup>17</sup> is used with appropriate tests to insure that the values obtained are proper. The expression is

$$F(\omega) = \frac{\sqrt{\pi}}{2} \epsilon^{-\omega^2} \tan \frac{\pi \omega}{2\sqrt{0.1}} - \frac{2\sqrt{0.1}}{\omega\sqrt{\pi}} \sum_{m=1,3,5,\dots} \frac{\epsilon^{-0.1m^2}}{\left(\frac{0.1m^2}{\omega^2} - 1\right)} \quad (20)$$

If the series fails to converge because of the value of  $\omega$  used, an unlikely possibility as indicated by numerous checks, a tenth order interpolation is made between tabulated values.

4. For  $\omega \geq 6$ , an asymptotic series<sup>16</sup> is used:

$$1 - 2\omega F(\omega) = - \left[ \frac{1}{2\omega^2} + \frac{1 \cdot 3}{(2\omega^2)^2} + \frac{1 \cdot 3 \cdot 5}{(2\omega^2)^3} + \frac{1 \cdot 3 \cdot 5 \cdot 7}{(2\omega^2)^4} + \dots \right] \quad (21)$$

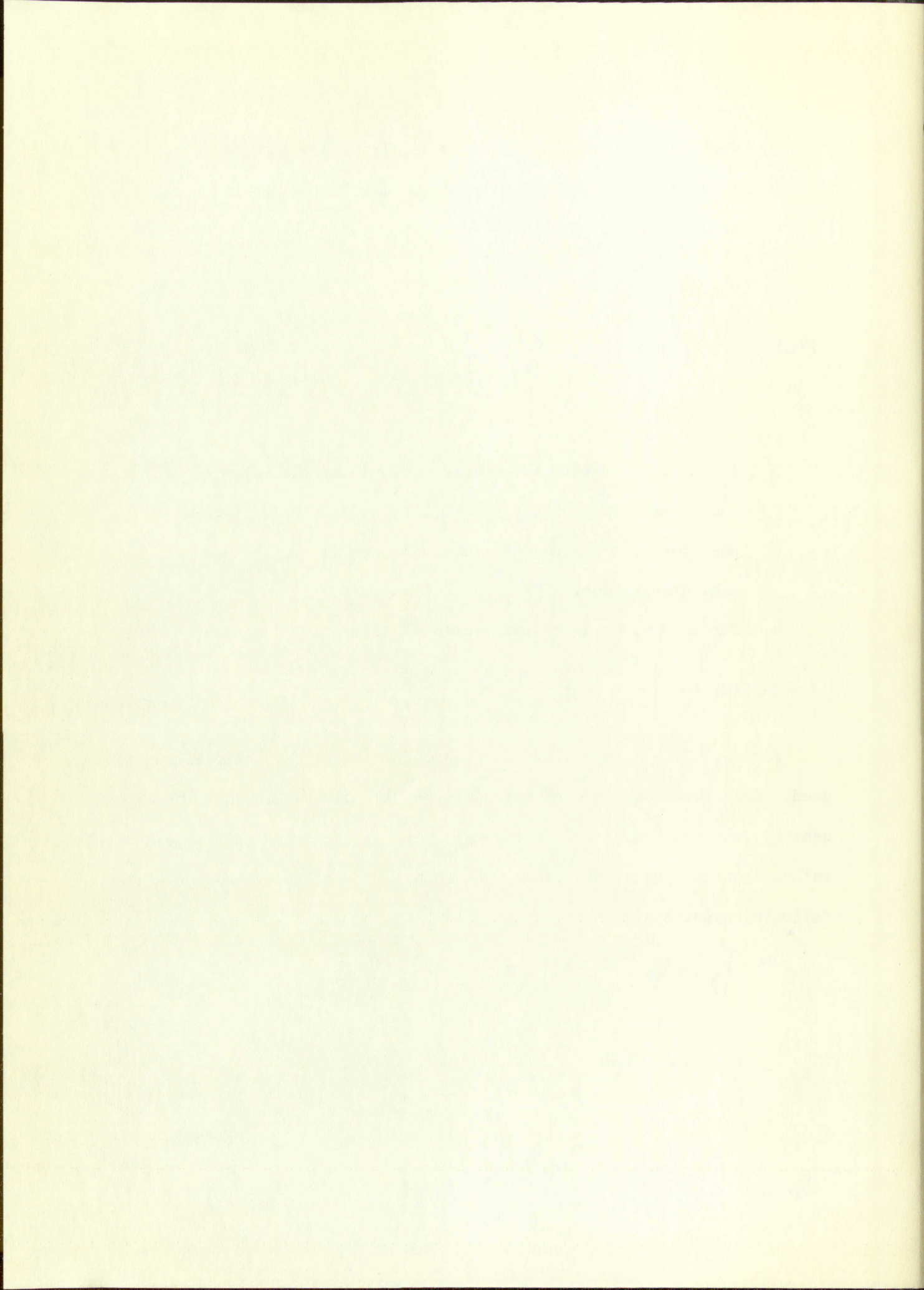
For  $\underline{a} > 0.8$ , an approximate integration technique due to Filon<sup>18</sup> is used. This technique is a modified Simpson's rule wherein just the exponential function (envelope) in the integrand is approximated with a parabola rather than the whole integrand. The method reduces to evaluation of the following quantities:

$$\int_0^{\infty} \epsilon^{-ax - \frac{x^2}{4}} \cos \omega x \, dx = \Delta x \left[ \beta S_{2r} + \gamma S_{2r-1} \right], \quad (22)$$

$$S_{2r} = \sum_{r=0}^n \epsilon^{-ax_{2r} - \frac{x_{2r}^2}{4}} \cos \omega x_{2r} - \frac{1}{2},$$

$$S_{2r-1} = \sum_{r=1}^n \epsilon^{-ax_{2r-1} - \frac{x_{2r-1}^2}{4}} \cos \omega x_{2r-1},$$





$$\beta = \frac{2}{\theta^2} \left[ 1 + \cos^2 \theta - \frac{\sin 2\theta}{\theta} \right], \quad (23)$$

$$\gamma = \frac{4}{\theta^2} \left[ \frac{\sin \theta}{\theta} - \cos \theta \right], \quad (24)$$

$$x_{2r} = 2r \Delta x,$$

$$\theta = \omega \Delta x,$$

where  $\Delta x$  is the integration increment and  $2n$  the number of integration increments. For  $\theta \leq 0.24$ , it is more convenient to use the first four terms of the MacLaurin expansion of the above expressions

$$\beta = \frac{2}{3} + \frac{2}{15} \theta^2 - \frac{4}{105} \theta^4 + \frac{2}{567} \theta^6, \quad (25)$$

$$\gamma = \frac{4}{3} - \frac{2}{15} \theta^2 + \frac{2}{270} \theta^4 - \frac{1}{11340} \theta^6. \quad (26)$$

Since the upper limit of the integral is infinite, it is necessary to decide at what value of  $x$  to stop summing. The value of  $\omega$  is constant for the integral, and hence the wavelength of the sinusoidal function does not change. With increase in the value of  $x$ , the net contribution of each succeeding oscillation of the integrand decreases as the envelope decreases and the rate of change of this contribution depends on the rate of decrease of the envelope function. Thus at a value of  $x$  for which the envelope is quite small compared to 1, the value at  $x = 0$ , the contribution of the next wave is small also, that is, the rate of decrease of the envelope is small compared to its initial drop. Thus it is sufficient to stop summing when the value of the envelope is small compared



... ..

... ..

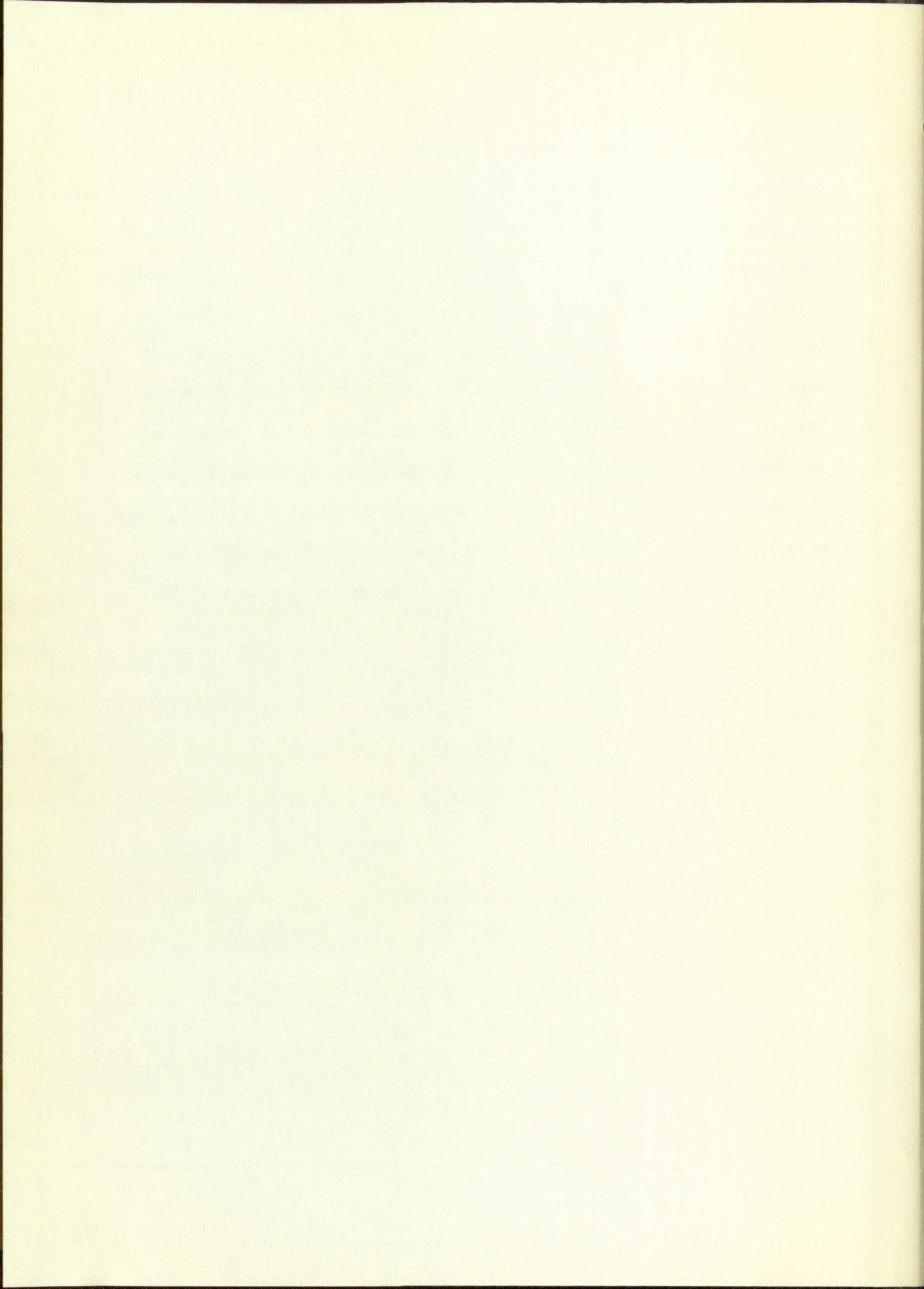
$$y = \frac{1}{2} + \frac{1}{2}x + \frac{1}{2}x^2 + \frac{1}{2}x^3 + \dots$$
$$y = \frac{1}{2} + \frac{1}{2}x + \frac{1}{2}x^2 + \frac{1}{2}x^3 + \dots$$

... ..

to 1. In this case small means machine accuracy ( $10^{-8}$ ) since differences between numbers of similar magnitude are involved in the summation.

Numerous test problems were run to determine the validity of these numerical techniques. Results were compared with the tables given in Mitchell and Zemansky<sup>19</sup> for the same values of  $\underline{a}$ . Filon's method was tested to determine the most efficient value of the integration increment in terms of accuracy desired and machine time consumed by comparing the results obtained using several different values of the integration increment. The range of convergence of the series approximation to the improper integral was tested by comparison with values computed by Filon's method. The upper useful limit of the series was determined to be for  $\underline{a} = 0.8$ , computed values for  $\underline{a} > 0.8$  being in error by more than 1%.





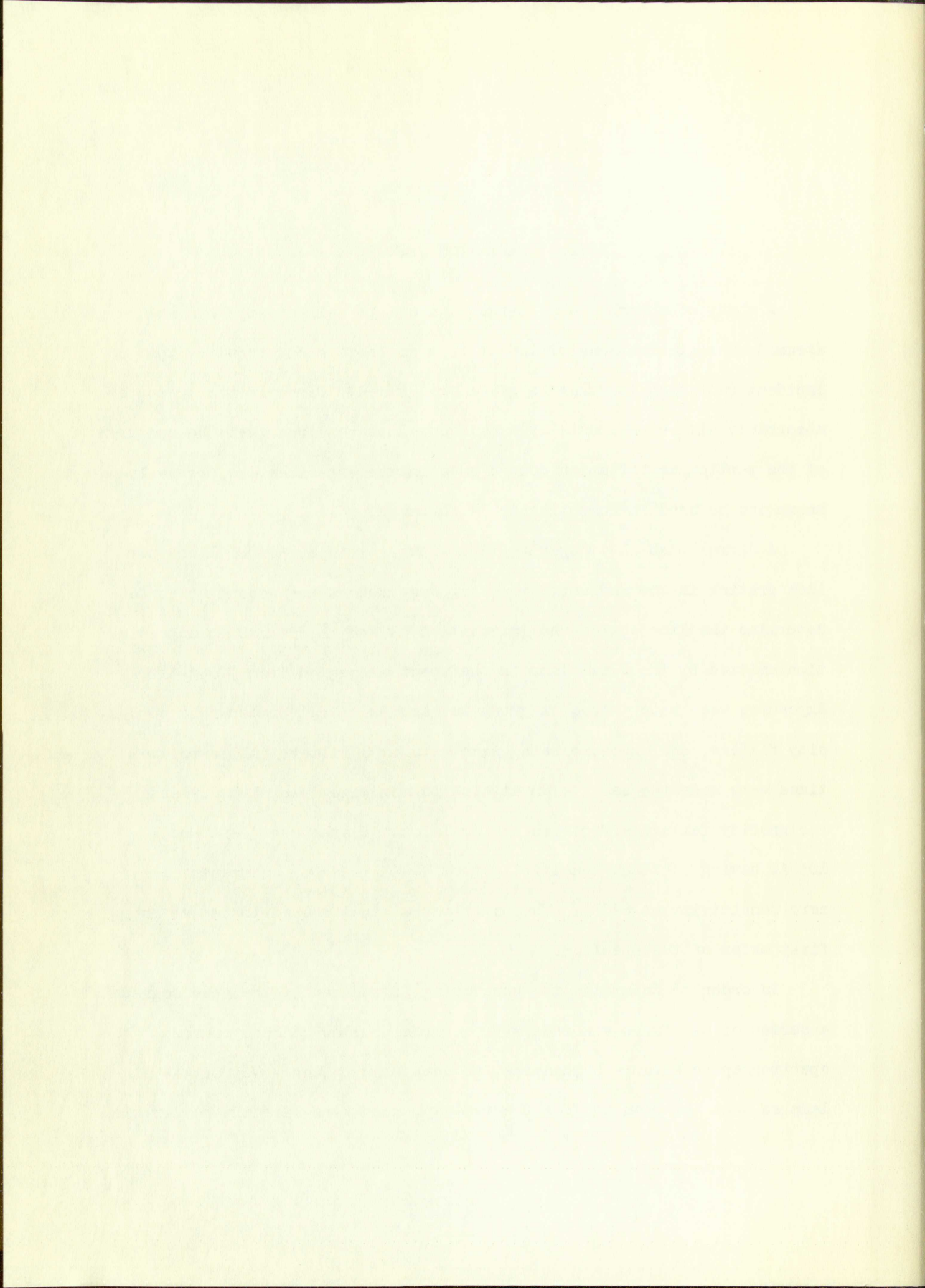
## INCIDENT RADIATION SPECTRUM

A study of absorbance as a function of optical density for various assumed characterizations of the absorption coefficient requires that an incident radiation spectrum be given or assumed. Comparison of computed absorbance with experimentally measured values requires that the spectrum of the particular radiation source used in the experiment be precisely known and be used in computing the absorbance.

A Jarrell-Ash 21 ft spectrograph with a  $4\frac{1}{2}$  inch, 30,000 lines per inch grating in the Wadsworth mounting was used in the second order to determine the line shapes and intensities of the  $^2\Sigma \rightarrow ^2\Pi$  OH band radiation emitted by the flash lamp in the spectral region from 3064A-3120A. Exposures were made through a graduated series of calibrated neutral density filters, one exposure being made without a filter. All exposure times were made the same in an attempt to minimize intermittency and reciprocity failure effects in the emulsion. Plates used were Kodak 103 AO having constant sensitivity from 2400A to 4400A and essentially zero sensitivity at 6200A. Thus a filter was not needed to remove the first order of the spectrum.

In order to determine the broadening introduced by the spectrograph a series of exposures was made with an iron, hollow-cathode source. The spectrographic setup was identical to that used in the study of the flash lamp so that the results from the two exposures were directly comparable.





Another precaution taken was to use only that portion of the flash lamp output which was actually used in the experimental shock tube calibration. To achieve this a rotating shutter was designed and set in the light path from the lamp to the slit of the spectrograph. A slot 0.725 inch wide and 0.425 inch deep was cut in the perimeter of an 8 inch Dural wheel. The wheel was attached to the axle of an 1800 rpm synchronous motor of sufficient size to stabilize the speed. Attached to the axle was a small magnet and to an external support an iron core and pickup coil. Output of the pickup coil was fed to an amplifier and pulse shaper to obtain a suitably fast-rising pulse. This pulse was fed through a microswitch controlled by an interval timer into the delay circuit of a Tektronix 545 oscilloscope. The scope delay output was fed to the lamp trigger to fire the flash lamp at the appropriate position of the wheel. The timer initiated the triggering sequence by closing the microswitch after the flash lamp capacitors had time to charge. Closing the switch completed the circuit so that at the next pulse from the pickup coil the previously described chain of events began and the lamp fired. Figure 1 shows a block diagram of the setup. Figure 2 is a circuit diagram of the amplifier and shaper circuit.

The lamp output was monitored by feeding the output of two photomultiplier tubes into a dual-input preamp on the oscilloscope. Each tube had a filter to exclude extraneous radiation and slits were used to limit incident intensity and prevent tube saturation. Two mirrors were arranged so that one tube saw the complete time history of the lamp output and the other saw only that which passed through the shutter to the spectrograph slit. Use of the dual input allowed a continuous check of the elapsed time between the initial firing of the lamp and the passage of light through



The first part of the report deals with the general situation of the country and the progress of the war. It is followed by a detailed account of the military operations in the various theaters of war. The author then discusses the political and economic conditions of the country and the impact of the war on these aspects. The report concludes with a summary of the findings and a list of recommendations for the future.

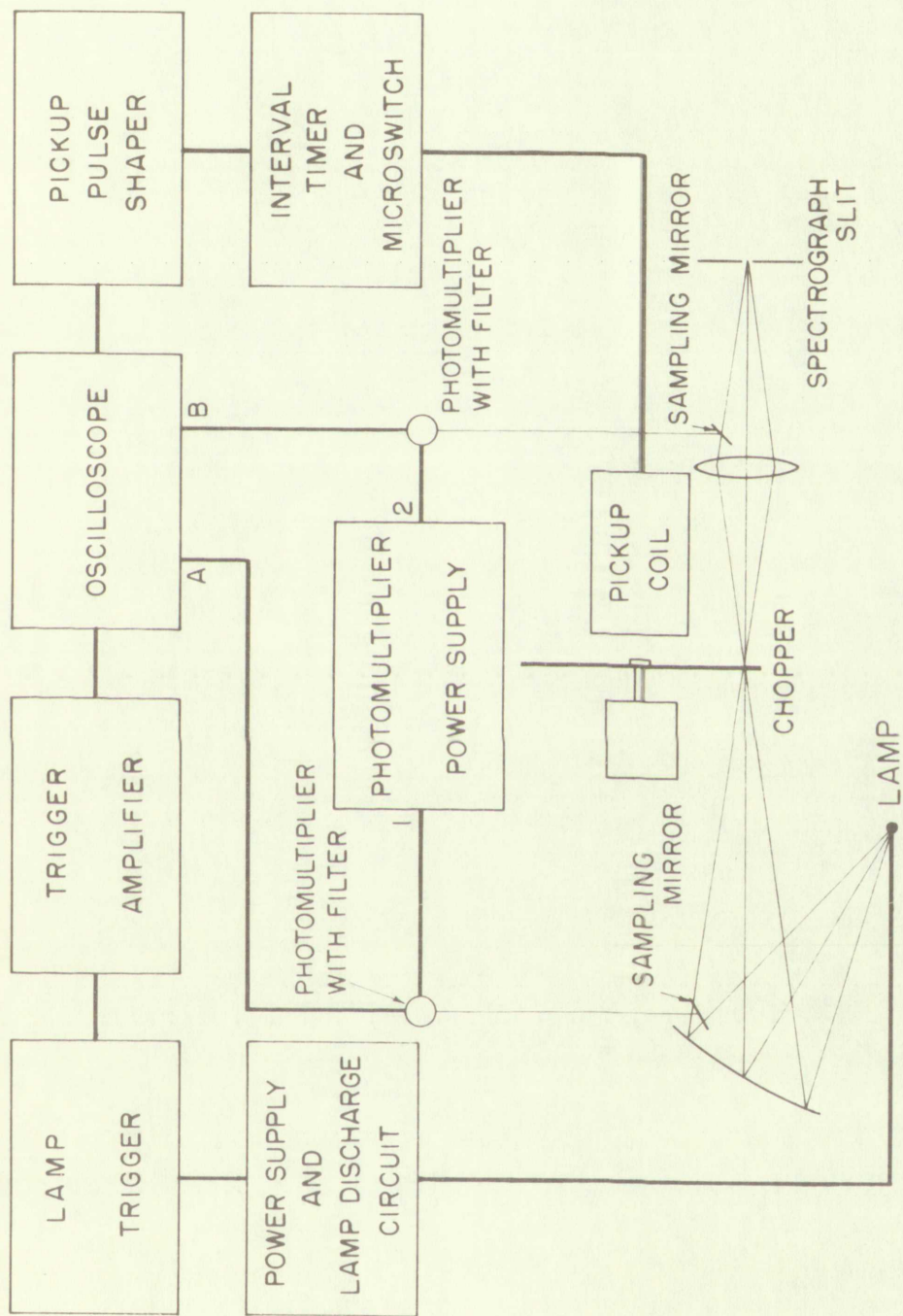
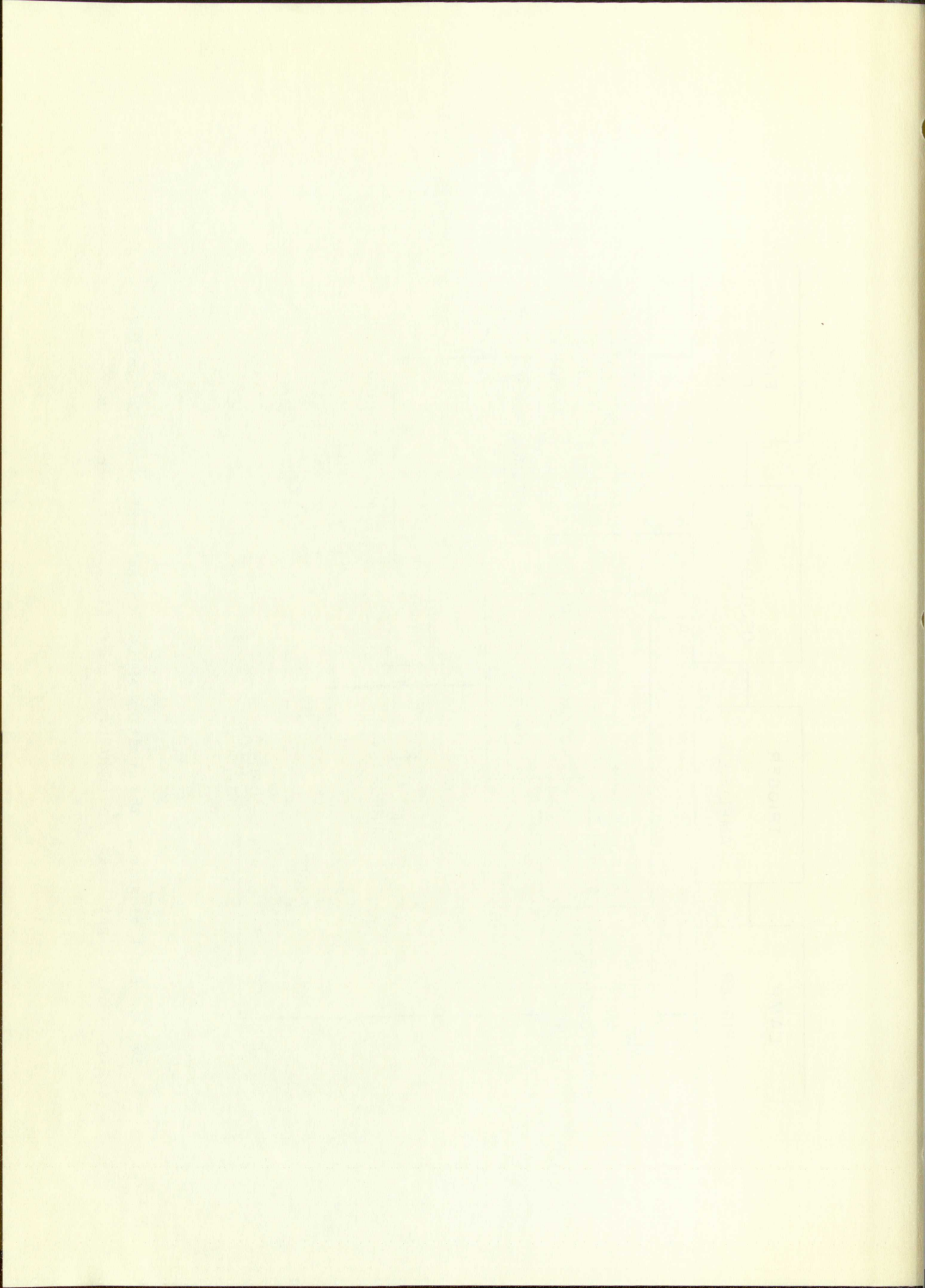


Fig. 1. Block diagram of the rotating shutter, flash control and monitoring apparatus. Light lines are light rays; heavy lines are electrical connections.





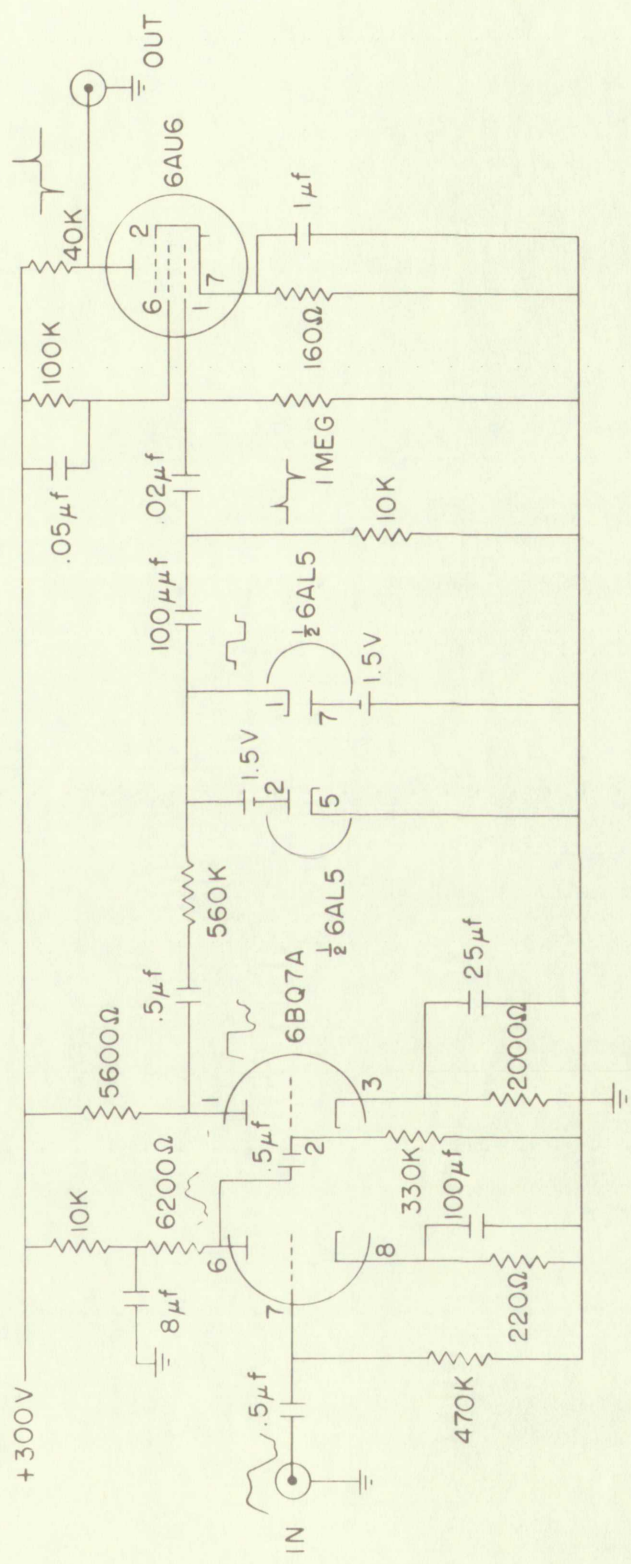


Fig. 2. Circuit diagram of the pulse amplifier and shaper.



Fig. 1. Schematic diagram of the experimental setup.



the shutter. It also permitted an accurate check on the time duration of light passage through the shutter. Figure 3 shows a photograph of the lamp output as monitored by the oscilloscope.

A Leeds & Northrup recording densitometer was used with an 8 micron scanning beam to measure the photographic density of the spectrograms. From each exposure maximum densities for selected lines in the region of the band spectrum used in the shock tube calibration experiment were measured. A plot of density versus log exposure was made for each line. These plots were then superimposed by aligning the log exposure axis and shifting the density axis. This gave a calibration curve which covered the full range of intensities. Relative intensities of all the lines from 3064A to 3120A were determined using this curve. Line shapes were determined for several lines of both high and low intensity, the low intensity lines having about 25% of the intensity of the strongest line.

Corrections for change in absorption of the neutral density filters over the range of wavelengths of interest were made. However, these corrections were small and perhaps superfluous in view of other larger errors and differences.

In addition to a knowledge of the details of the incident radiation spectrum the optical path length of the radiation through the absorbing gas and the transmission function of the monochromator must be known. The optical path length was 10 cm. The transmission function of the monochromator may be computed given the focal length of the monochromator, the dispersion, and the width of the entrance and exit slits.<sup>20</sup> At the settings used for the OH calibration experiments transmission was essentially constant for the 8A interval containing 31 lines from 3089.008A to 3096.830A and zero for lines centered outside this region.



The first part of the paper is devoted to a general discussion of the problem of the stability of the equilibrium of a system of particles. It is shown that the stability of the equilibrium depends on the nature of the forces acting between the particles. In particular, it is shown that the equilibrium is stable if the forces are attractive and the particles are distributed in a regular lattice. The second part of the paper is devoted to a detailed study of the stability of the equilibrium of a system of particles in a regular lattice. It is shown that the equilibrium is stable if the forces are attractive and the particles are distributed in a regular lattice. The third part of the paper is devoted to a study of the stability of the equilibrium of a system of particles in a regular lattice. It is shown that the equilibrium is stable if the forces are attractive and the particles are distributed in a regular lattice. The fourth part of the paper is devoted to a study of the stability of the equilibrium of a system of particles in a regular lattice. It is shown that the equilibrium is stable if the forces are attractive and the particles are distributed in a regular lattice. The fifth part of the paper is devoted to a study of the stability of the equilibrium of a system of particles in a regular lattice. It is shown that the equilibrium is stable if the forces are attractive and the particles are distributed in a regular lattice. The sixth part of the paper is devoted to a study of the stability of the equilibrium of a system of particles in a regular lattice. It is shown that the equilibrium is stable if the forces are attractive and the particles are distributed in a regular lattice. The seventh part of the paper is devoted to a study of the stability of the equilibrium of a system of particles in a regular lattice. It is shown that the equilibrium is stable if the forces are attractive and the particles are distributed in a regular lattice. The eighth part of the paper is devoted to a study of the stability of the equilibrium of a system of particles in a regular lattice. It is shown that the equilibrium is stable if the forces are attractive and the particles are distributed in a regular lattice. The ninth part of the paper is devoted to a study of the stability of the equilibrium of a system of particles in a regular lattice. It is shown that the equilibrium is stable if the forces are attractive and the particles are distributed in a regular lattice. The tenth part of the paper is devoted to a study of the stability of the equilibrium of a system of particles in a regular lattice. It is shown that the equilibrium is stable if the forces are attractive and the particles are distributed in a regular lattice.

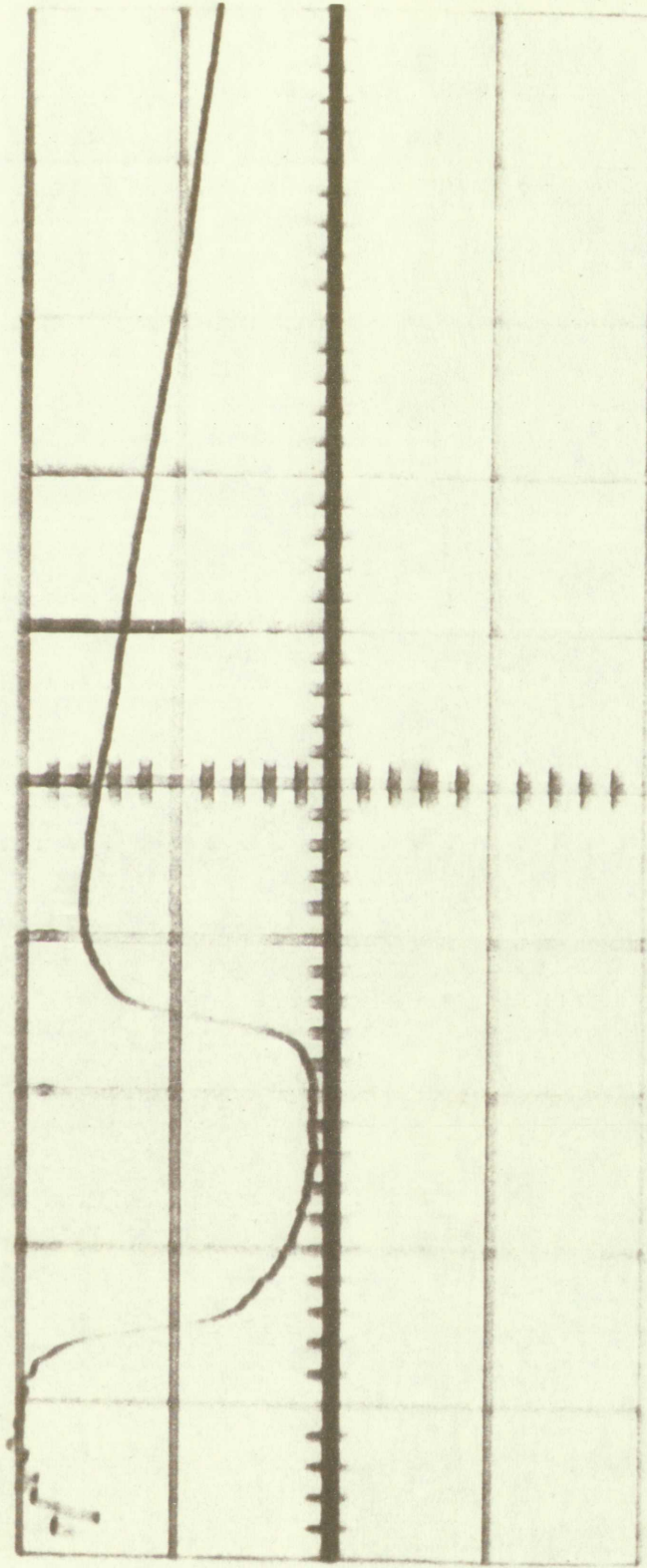


Fig. 3. Oscilloscope trace showing flash duration and synchronization of rotating shutter. Major divisions of graticule are 500  $\mu$ sec. Duration of flash seen by spectrograph is approximately 1 msec.



1947

1. The first part of the report deals with the general situation of the country and the progress of the work done during the year.

2. The second part deals with the results of the various investigations carried out during the year.

3. The third part deals with the conclusions drawn from the results of the investigations.



### Film Calibration Errors

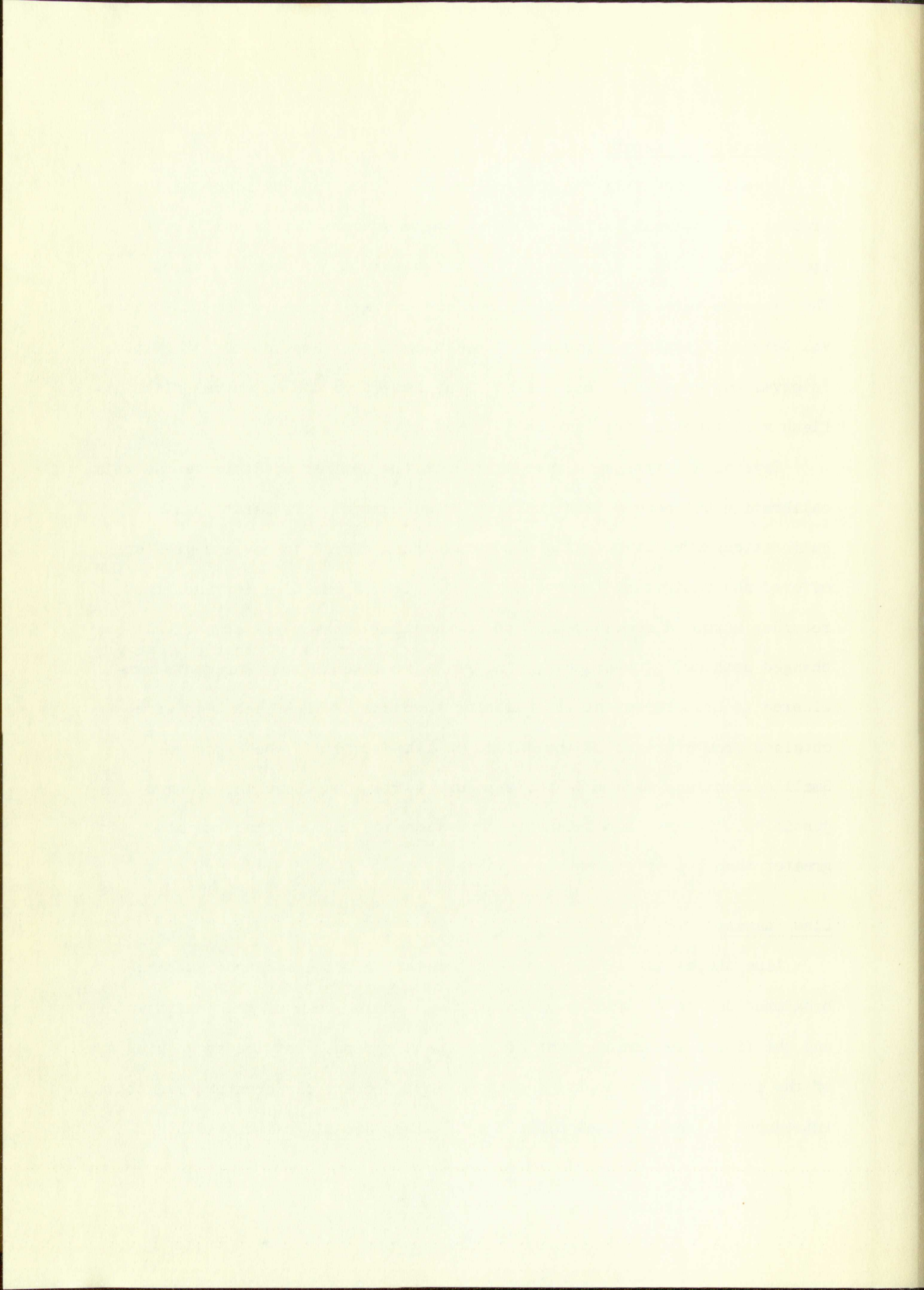
A really good film calibration was difficult to obtain due to the presence of apparent variations in relative intensities for different spectrograms. Small exposure variations seemed to be present, also. The exposure variations may have been due to variations in the time interval between flashes. Exposure was based on the assumption that this time interval was constant. Both effects may have been due to actual flash-to-flash variations in the lamp as is noted in D. C. arcs.<sup>21</sup>

Several attempts were made to reduce the scatter and improve the film calibration but none were significantly successful. Preparation of a calibration curve by omitting exposures which seemed to deviate greatest offered no significant improvement. Nor did compensation for incorrect recorder zero. A remeasurement of the neutral density filter calibration changed nothing. Consequently, the relative intensity measurements considered to best represent the emission spectrum of the flash lamp were obtained from averages of the values obtained from all the exposures. Small corrections were made for exposure variations where they seemed justified. The maximum intensity deviation for any one line was not greater than 10% of its measured value.

### Line Shapes

Line shapes as read by the densitometer from the spectrograms are broadened due to the finite width of the scanning beam of the densitometer and the finite resolving power of the spectrograph. But the broadening of the iron lines due to the densitometer is relatively greater than that introduced to the OH lines since the OH lines are of greater width. Hence





the measured width of the iron lines represents the maximum possible broadening function of the system.

The measured shape of the iron lines is nearly Gaussian of half-width  $0.017 \pm 0.001A$ , but is slightly asymmetrical. The actual width of the iron lines is approximately  $0.005A$  as computed for the estimated temperature and measured using a Fabry-Perot interferometer. The width of the scanning beam of the densitometer corresponds to approximately  $0.005A$ . It can be shown that the width of the scanning beam of the densitometer does not alter the width of the lines on the spectrograms by more than  $0.001A$ . Assuming the shape of the measured spectrograph function to be Gaussian, the correction for the narrow iron lines leaves a spectrograph function of half-width  $0.0162A$ . It is apparent then that the measured shape is essentially the spectrograph broadening function. The width of the spectrograph function indicates a resolution of about 180,000.

Line shape measurement of both low (25% of maximum) and high intensity OH lines shows that in addition to the slight asymmetry noted in the iron lines, the high intensity lines are broadened somewhat due to self-absorption. The major portion of the low intensity lines is essentially Doppler in shape, but the wings are not so small as for a pure Doppler line, indicating the presence of some small extra broadening effect. The measured half-width of a high intensity line is  $0.045 \pm 0.001A$ ; a low intensity line  $0.040 \pm 0.001A$ . Taking a Doppler line at  $4200^{\circ}K$  ( $0.0348A$ ) and putting in the spectrograph shape as measured gives a width of  $0.040A$ , the same as measured directly for the low intensity line. It can be concluded that the basic line shape is essentially Doppler corresponding to  $4200^{\circ}K$ . The more intense lines are broadened by self-absorption. All lines are affected by a small amount by collision or other broadening.



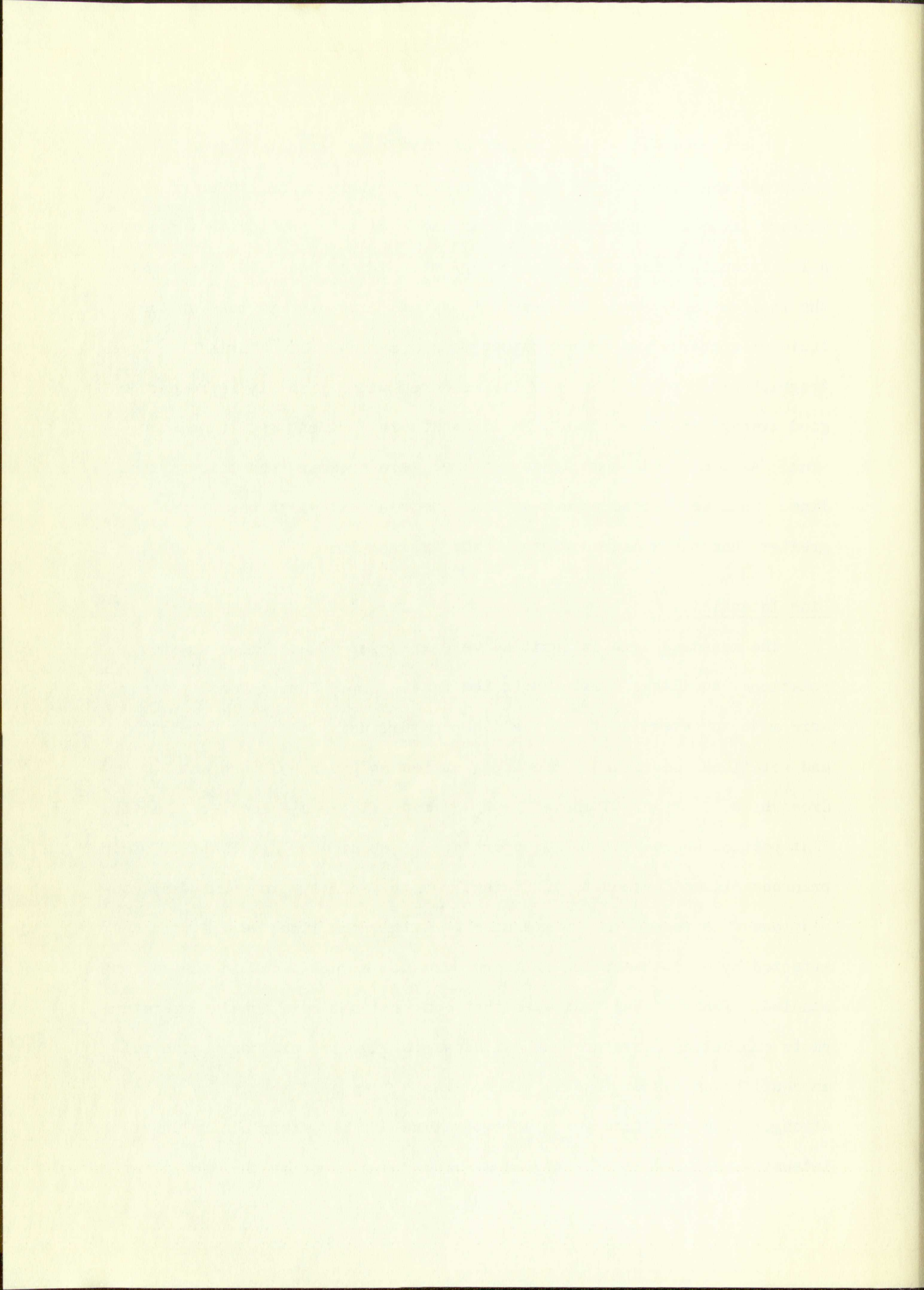
Faint, illegible text covering the page, possibly bleed-through from the reverse side.

Since the measured line shapes of the lower intensity lines were broadened significantly by the spectrograph, there seemed to be no advantage in measuring the intensity of each point in the incident spectrum. A low intensity line was taken as typical (Fig. 4) and used to generate the incident spectrum. The measured typical line used to make up the incident spectrum was chosen rather than a narrower line having the spectrograph width removed because its measured width probably represents a good average of the width of the lines of the incident radiation spectrum. As mentioned, some lines measured were broader than this typical line. Some were broad enough so that their actual width was probably greater than the measured width of the typical line.

#### Line Intensities

The measured line intensities were analyzed to determine whether rotational equilibrium existed in the flash lamp. Conventional plots were made to determine rotational temperature using the line strengths and rotational energies of the upper states as given by Dieke and Crosswhite.<sup>22</sup> Figure 5 shows the  $R_2$  branch which has a long, relatively flat portion equivalent to a temperature of about  $4200^\circ\text{K}$ . Plots of other branches did not extend to sufficiently high J-numbers to permit any conclusions with regard to a temperature. Either the lines were strong and affected by self-absorption or there were not enough lines in the region studied. Penner<sup>23</sup> has indicated that conventional rotational temperature plots exhibiting curvature such as shown in Fig. 5 could correspond to an equilibrium system in which there exists some self-absorption of the stronger lines but from which a temperature may be determined by using the intensity measurements for higher J-numbers. A check by the iso-intensity





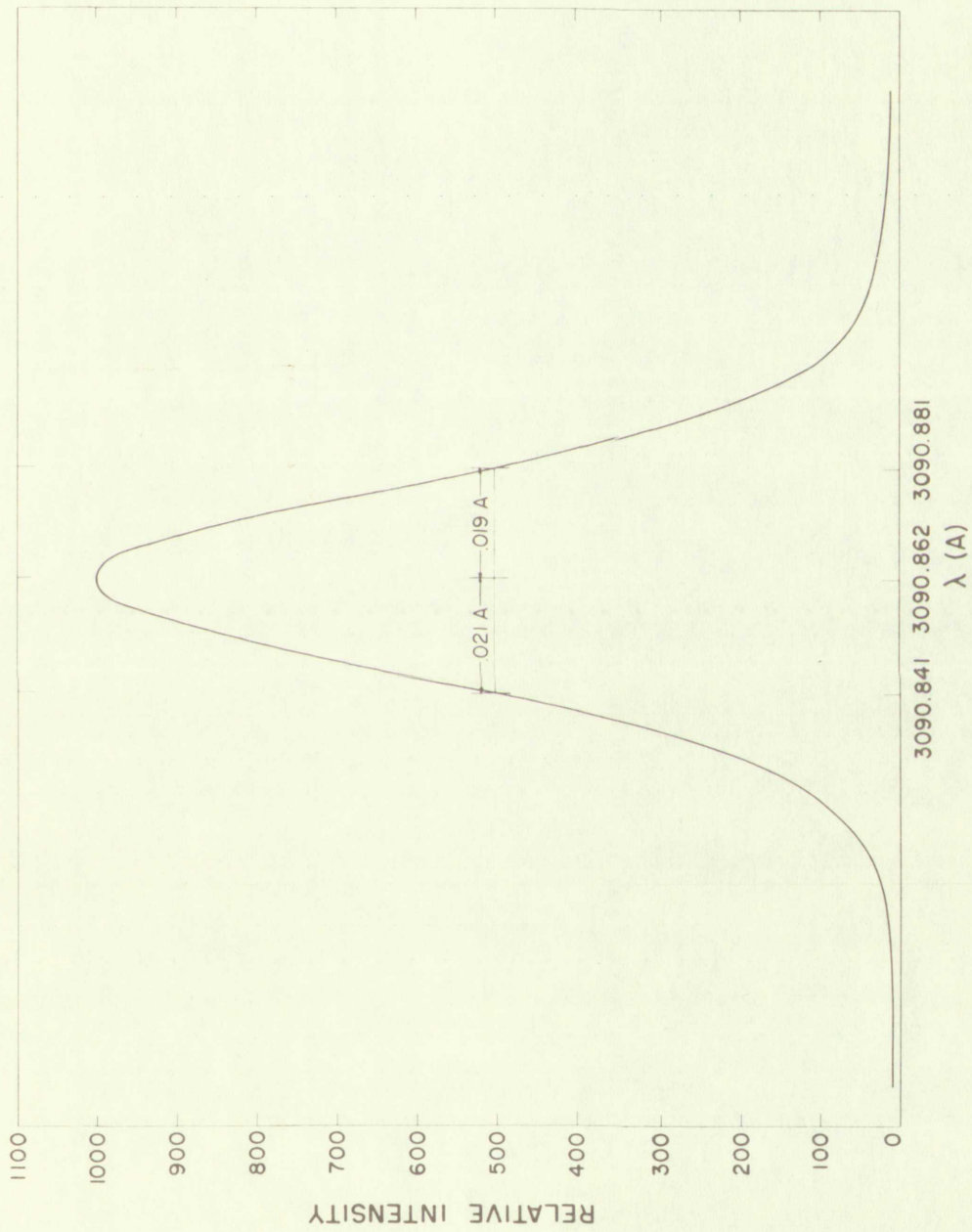
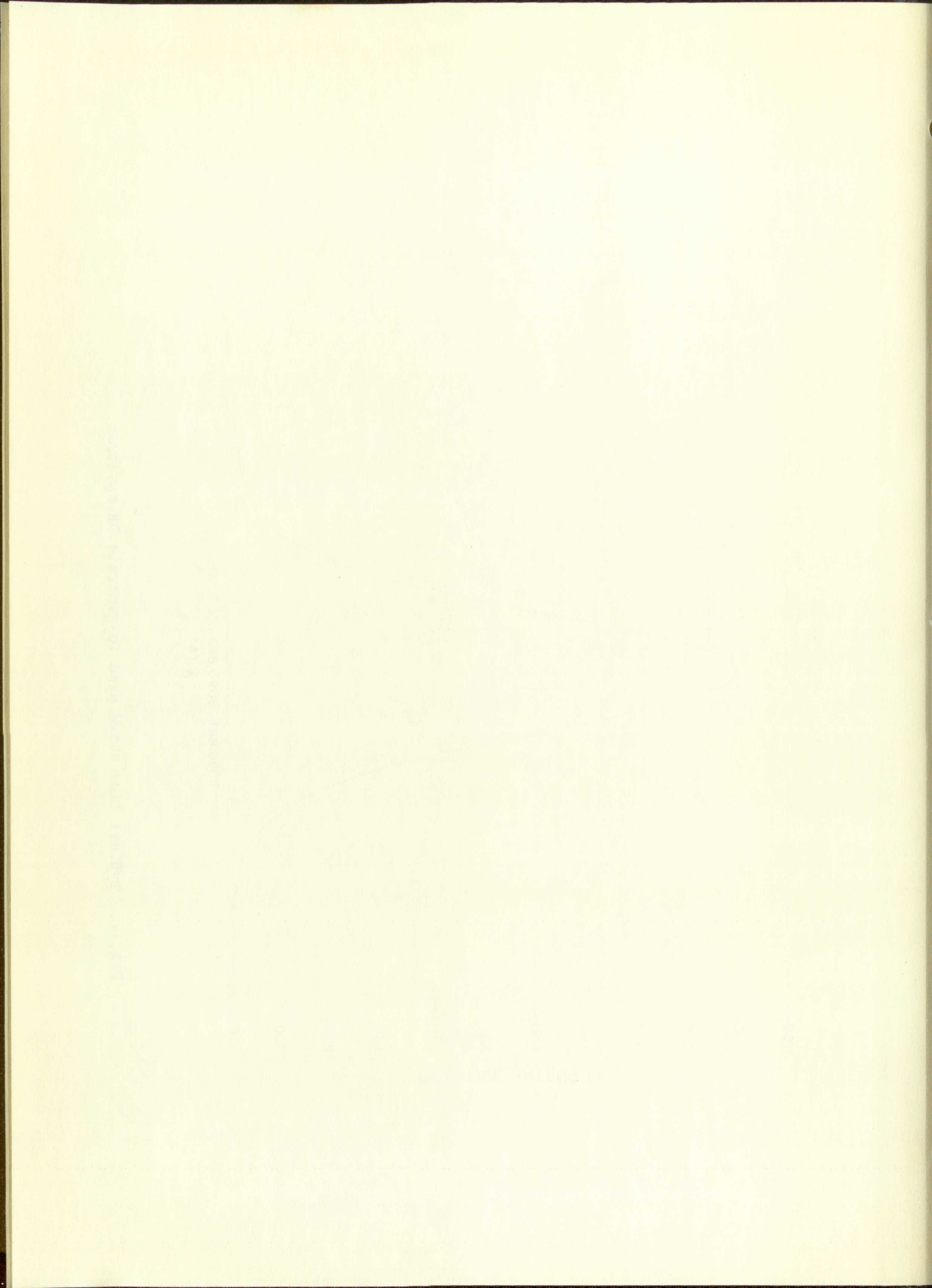


Fig. 4. Typical line shape used to generate OH spectrum.





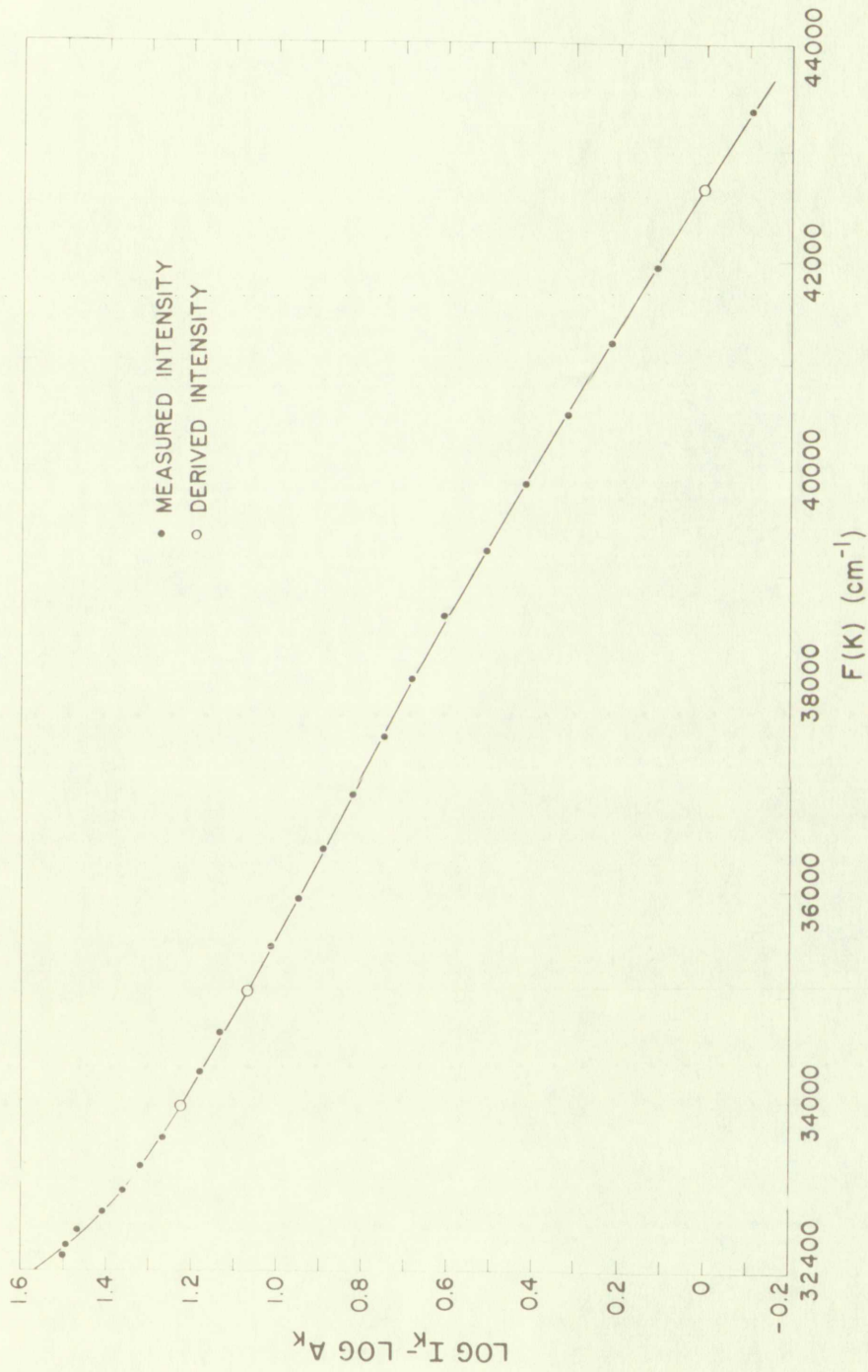


Fig. 5. Graph using the measured relative intensities ( $R_2$  branch) along with the line strengths and energy levels from ref. 22 to determine the rotational temperature of the emitter, approx. 4200°K, and obtain relative intensities of lines in blends.



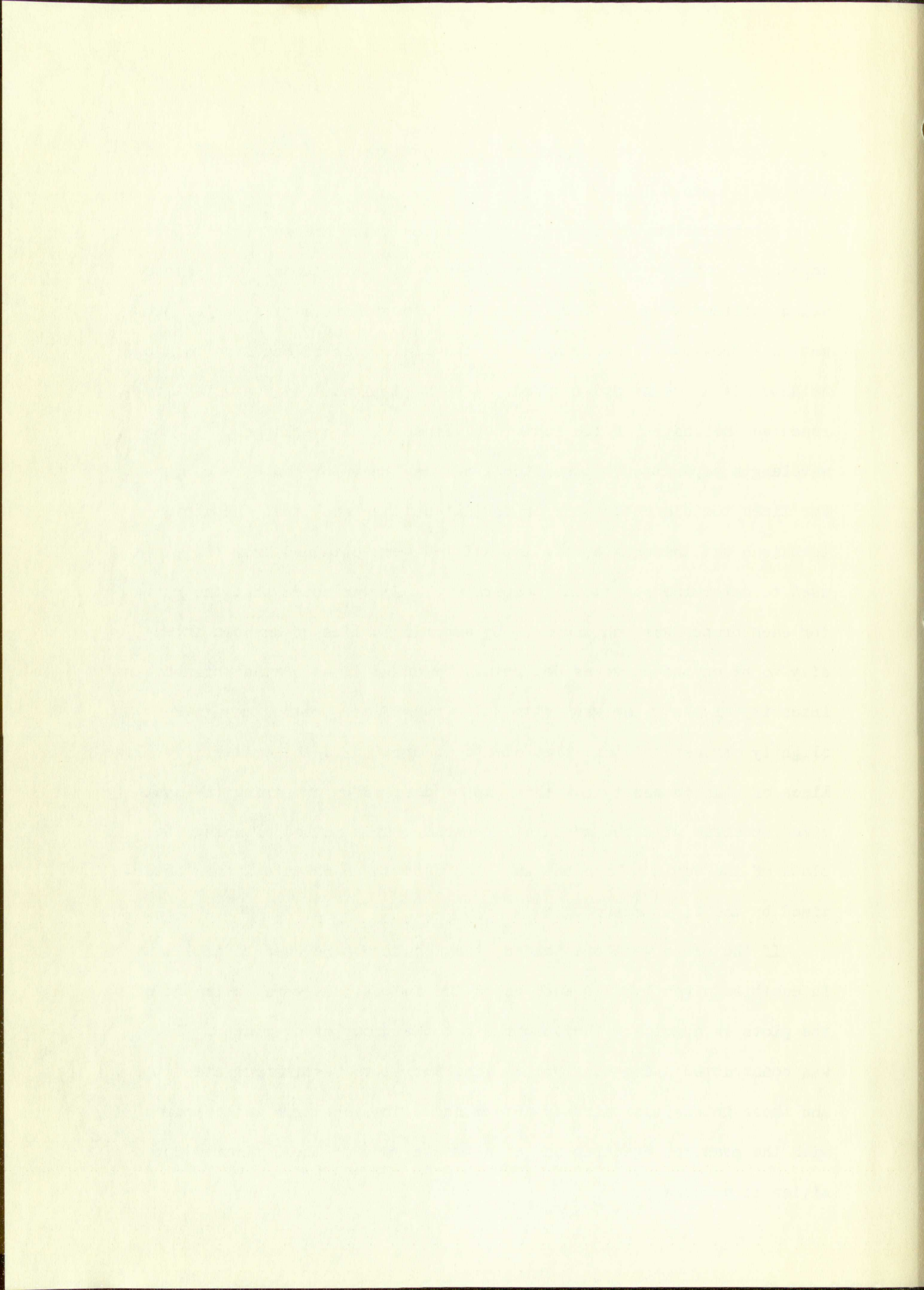


method gives a similar temperature. The existence of rotational equilibrium is open to question.

Determinations of intensities of lines which are sufficiently close together not to be resolved were obtained by two methods. One method which sufficed when distinct peaks were present was a first order summation approximation assuming: (1) the distortion of one line by its neighbor is a second order effect, (2) the typical line shape best represented the shapes of the individual lines which overlapped, (3) the wavelength separation between the lines was known or could be computed. For lines too close together or for intensities such that the above technique was inadequate, the intensities were obtained from the plots used to determine rotational temperature. It was noted that the curve for each branch was continuous. By assuming a line of unknown intensity to be on the curve as determined by other lines of that branch, the intensity of that line was estimated. Use of this method may give slightly erroneous intensities due to absorption in the emitter for close lines of high intensity but this can be checked by comparing the synthesized spectrum with the measured spectrum. This method of using the plots of the various branches was also used to check intensities determined by the first method.

If the plots were open-ended, they could not be used to determine intensities directly. In such cases the intensities were estimated using the plots as a guide. The spectrum for the group of overlapping lines was constructed using the typical line shape, the estimated intensities, and those intensities already determined. This spectrum was compared with the measured spectrum and adjustments made to the estimated intensities if necessary.



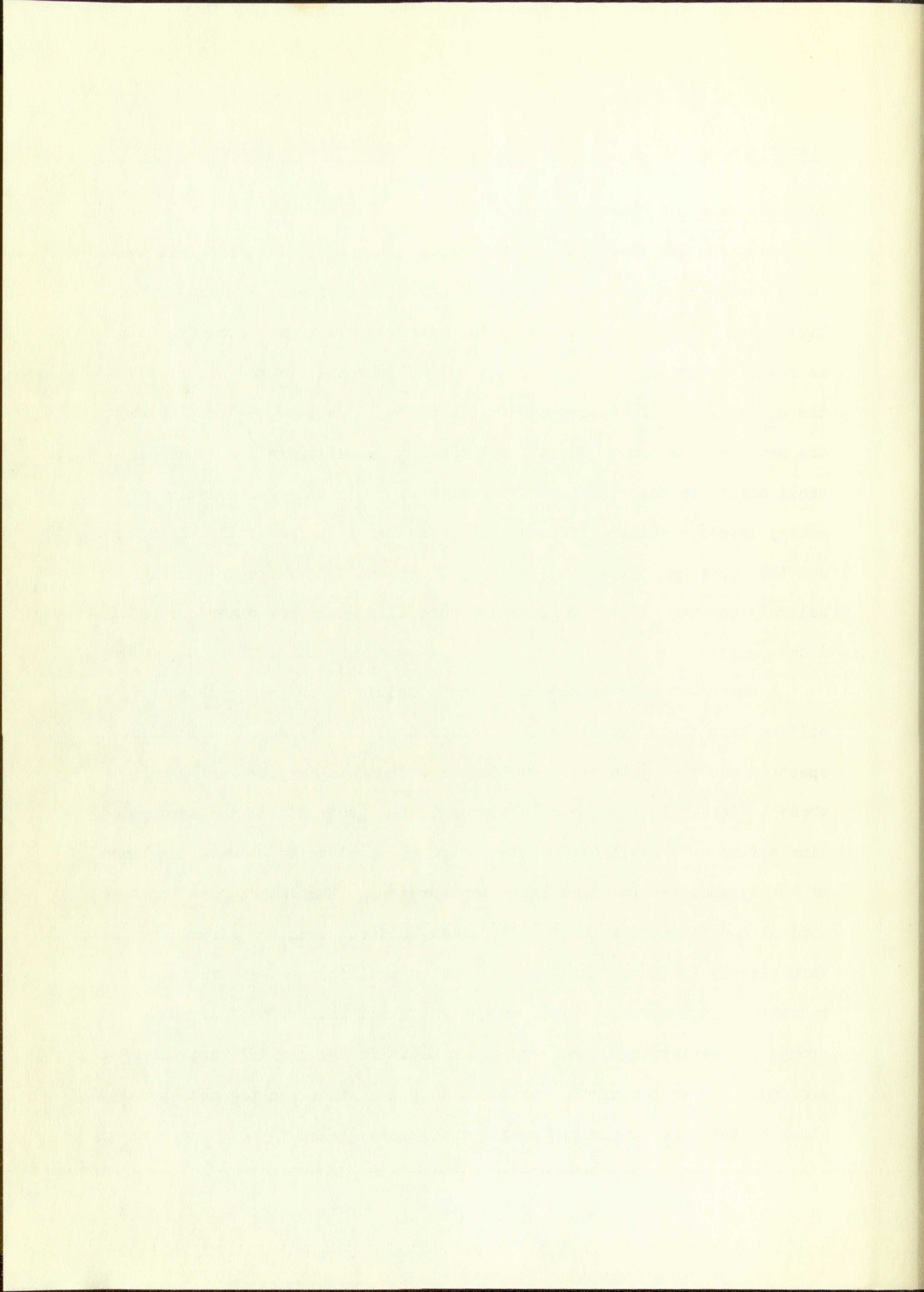


Comparison of the Measured Spectrum with that Synthesized from a TypicalLine and Measured Intensities

Plotting the incident spectrum as synthesized by the code from computed vacuum wavelengths, measured relative intensities, and the typical line shape allows comparison with the measured spectrum. From Fig. 6 it is readily seen that the  $Q_{12}(4)$  and  $Q_2(4)$  lines superimpose nicely but the  $Q_{12}(1)$  and  $Q_2(1)$  lines are displaced toward shorter wavelengths from the measured spectrum. These displacements probably are the result of small errors in the Dieke and Crosswhite study in the determination of energy levels. Actual differences between the spectrum of the flash lamp and the spectrum of the flame used by Dieke and Crosswhite are considered unlikely but may exist. Differences were also noted for other groups of lines.

A check was made to determine the possible error in absorbance resulting from these displacements. Absorbance for the measured incident spectrum and the synthesized incident spectrum was computed using only these 4 lines. In this computation as in the general code the absorption line maxima were positioned at the computed wavelengths as were the lines of the synthesized incident radiation spectrum. The absorbances for some typical conditions for the two different incident spectra differed by 22%. This clearly indicated that differences in positions between incident radiation and absorption lines were significant insofar as individual groups of overlapping lines were concerned. It was decided that the best procedure was to center the incident radiation lines and the absorption lines at the same wavelength positions. There seemed to be no good reason





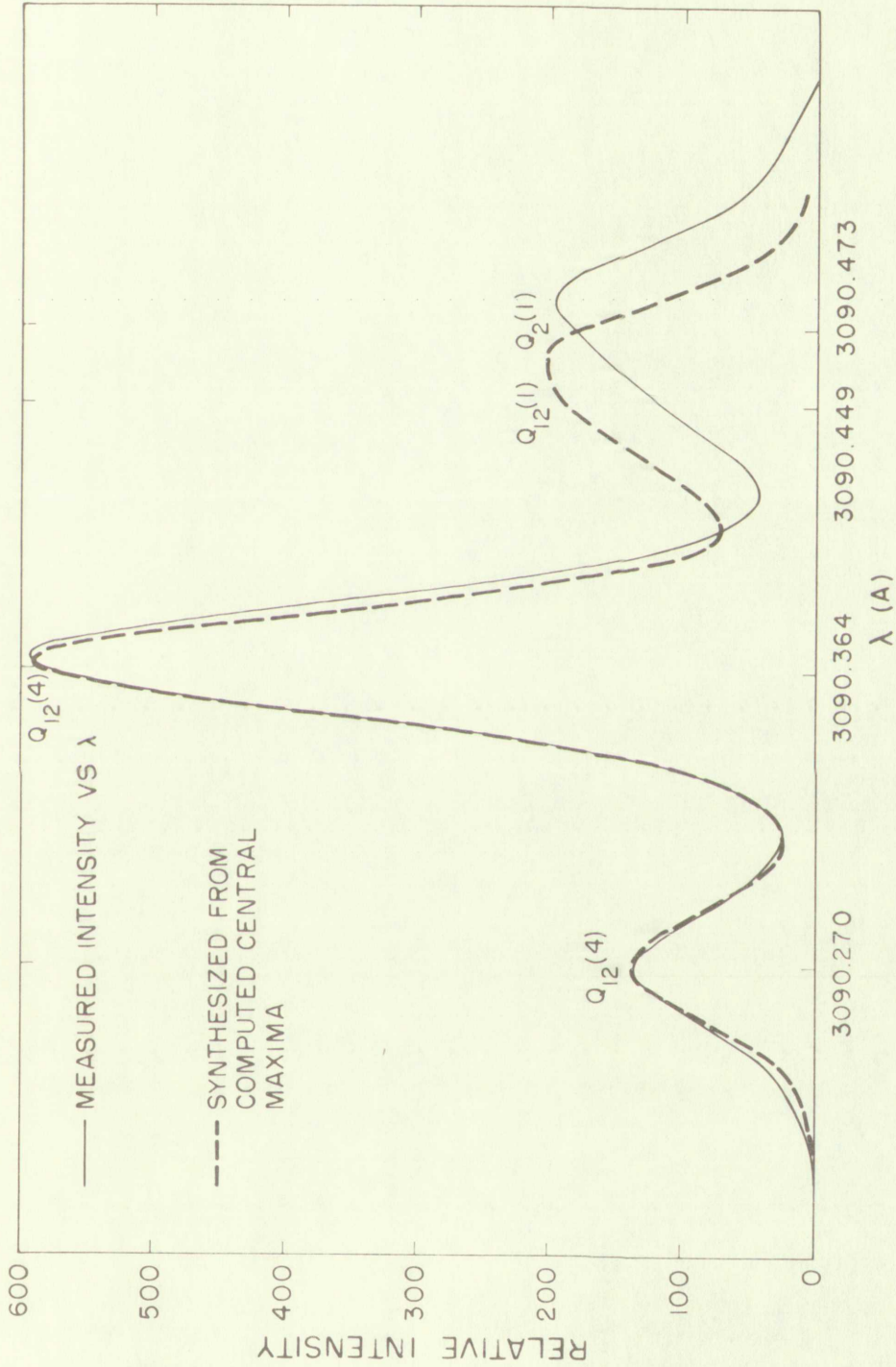
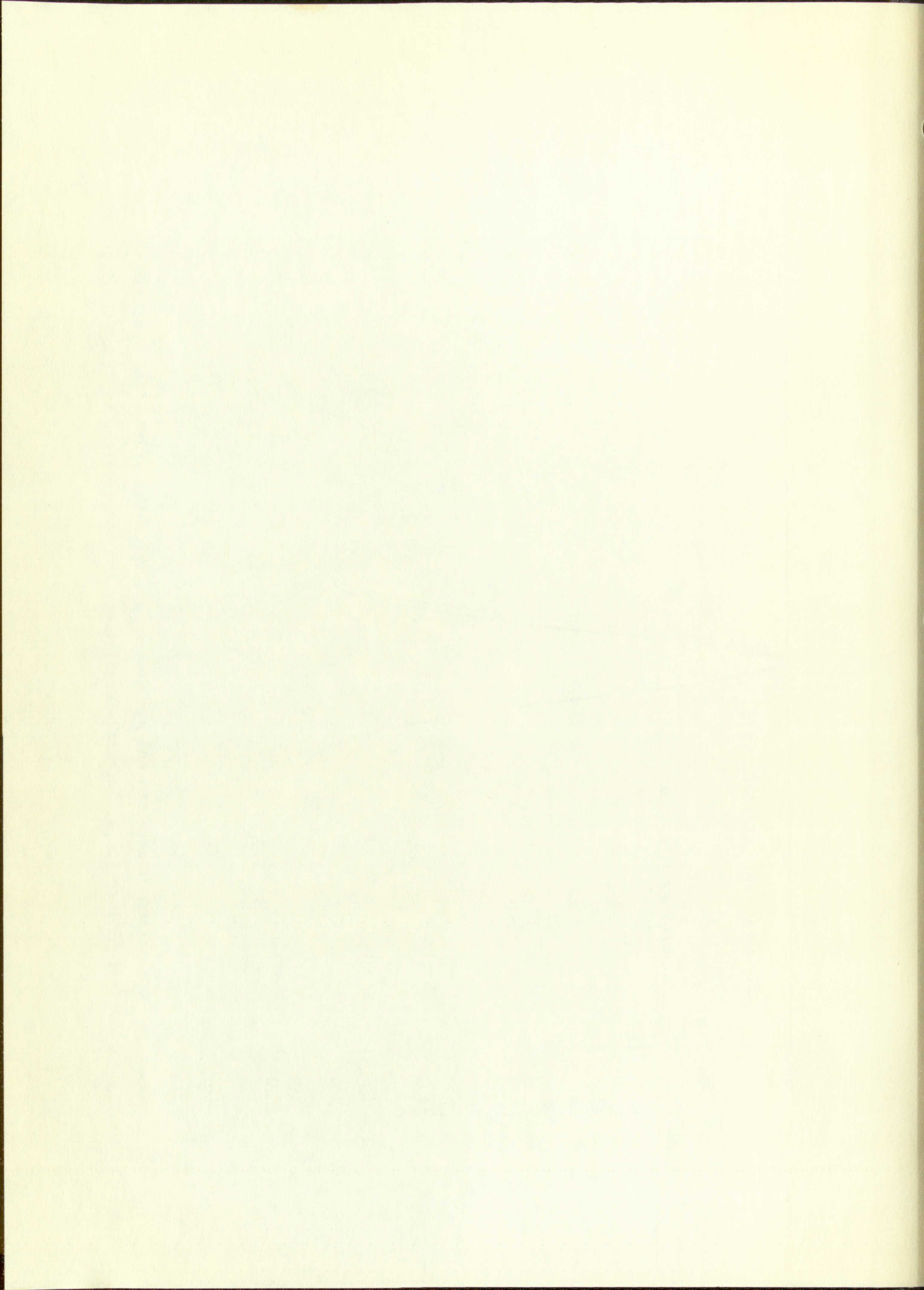


Fig. 6. Comparison of measured and synthesized spectra. The synthesized spectrum used the typical line shape, measured intensities, and the wavelengths from ref. 22.





why the wavelengths of the lines from the flash lamp should differ substantially and inconsistently from those of the absorbing gas.

Errors arising from locating central maxima at discrete mesh points instead of at measured wavelengths are small in comparison to the possible error due to the uncertainty in position of the central maxima. It is difficult to estimate the error introduced by assuming the computed vacuum wavelengths as correct and that maxima of the absorption and incident radiation lines fall at the same place, but it is probably safe to say it is only a few percent. The presence of a number of well-isolated and intense lines reduces the significance of these possible errors.

A rather elementary check of possible shift between the incident radiation spectrum produced by the lamp and the absorption spectrum indicated that shift was not a cause of any significant error. At low pressures, shift of the absorption spectrum would be small. At high pressures the absorption lines are broad and the shift due to pressure would have to be unreasonably large to make any significant error in absorbance.



The first part of the report deals with the general situation of the country and the progress of the work. It is followed by a detailed account of the various projects and the results achieved. The report concludes with a summary of the work done and the prospects for the future.

The work has been carried out in accordance with the programme of work approved by the Council of the League of Nations. It has been a most successful one and has resulted in the completion of a number of important projects. The results of this work are set out in the following pages.

The first project was the study of the economic situation of the country. This was done by a number of experts who have prepared a report on the subject. The results of this study are set out in the following pages.

The second project was the study of the social situation of the country. This was done by a number of experts who have prepared a report on the subject. The results of this study are set out in the following pages.

The third project was the study of the political situation of the country. This was done by a number of experts who have prepared a report on the subject. The results of this study are set out in the following pages.

The fourth project was the study of the legal situation of the country. This was done by a number of experts who have prepared a report on the subject. The results of this study are set out in the following pages.

The fifth project was the study of the educational situation of the country. This was done by a number of experts who have prepared a report on the subject. The results of this study are set out in the following pages.

The sixth project was the study of the health situation of the country. This was done by a number of experts who have prepared a report on the subject. The results of this study are set out in the following pages.

The seventh project was the study of the cultural situation of the country. This was done by a number of experts who have prepared a report on the subject. The results of this study are set out in the following pages.

The eighth project was the study of the international situation of the country. This was done by a number of experts who have prepared a report on the subject. The results of this study are set out in the following pages.

The ninth project was the study of the military situation of the country. This was done by a number of experts who have prepared a report on the subject. The results of this study are set out in the following pages.

The tenth project was the study of the financial situation of the country. This was done by a number of experts who have prepared a report on the subject. The results of this study are set out in the following pages.

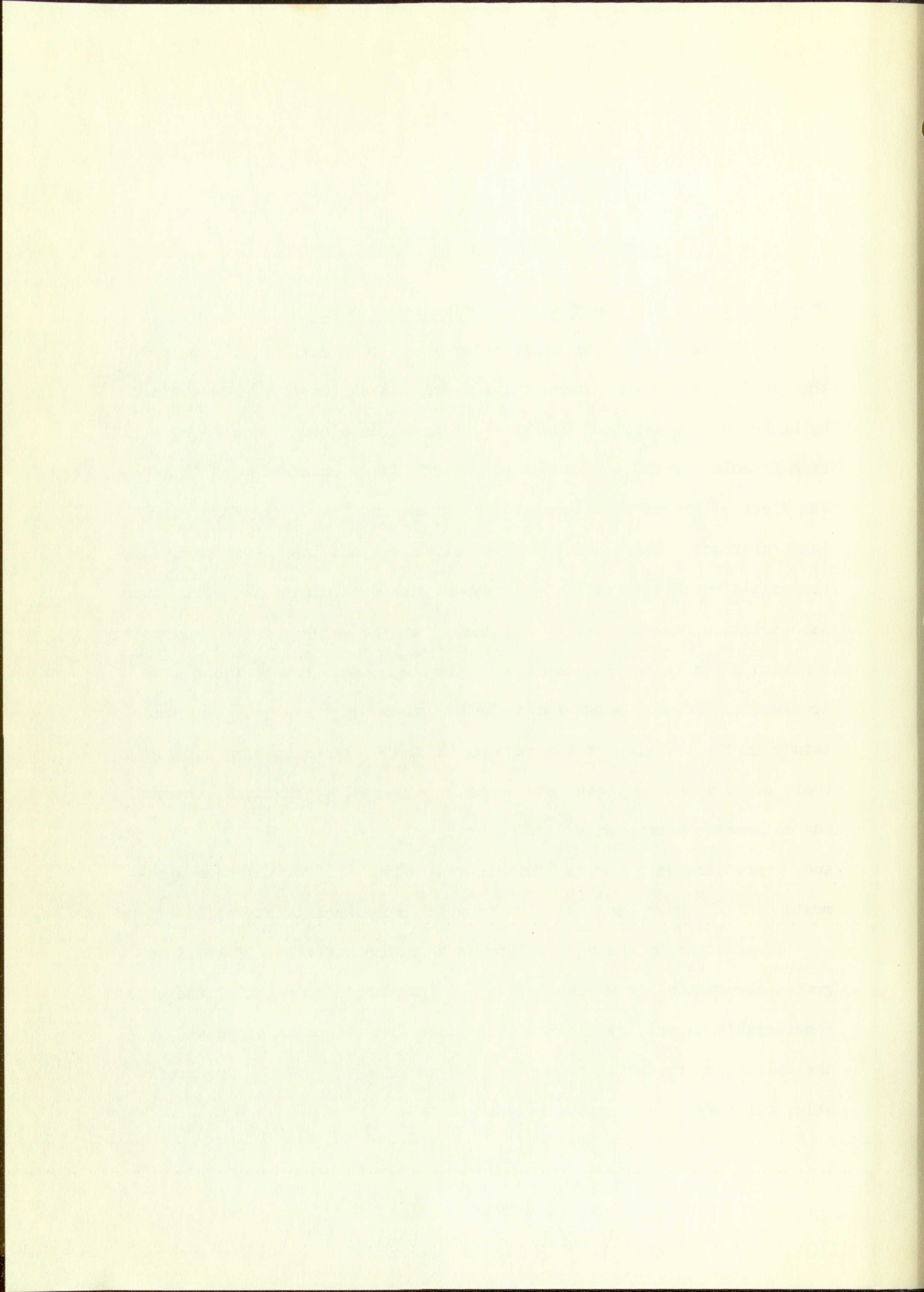
## COMPUTATIONAL STUDY OF ABSORBANCE

### Uncertainties in the Spectral Absorption Coefficient

In the expression for the Doppler absorption maximum,  $P'$ , most of the quantities are well known. The energy levels have been determined by Dieke and Crosswhite. The line strengths have been computed by Earls<sup>24</sup> from formulas, based on quantum mechanics, first obtained by Hill and Van Vleck.<sup>25</sup> These were tabulated by Dieke and Crosswhite for convenient reference. These are probably reliable since they seem to give reasonable results in rotational temperature determinations. The internal partition function can be computed from the values of the free energy function given in the NBS tables.<sup>15</sup> The  $\lambda_0$ , measured by Dieke and Crosswhite, are well known for isolated lines but there is some uncertainty in the position of the central maxima of lines in blends. However, effects due to these uncertainties are small. Physical, chemical, and mathematical constants such as  $e$ ,  $c$ ,  $m$ ,  $M$ ,  $R$ ,  $h$ ,  $k$ ,  $\pi$ , and  $\epsilon$  are also well known. This leaves only  $F$ , for which measurements<sup>4-7,26-28</sup> have been made but in which some uncertainty still exists.

In addition to the uncertainty in the absolute value of the integrated absorption, of which  $F$  may be considered the measure, there is considerable uncertainty in the absorption line shape as expressed by the collision broadening factor  $\underline{a}$ . Values of  $\underline{a}$ <sup>4-7,26,27,29</sup> are available, but they cover quite a range.





Thus the spectral absorption coefficient is uncertain to the extent of the uncertainties in  $F$  and  $\underline{a}$ . The computed absorbance is also uncertain to the extent of the possible error in the measurement of the relative intensities and line shapes of the incident radiation spectrum. Errors in the relative intensities are at least as small as errors in the other uncertain quantities. However, errors in line shapes of the incident spectrum due to lack of sufficient resolution could be significant. Since the absorbance is uncertain to the extent of the uncertainties in the quantities noted above, the absorbance was studied by varying one of these quantities while holding the other two constant for the temperatures of interest and a range of optical densities. In each case absorbance was computed for a sufficient number of optical densities, usually six, in the range of interest to definitely establish the position of the absorbance curve.

#### Absorbance as a Function of Absorber Characteristics

Analysis of the behavior of absorbance as a function of optical density for various assumed characterizations of the absorption coefficient is simplified by the definition of a typical absorption line. Most of the lines in this particular wavelength region have low rotational quantum numbers and are strong absorbers. Thus they dominate the behavior of the absorbance, and the effects due to the whole absorption spectrum are conveniently described in terms of them as typical lines or typical absorption maxima.

Values of absorbance as a function of optical density were computed and plotted for 1500°K, 2000°K, and 2500°K (Fig. 7) using the  $F$  of Carrington,<sup>6</sup>  $3.24 \cdot 10^{-4}$ , assuming a pure Doppler absorption line ( $\underline{a} = 0$ ),



The present paper is devoted to the study of the  
... and the ...  
... of the ...  
... as well as ...  
... in the ...  
... of the ...  
... in the ...  
... of the ...  
... of the ...  
... of the ...  
... of the ...

References

1. ...  
2. ...  
3. ...  
4. ...  
5. ...  
6. ...  
7. ...  
8. ...  
9. ...  
10. ...

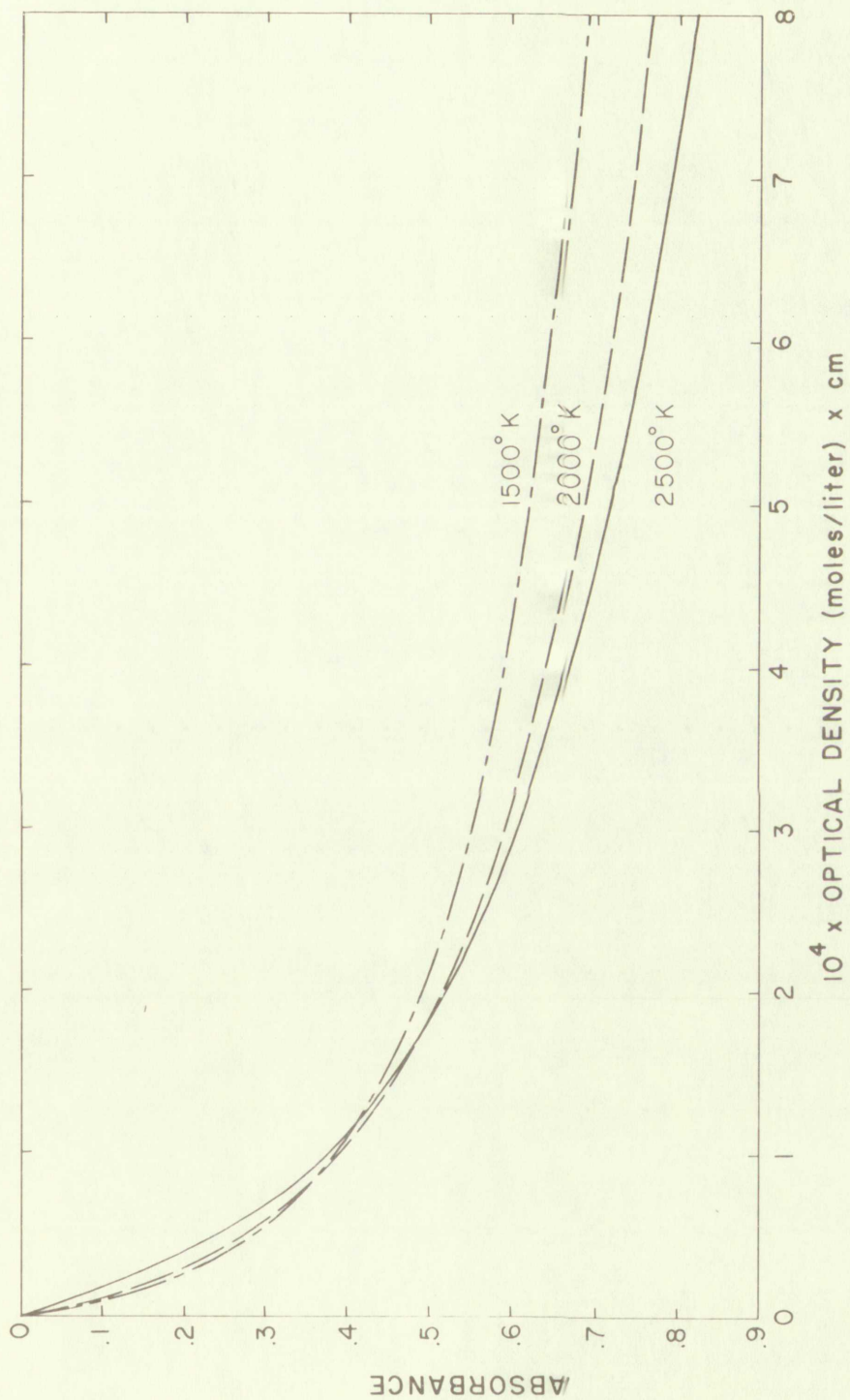
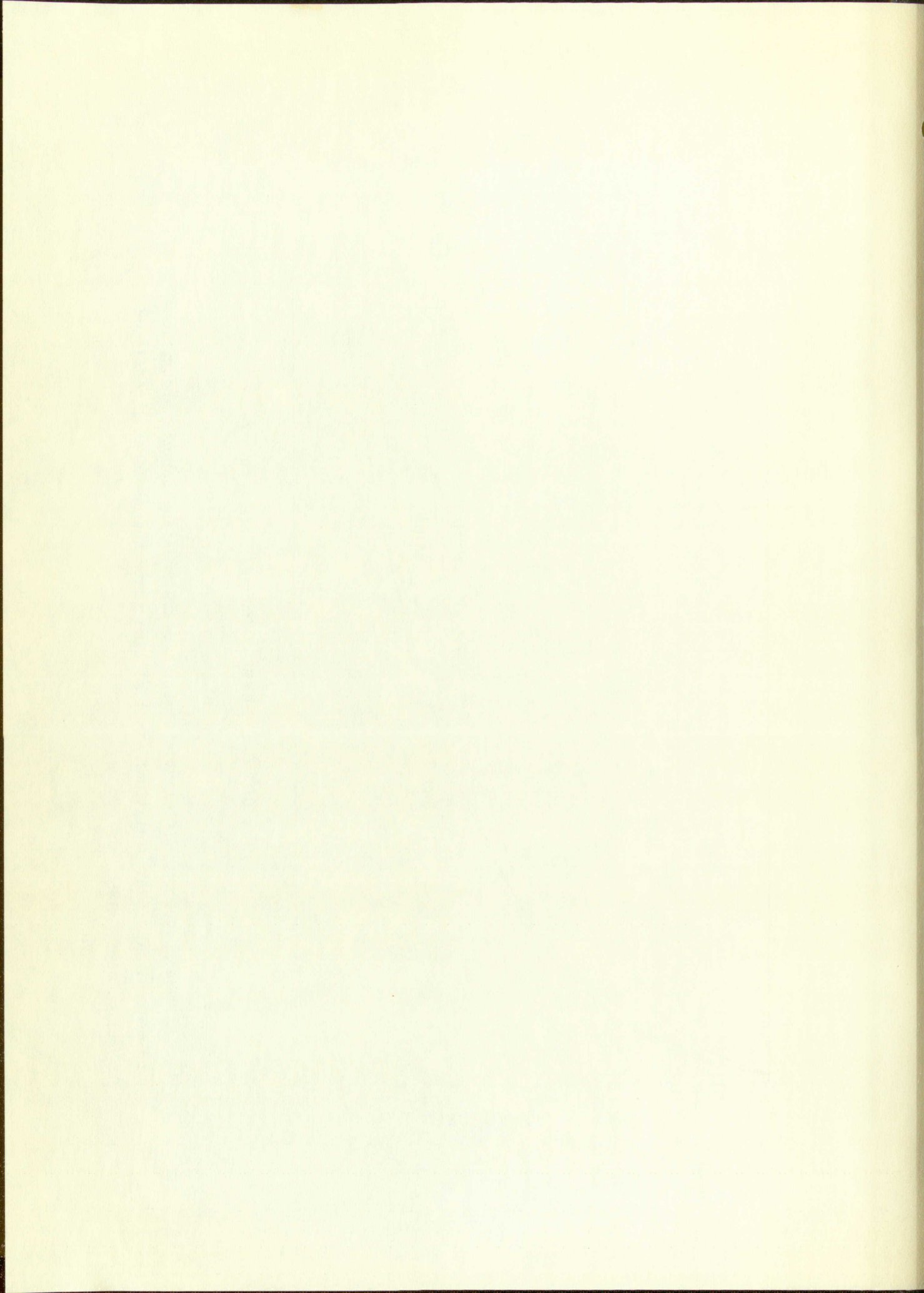


Fig. 7. Absorbance for different absorber temperatures and Doppler absorption line shapes. Incident radiation: typical line shape and measured intensities. Absorption coefficient:  $F = 3.24 \cdot 10^{-4}$ .





and using an incident spectrum synthesized from the typical line shape and measured intensities. A look at these results shows a decrease in absorbance with increase in temperature at low optical densities but an increase in absorbance with temperature at high optical densities. The reason for this behavior is that the typical absorption maximum decreases as temperature increases due to a decrease in population of the predominating absorbing states with increase in temperature and to an increase in the Doppler width of the absorber to which the absorption maximum is inversely proportional. The behavior of the typical absorption maximum is the significant factor at low optical densities and the absorbance is less at high temperatures for these optical densities. At higher optical densities the width of the absorbing line becomes the significant factor, and the absorbance at higher temperatures is greater than at lower temperatures.

Using a pure Doppler absorption line shape and the typical line input spectrum, values of absorbance as a function of optical density were computed and plotted for a temperature of  $2500^{\circ}\text{K}$  and 3 different values of  $F$ , each within the overall range of previous measurements (Fig. 8). Clearly the absorbance increases as  $F$  increases. It should be noted that a change in  $F$  is equivalent to changes in concentration of absorber as far as computed absorbance is concerned, and at different temperatures for sufficiently large changes in  $F$  one might expect behavior as noted in the previous paragraph.

In order to study the absorbance at different temperatures for the same value of the collision broadening parameter  $a$ , the absorbance was computed for  $a = 0.4$  at  $1500^{\circ}\text{K}$ ,  $2000^{\circ}\text{K}$ , and  $2500^{\circ}\text{K}$  using the typical line incident spectrum and the  $F$  of Carrington (Fig. 9). The differences



The following table shows the results of the experiments conducted in the laboratory of the University of California, Berkeley, during the summer of 1925. The experiments were conducted by the author and his assistants, and the results are given in the following table. The table is divided into two parts, the first part giving the results of the experiments conducted at a constant temperature of 25°C, and the second part giving the results of the experiments conducted at a constant temperature of 30°C. The results are given in terms of the rate of reaction, expressed as a percentage of the initial concentration of the reactants, per unit time. The rate of reaction is given in the first column of the table, and the initial concentration of the reactants is given in the second column. The results are given for three different concentrations of the reactants, and for two different temperatures. The results show that the rate of reaction increases with increasing concentration of the reactants, and with increasing temperature. The results also show that the rate of reaction is independent of the initial concentration of the products.

Initial Concentration of Reactants	Rate of Reaction at 25°C	Rate of Reaction at 30°C
0.1 M	1.0	1.5
0.2 M	2.0	3.0
0.3 M	3.0	4.5

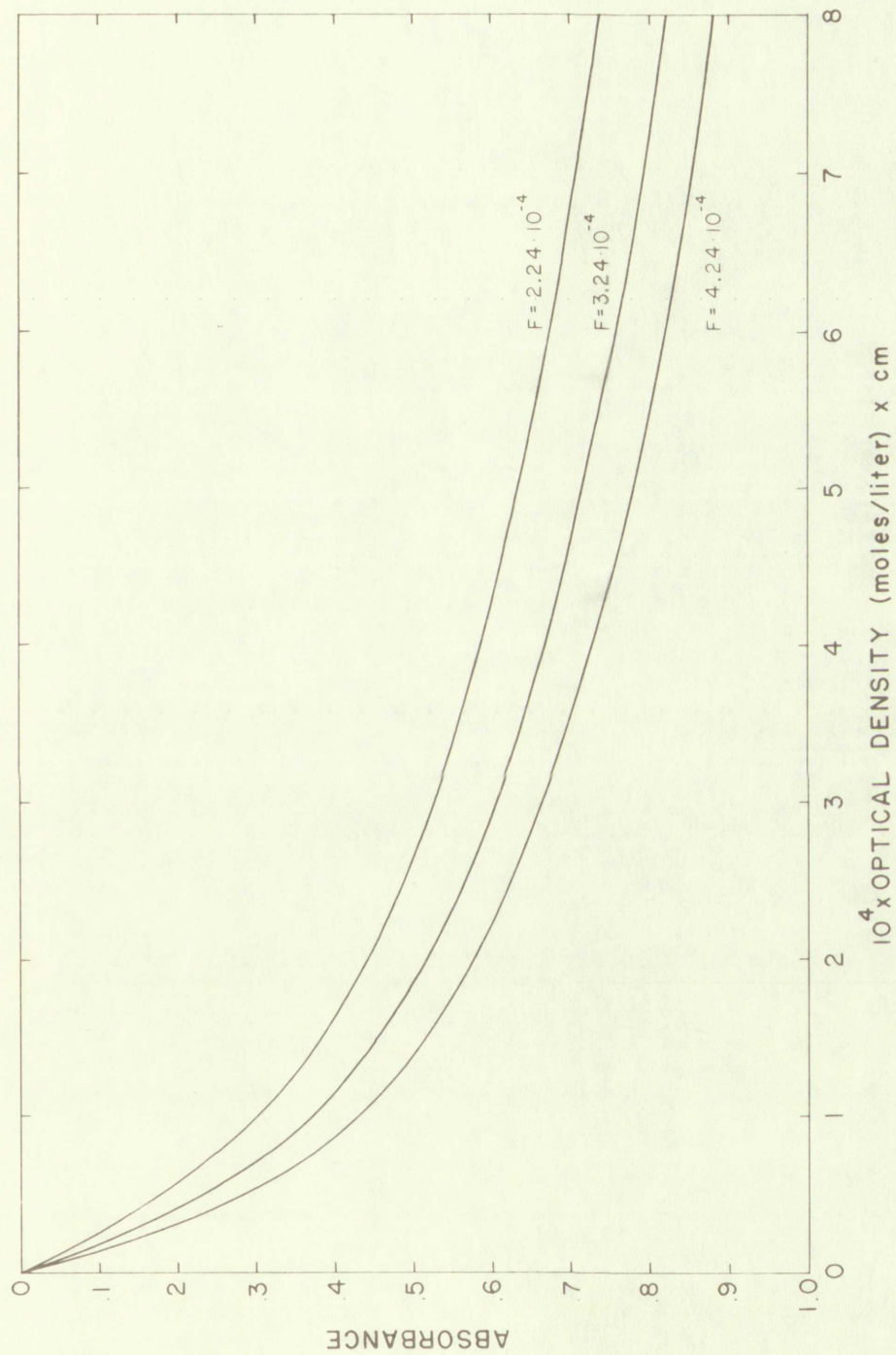
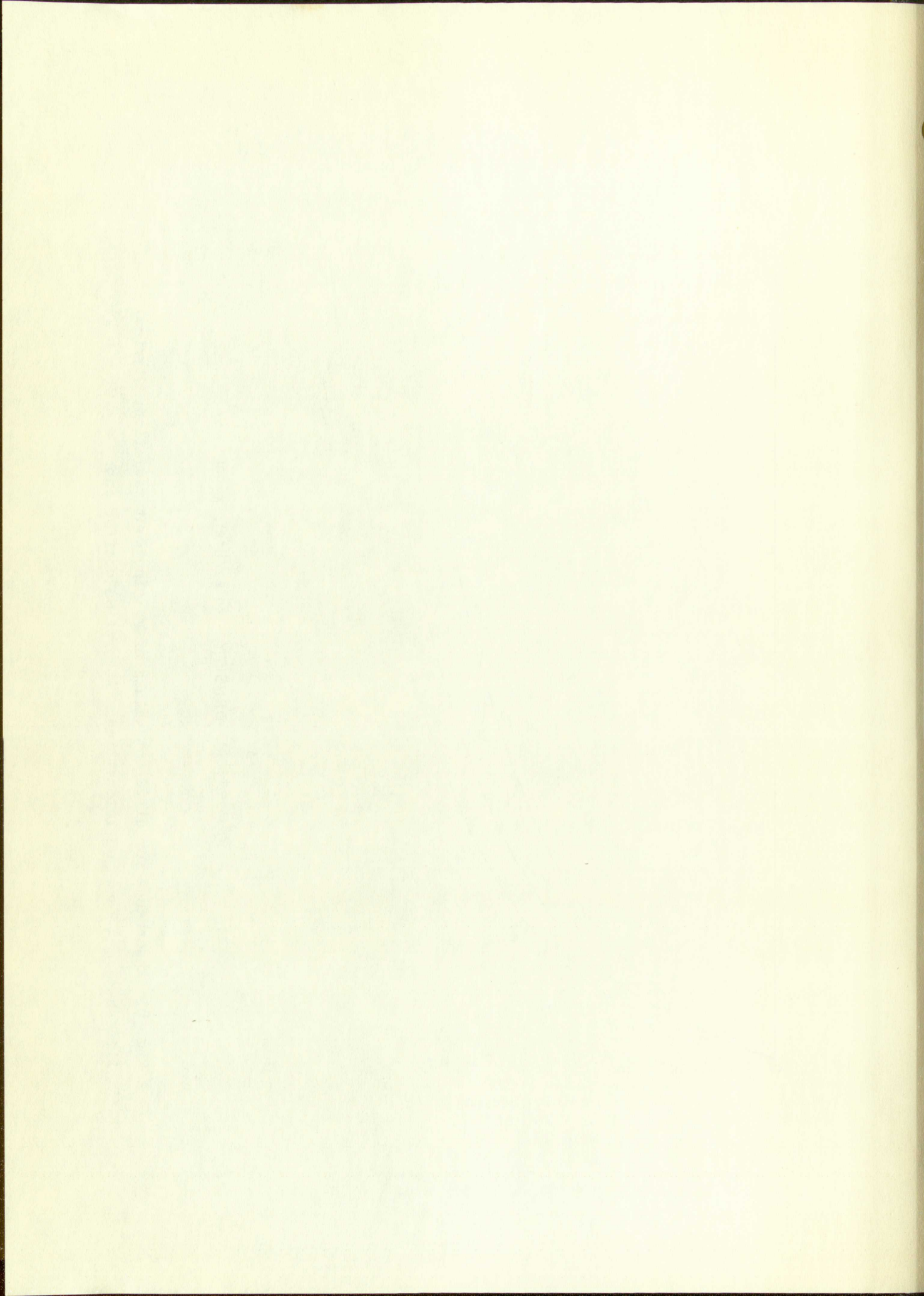


Fig. 8. Absorbance for different values of  $F$ . Incident radiation: typical line shape and measured intensities. Absorption coefficient:  $a = 0$ ;  $T = 2500^\circ\text{K}$ .





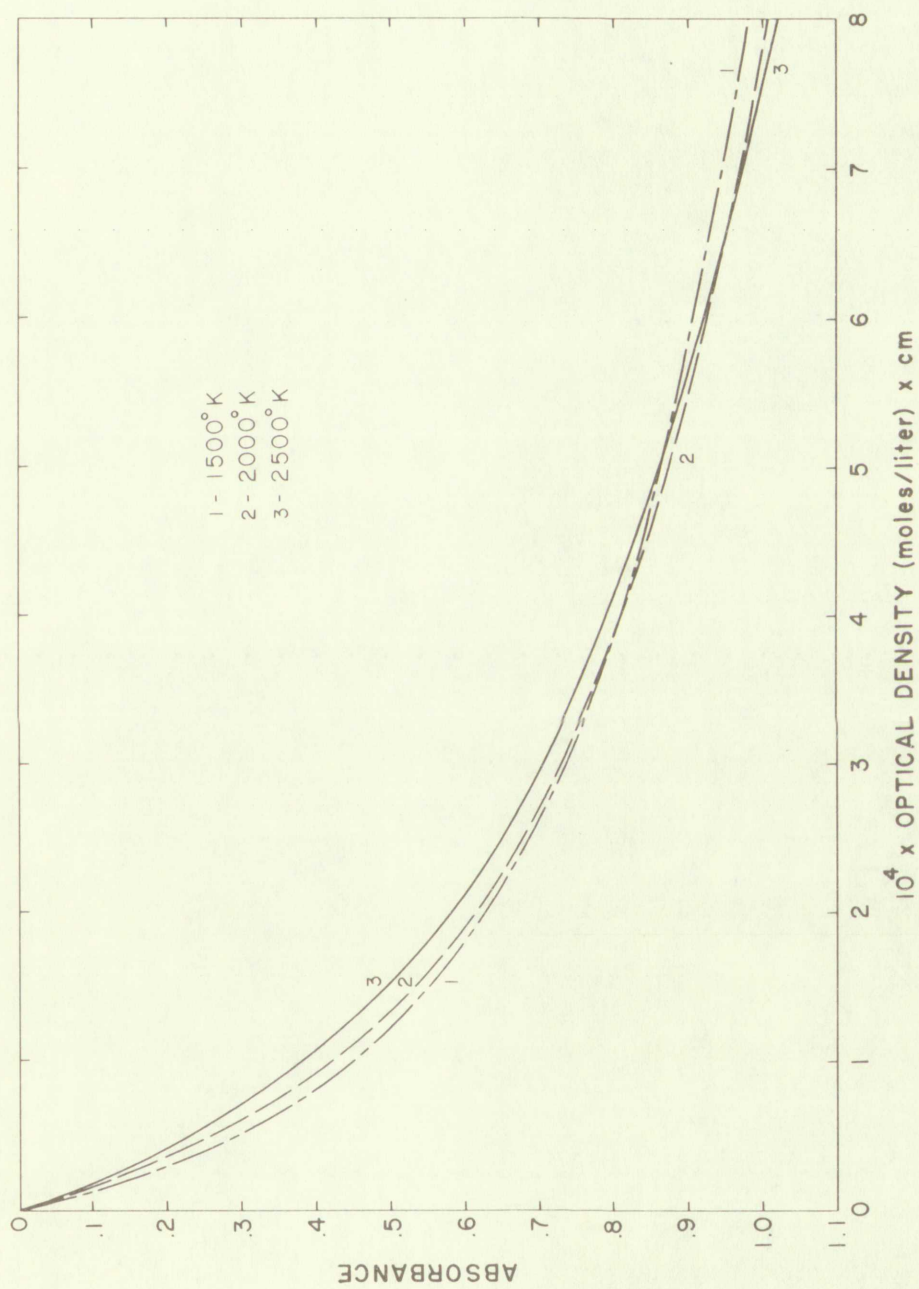
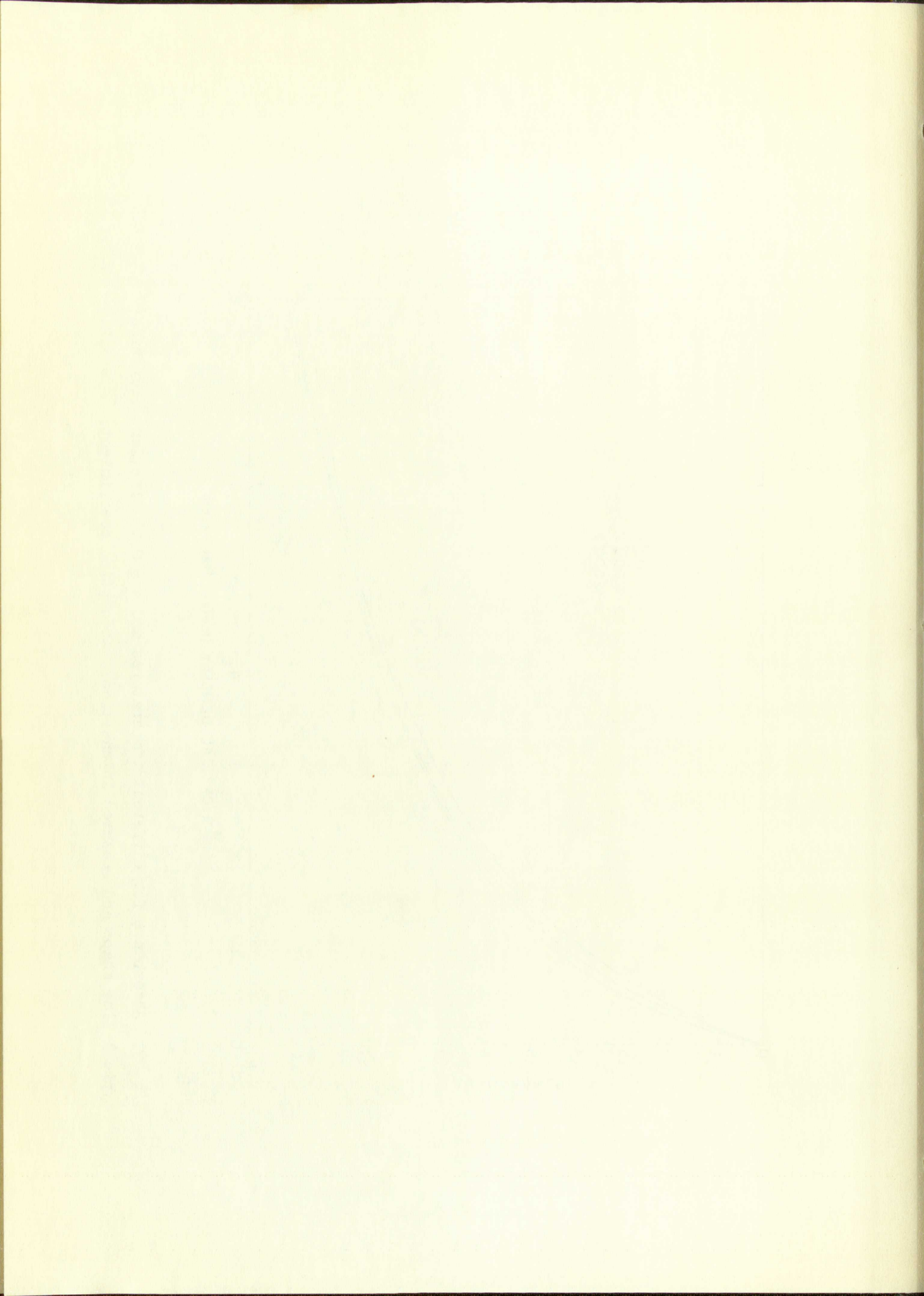


Fig. 9. Absorbance for different temperatures and  $\underline{a} = 0.4$ . Incident radiation: typical line shape and measured intensities. Absorption coefficient:  $F = 3.24 \cdot 10^{-4}$ .





in absorbance at the 3 temperatures and low optical densities are similar but of greater magnitude than those for the pure Doppler lines at the same temperatures. The greater absorbance at lower temperatures is due to the greater line width being more significant than the decrease in the central maximum.

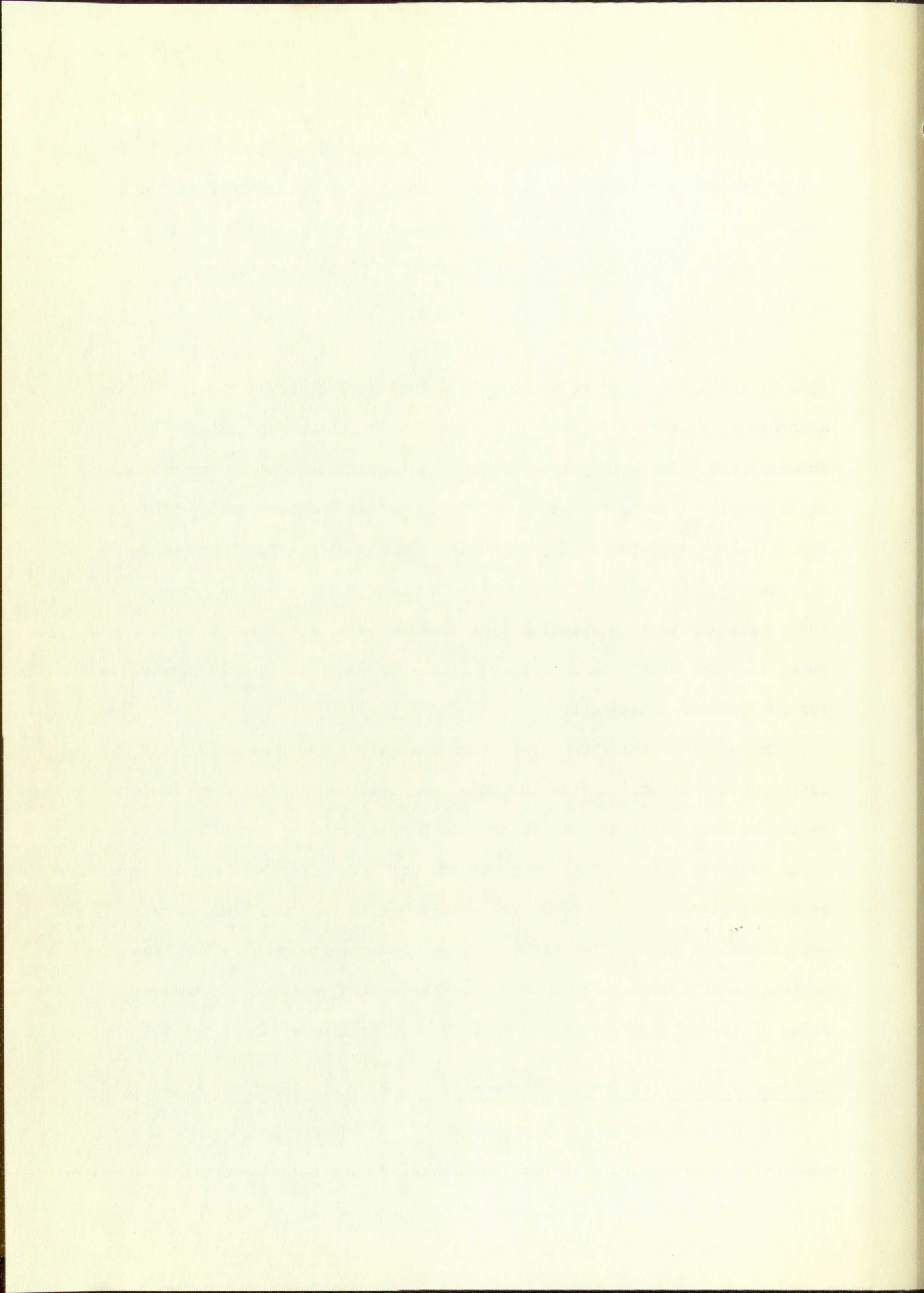
The curves of Fig. 10 were each computed at the same temperature,  $2562^{\circ}\text{K}$ , and a series of values of  $\underline{a}$ . A look at the curves shows that the absorbance is decreasing as  $\underline{a}$  increases for low optical densities. At intermediate values of optical density whether absorbance is increasing or decreasing depends on the value of  $\underline{a}$ . This is better shown by noting Fig. 11 where absorbance is plotted as a function of  $\underline{a}$  for constant optical density. It is readily seen that for intermediate optical densities there exists a maximum absorbance at some value of  $\underline{a}$ . This plot also shows that the change in absorbance with  $\underline{a}$  is small and nearly linear for low optical densities.

The computed absorbance for other conditions provides some interesting observations. If the absorbance is computed for narrower incident radiation lines, the maximum absorbance for all optical densities will occur at lower values of  $\underline{a}$ . The maximum for lower absorber temperatures occurs at higher values of  $\underline{a}$ . The conclusion to be drawn from these observations and those noted previously is that absorbance as a function of optical density depends upon the competition of effects due to the peak value of the central absorption maximum and the line width of the absorber.

#### Absorbance as a Function of Different Incident Radiation Line Shapes

The above paragraphs explain in brief the effects produced in the absorbance by assuming different characteristics for the absorption





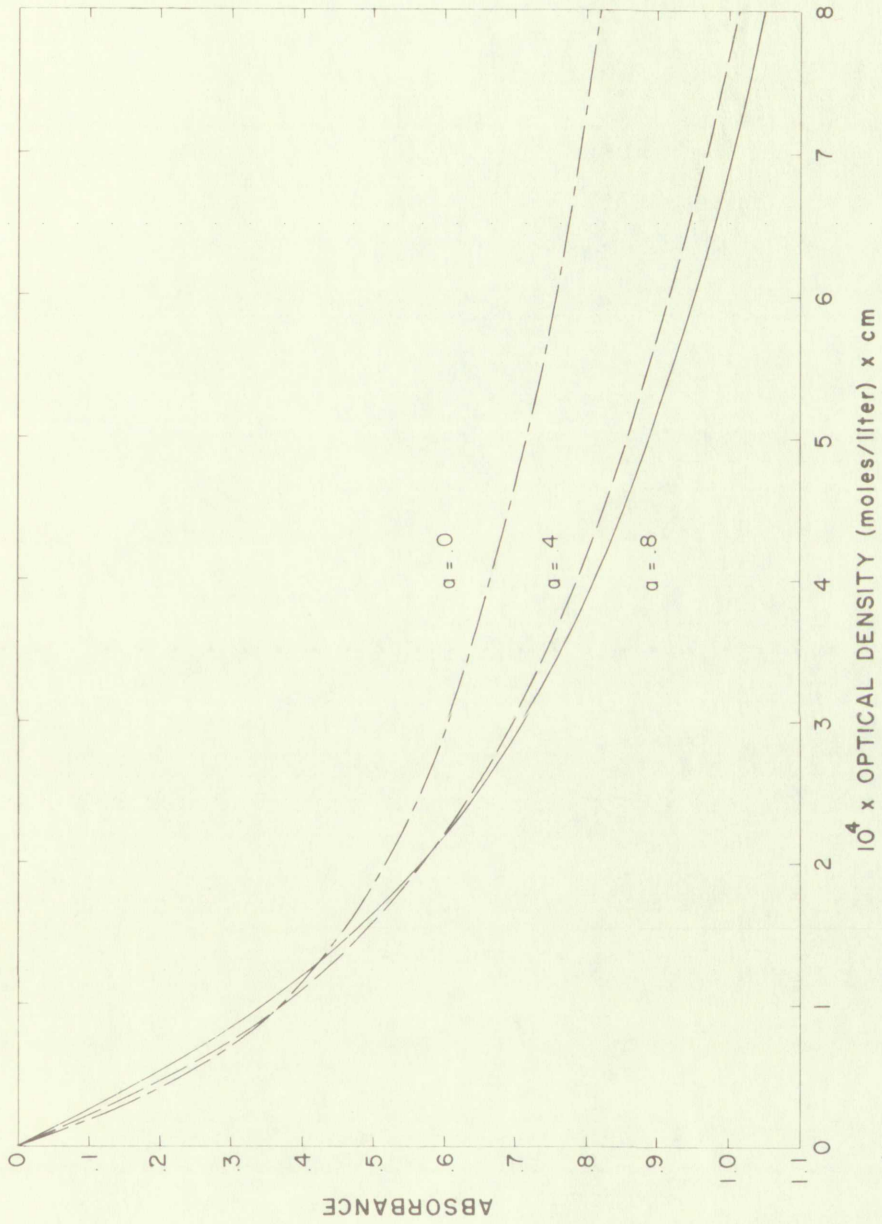


Fig. 10. Absorbance for different values of  $a$ . Incident radiation: typical line shape and measured intensities. Absorption coefficient:  $T = 2562^\circ \text{K}$ ;  $F = 3.24 \cdot 10^{-4}$ .



1. The first part of the paper discusses the general theory of the subject and the various methods of investigation.

### 2. The second part of the paper discusses the experimental results.



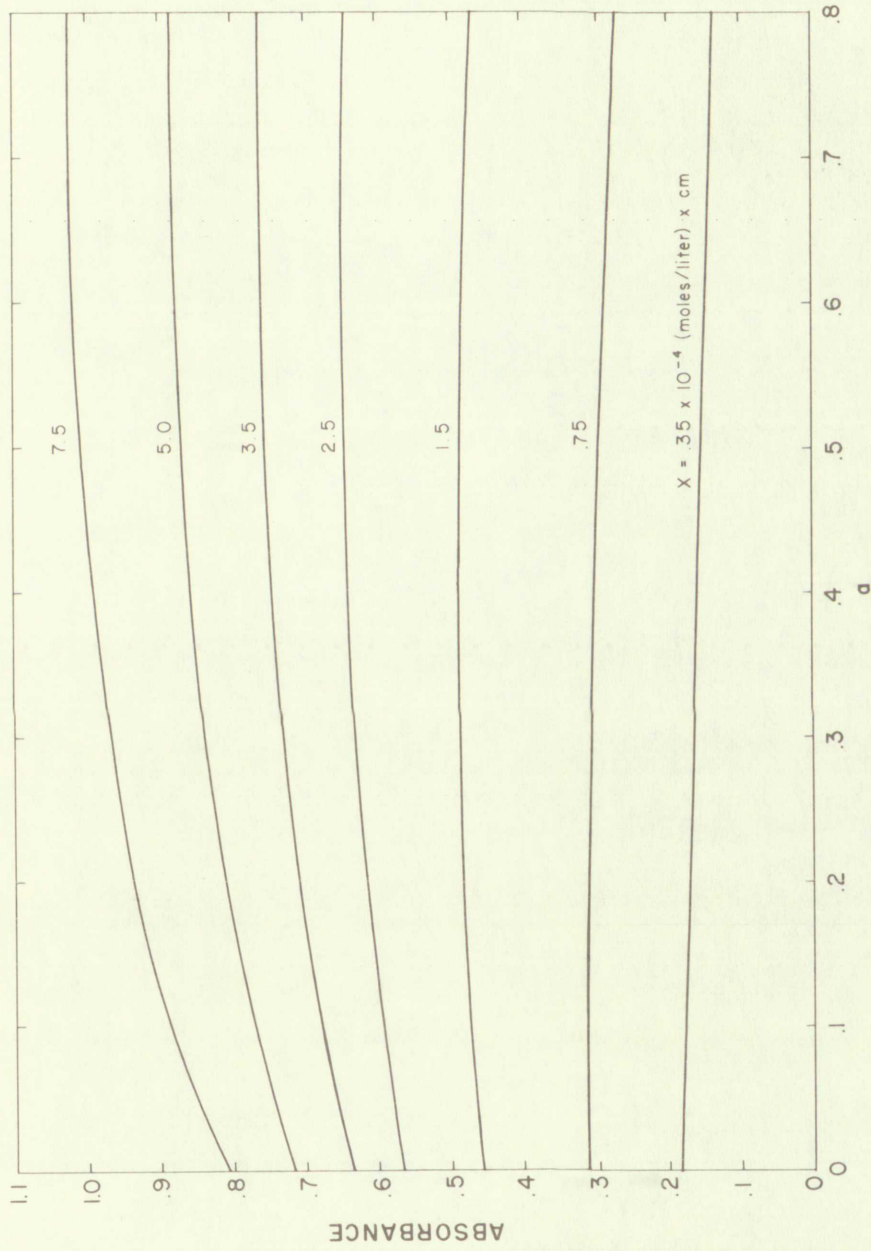
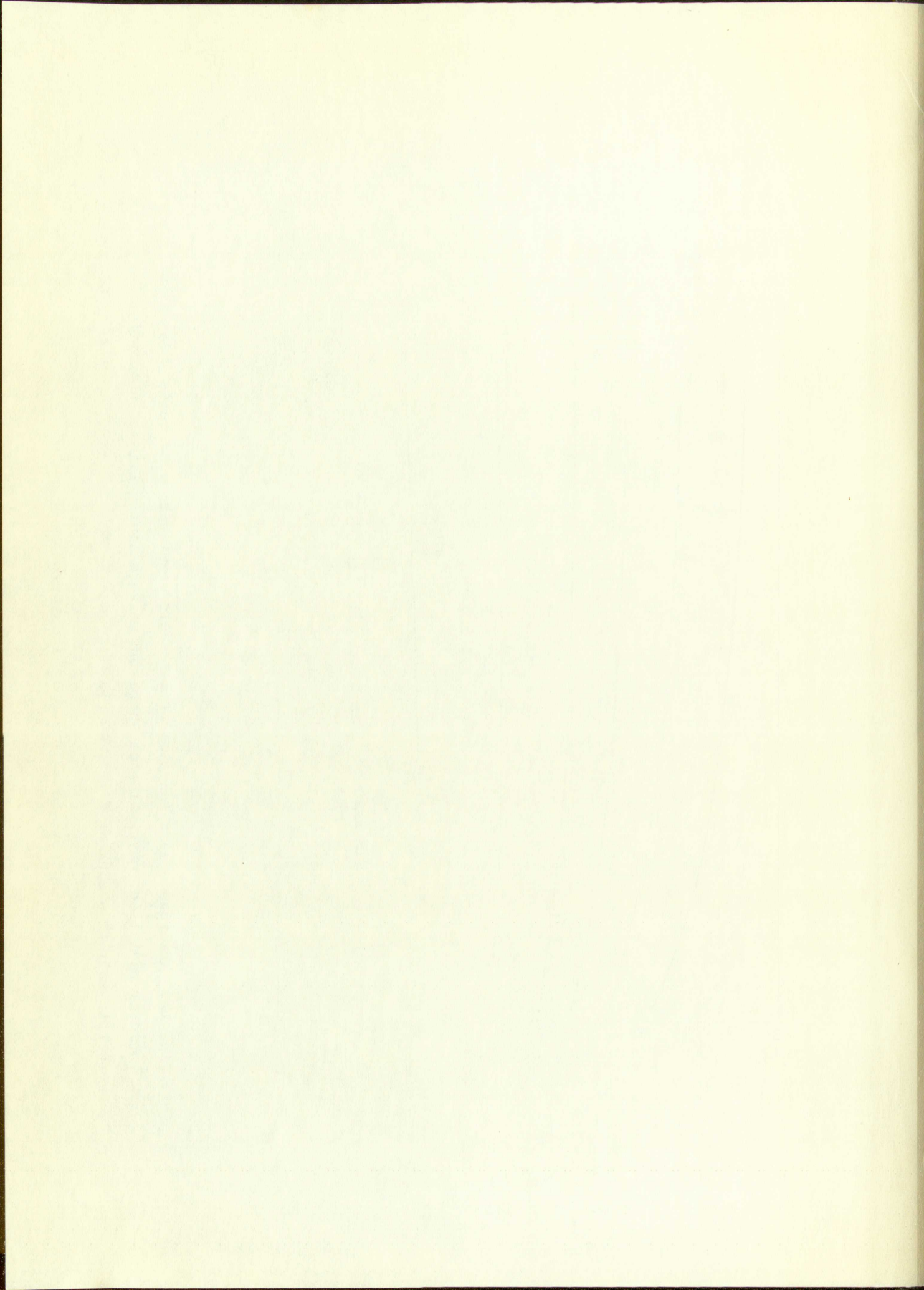


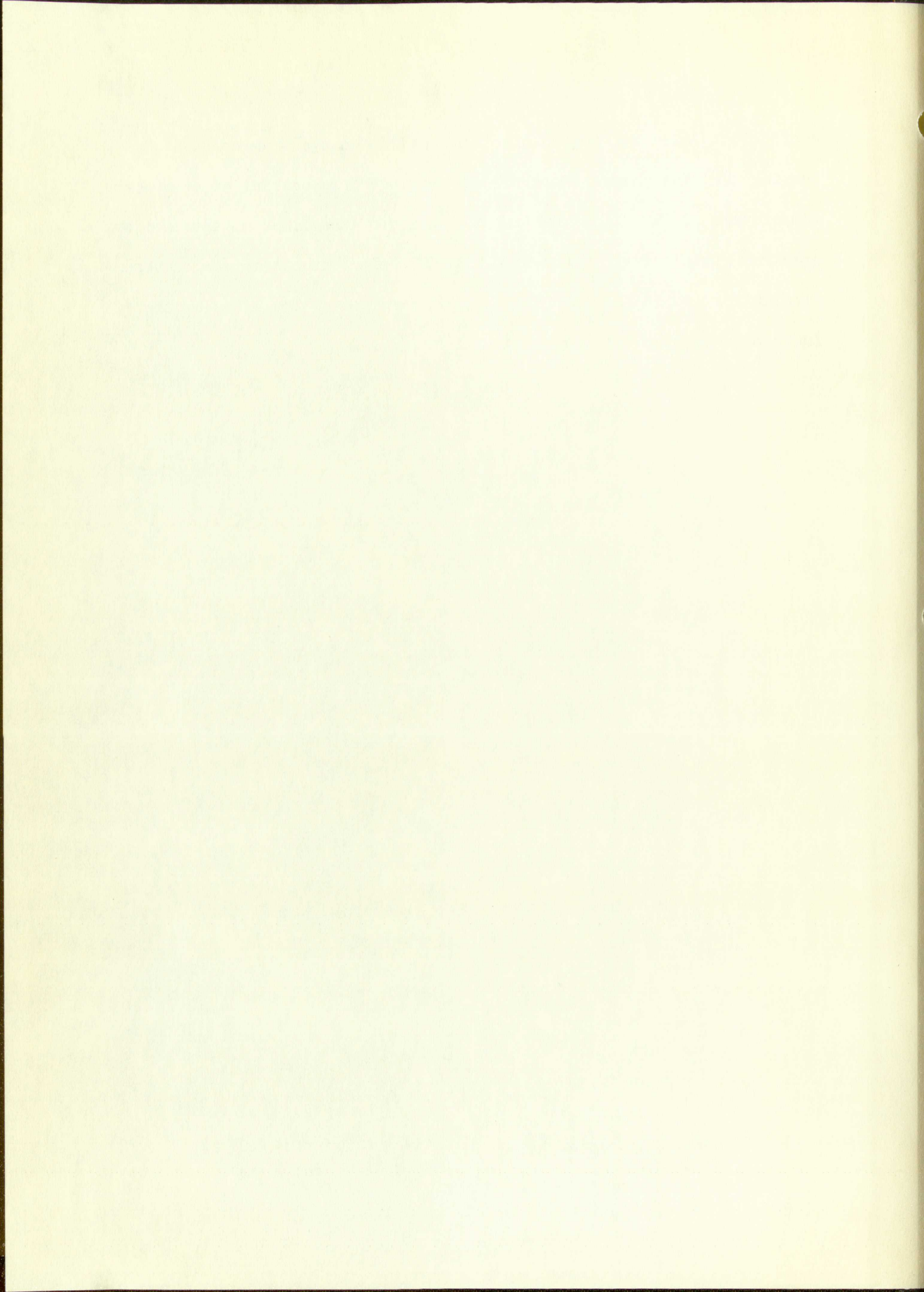
Fig. 11. Absorbance as a function of  $a$  for different values of optical density. Incident radiation: typical line shape and measured intensities. Absorption coefficient:  $T = 2562^{\circ}\text{K}$ ;  $F = 3.24 \cdot 10^{-4}$ .





coefficient while holding the incident radiation spectrum constant. Keeping the line shapes (Doppler) of the absorber constant at an absorber temperature of  $2500^{\circ}\text{K}$  and varying the shape of the lines of the incident spectrum gives curves as shown in Fig. 12. The effects appear rather straightforward in that the absorbance increases as the lines of the incident radiation spectrum become narrower.





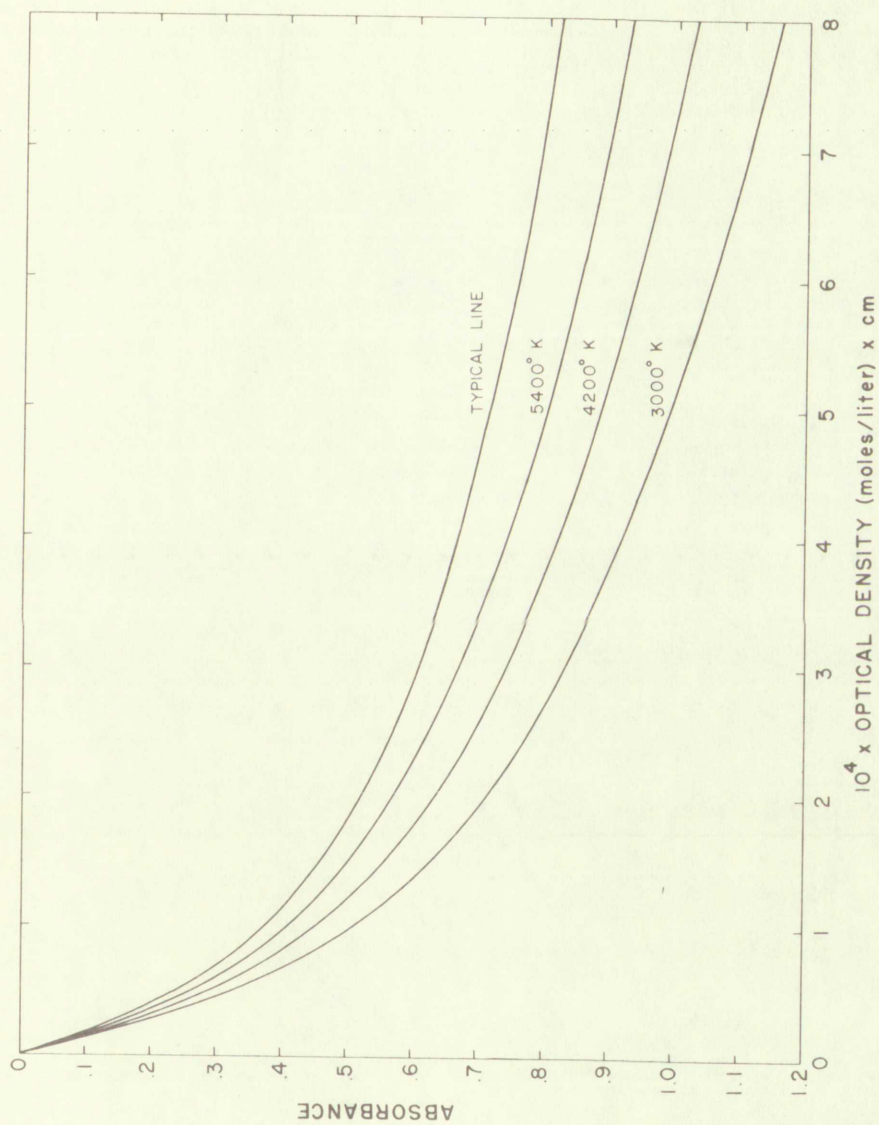
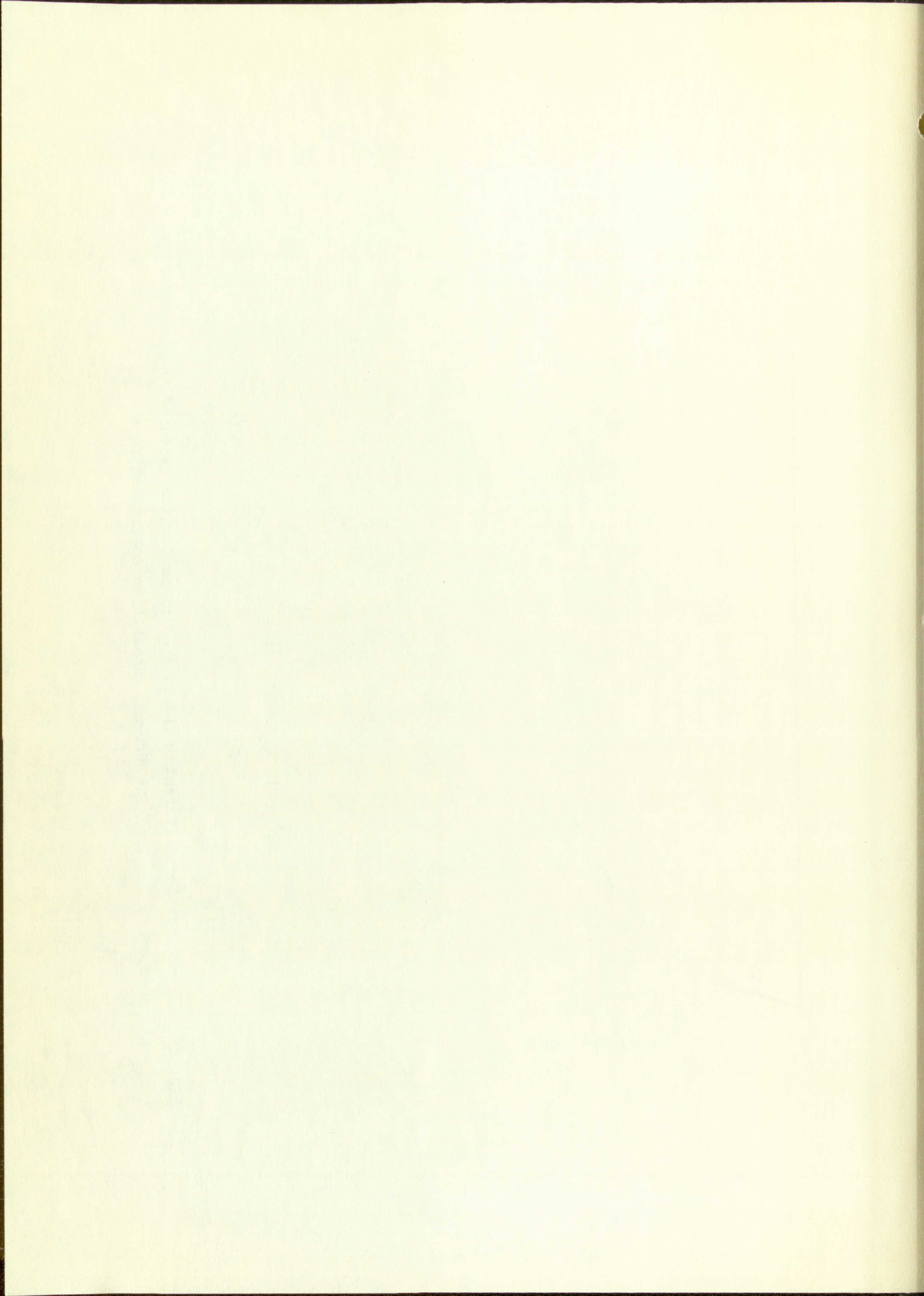


Fig. 12. Absorbance for different incident spectra having the measured intensities. Temperatures specify Doppler line shapes. Absorption coefficient:  $\underline{a} = 0$ ;  $T = 2500^\circ\text{K}$ ;  $F = 3.24 \cdot 10^{-4}$ .



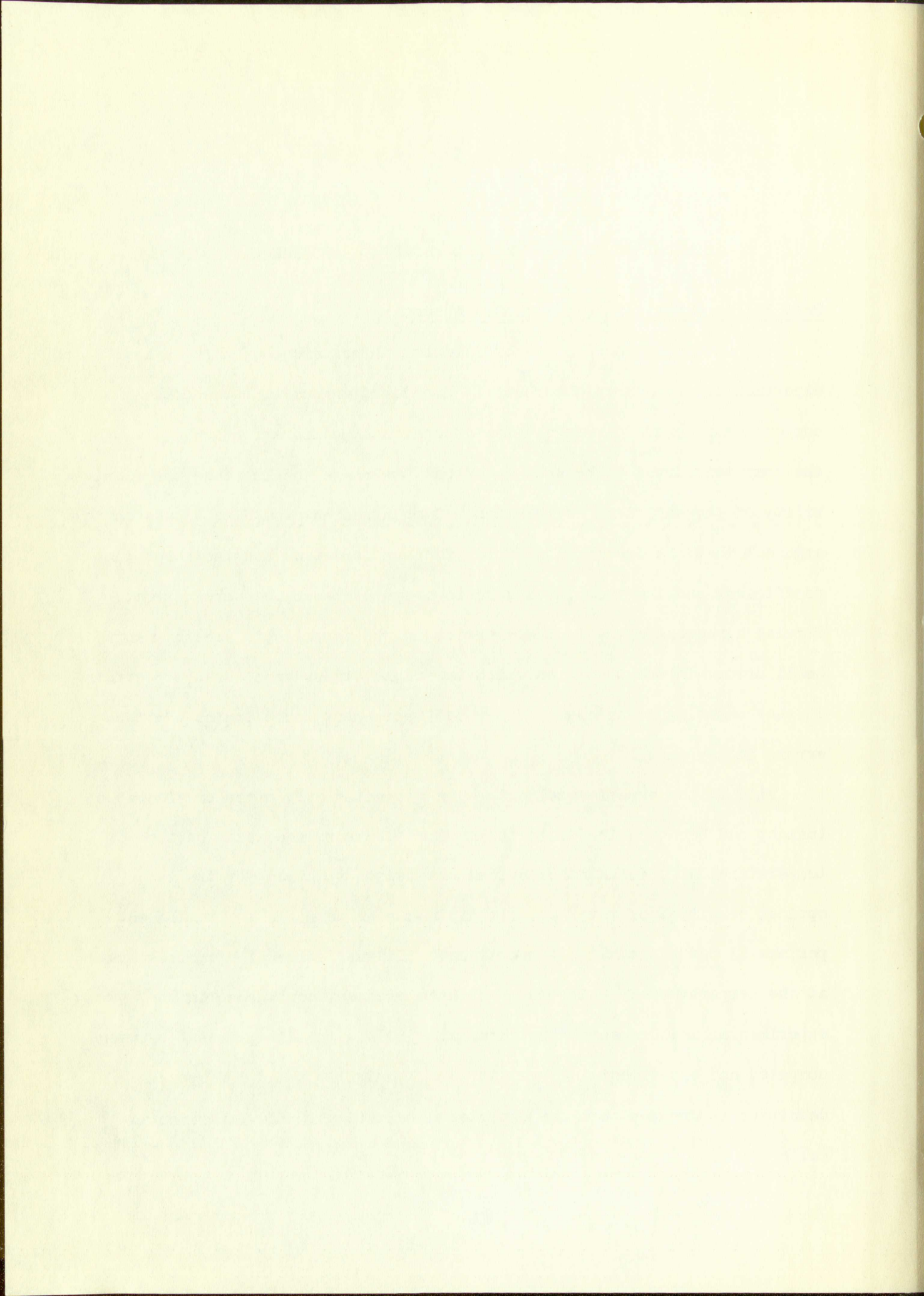


## COMPARISON OF COMPUTED AND MEASURED ABSORBANCE

### Best Fit to Experimentally Measured Absorbance

For several reasons it is of interest to compare the computed and experimentally measured absorbance. Excellent agreement between the computed absorbance curves and the experimental calibration would allow the computed curves to be used to extend the range and increase the flexibility of the empirical calibration. Such agreement would be a substantial argument that the description of the incident spectrum and the absorption coefficient and the techniques used to compute absorbance were correct. Partial agreement might indicate errors in the experimental measurements, small errors in the theory on which the computations were based, or errors in the computing techniques. Violent disagreement could indicate gross errors in any part.

Fits to the experimental data were attempted only after considerable insight had been acquired into the nature of absorbance as a function of temperature,  $F$ ,  $\underline{a}$ , and the incident radiation spectrum for the range of optical densities of interest. It did not seem possible to fit the experimental curves at all 3 temperatures. It was decided to fit the curves at the temperature at which there existed greatest confidence in the experimental measurements, the curve at 2562°K. The disagreement between computed and experimental curves at 1520°K and 2000°K and low optical densities is greater than the expected uncertainty in the experimental calibration.





The computed absorbance versus optical density curves using the incident radiation spectrum synthesized from the typical line and measured intensities and giving best agreement with the experimental data are shown in Fig. 13-15. The experimental data plotted include points obtained for temperatures up to  $170^{\circ}\text{K}$  above or below the temperature of interest. The absorption coefficient used a value for  $F$  of  $3.32 \cdot 10^{-4}$  and the expression proposed by Kaskan<sup>29</sup> for the collision broadening factor,  $\underline{a} = \frac{450p}{T}$  ( $p \equiv$  total pressure in atmospheres;  $T \equiv$  temperature in degrees Kelvin). This expression for  $\underline{a}$  is based on the Lorentz collision broadening theory which gives the Lorentz half-width as proportional to the total pressure and inversely proportional to the square root of the absolute temperature.<sup>30</sup> Expressing  $\underline{a}$  as the ratio of the Lorentz half-width to the Doppler half-width, a good approximation,  $\underline{a}$  is seen to be proportional to the pressure and inversely proportional to the absolute temperature. Kaskan's work indicated that the constant of proportionality should be 450.

The experimental data at  $2562^{\circ}\text{K}$  could be fitted almost as well by using an incident spectrum synthesized from the measured intensities and lines of Doppler shape equivalent to  $4400^{\circ}\text{K}$  (Fig. 16). The absorption coefficient in this case required a value of  $F$  of  $2.57 \cdot 10^{-4}$  and an expression for the collision broadening factor,  $\underline{a} = \frac{260p}{T}$ . Comparing the two computed curves at the absorber temperature of  $2562^{\circ}\text{K}$  shows no great difference in their shapes. A very close comparison shows that this curve has slightly greater curvature than that using the typical line incident spectrum.



Faint, illegible text covering the majority of the page, likely bleed-through from the reverse side.

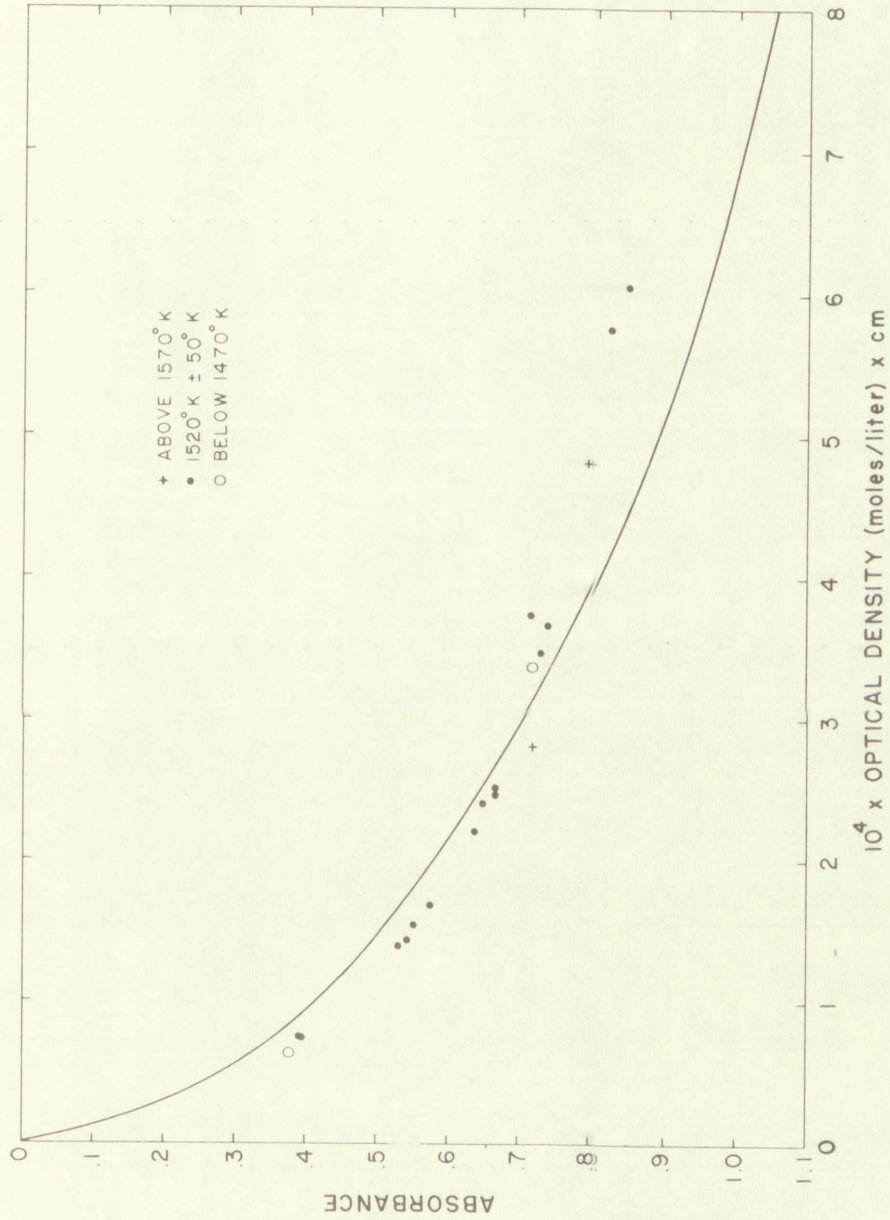
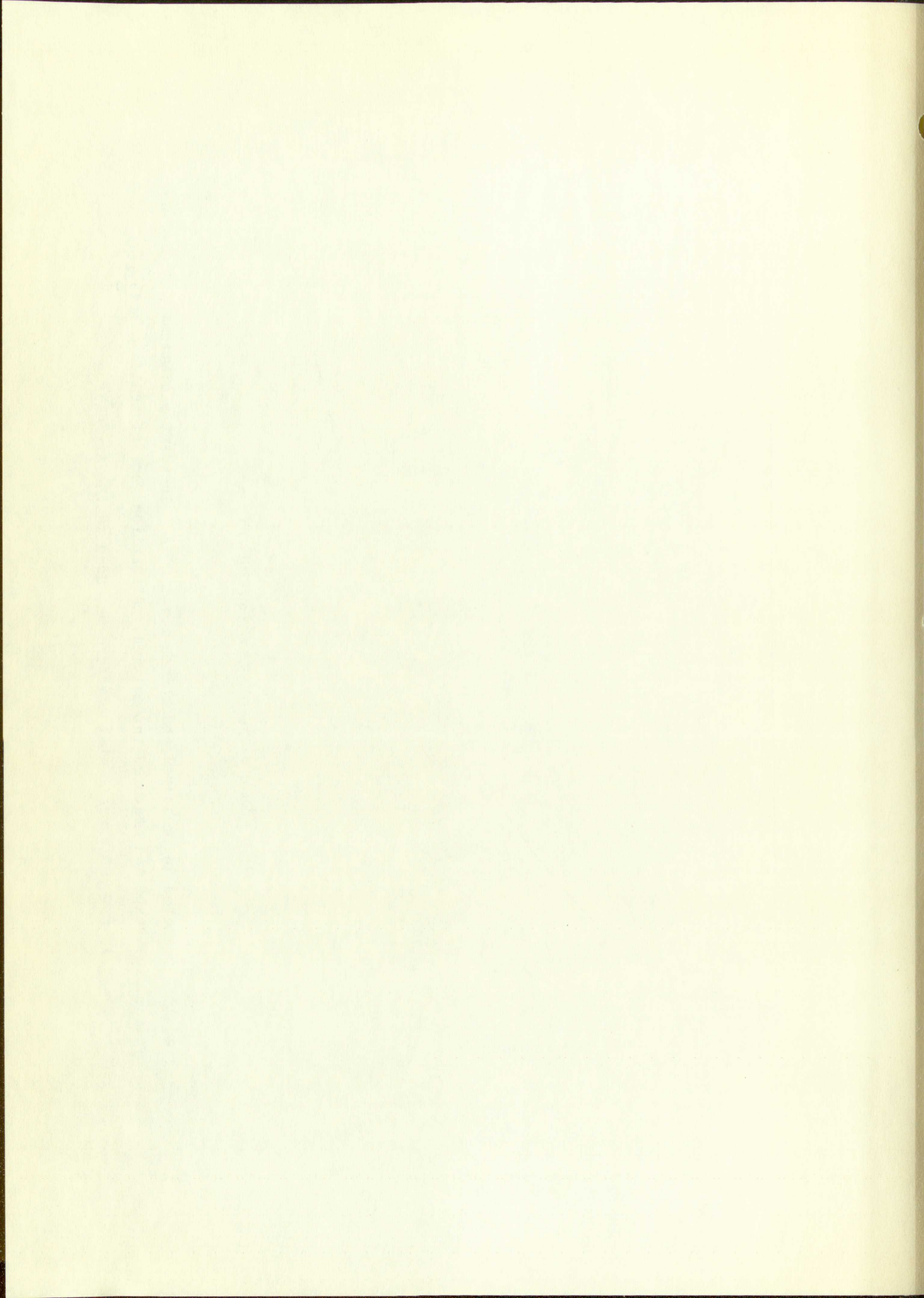


Fig. 13. Computed and measured absorbance for 1520°K. Incident radiation: typical line shape and measured intensities. Absorption coefficient:  $\underline{a} = \frac{450p}{T}$ ;  $F = 3.32 \cdot 10^{-4}$ . The experimental pressure was used in the expression for  $\underline{a}$ .





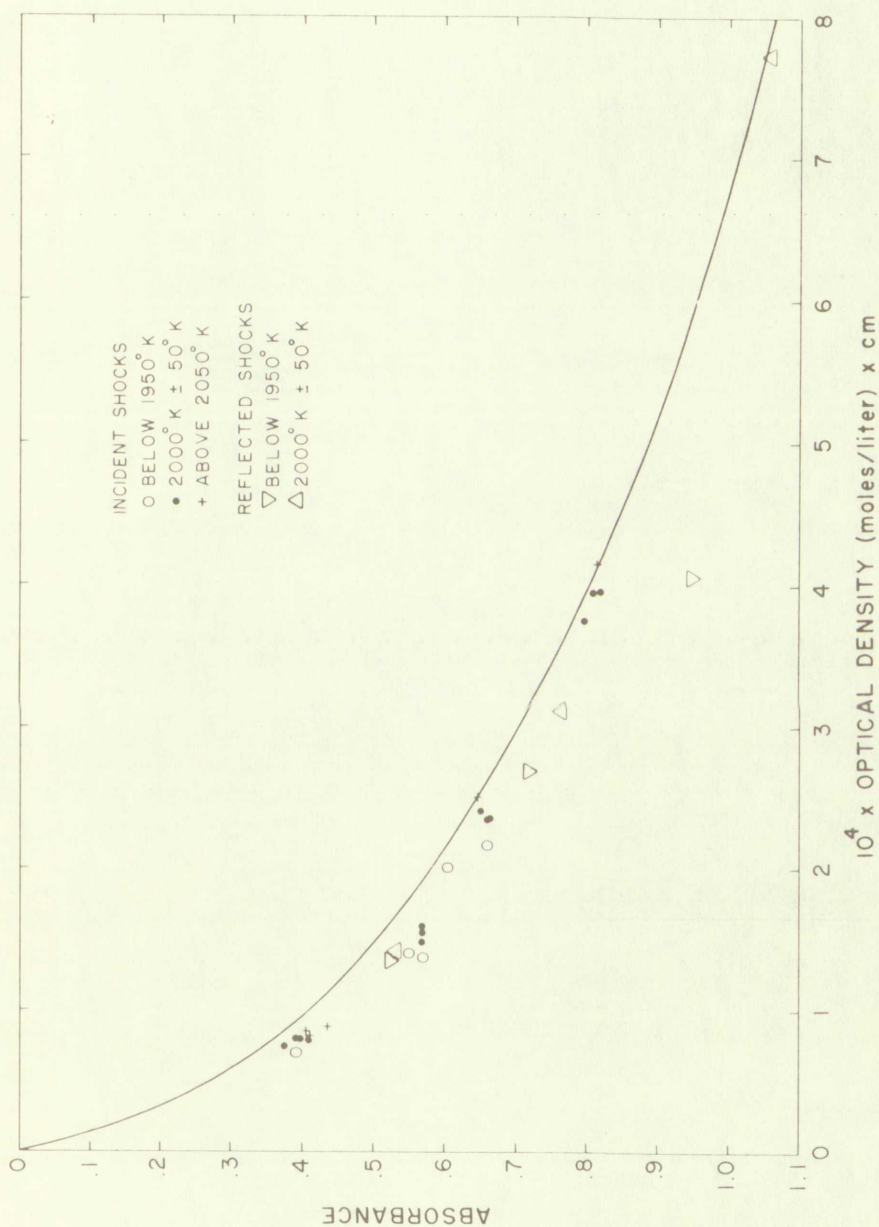
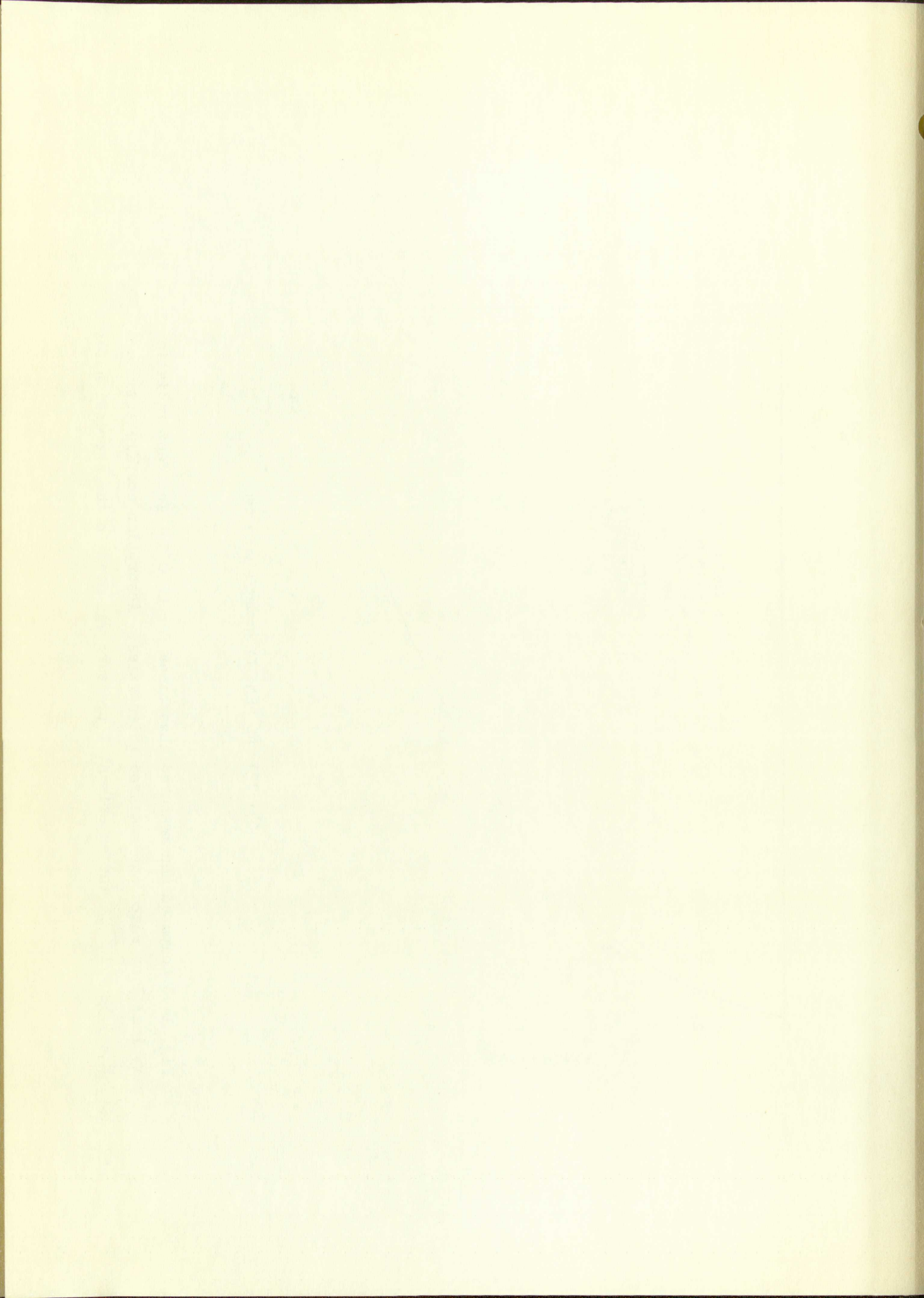


Fig. 14. Computed and measured absorbance for  $2000^\circ \text{K}$ . Incident radiation: typical line shape and measured intensities. Absorption coefficient:  $a = \frac{450p}{T}$ ;  $F = 3.32 \cdot 10^{-4}$ . The experimental pressure was used in the expression for  $a$ .



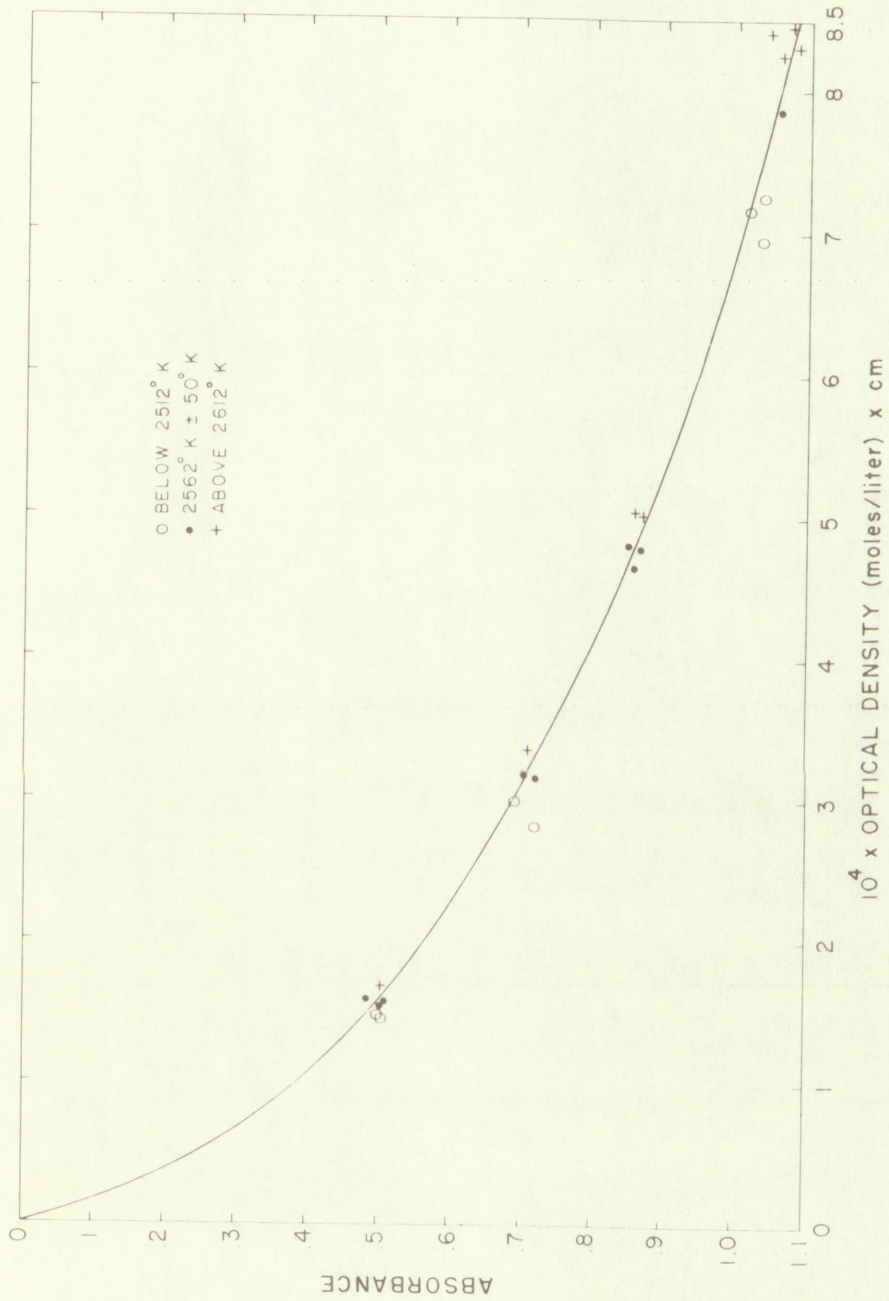
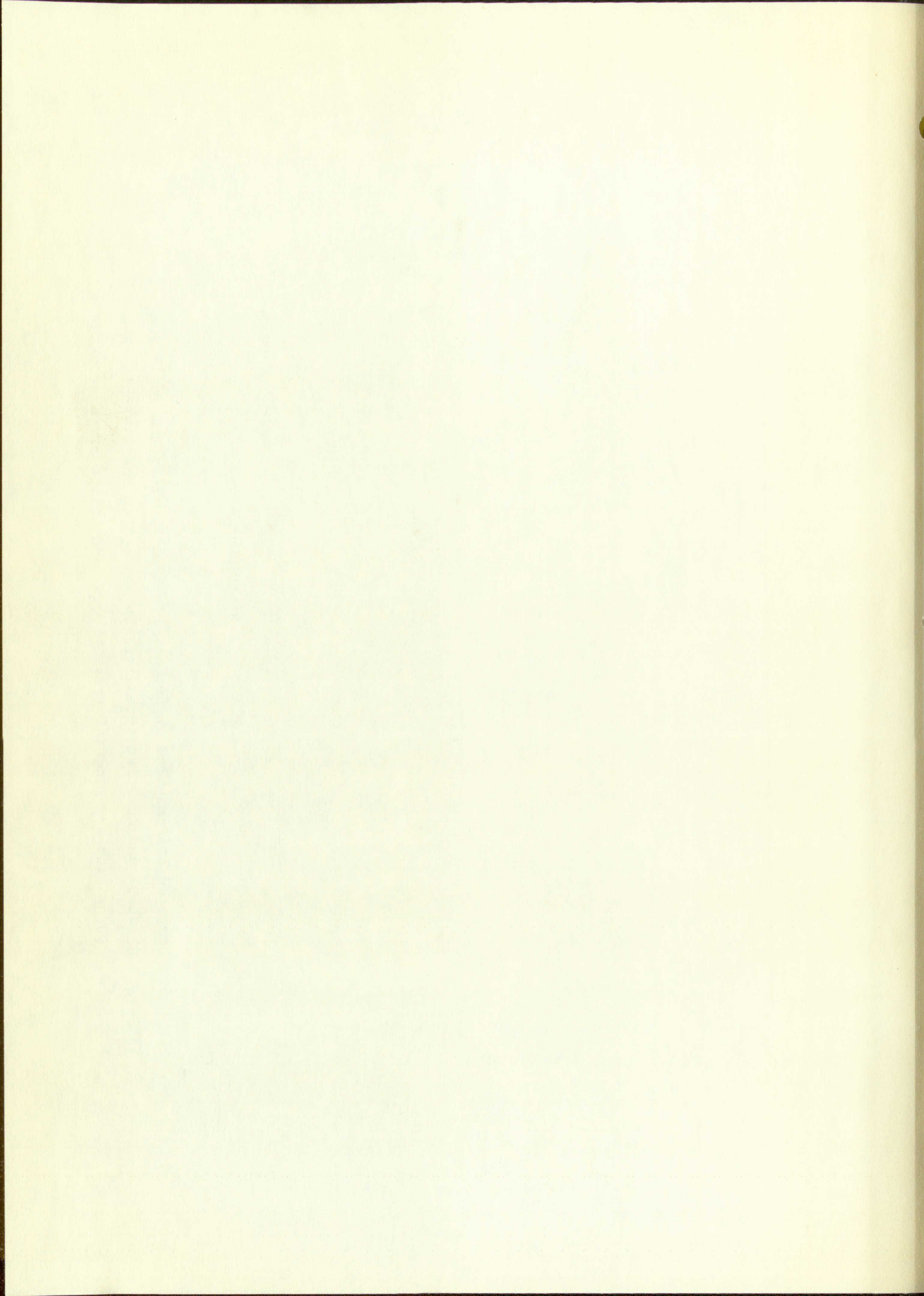


Fig. 15. Computed and measured absorbance for 2562°K. Incident radiation: typical line shape and measured intensities. Absorption coefficient:  $\underline{a} = 450p$ ;  $F = 3.32 \cdot 10^{-4}$ . The experimental pressure was used in the expression for  $\underline{a}$ .





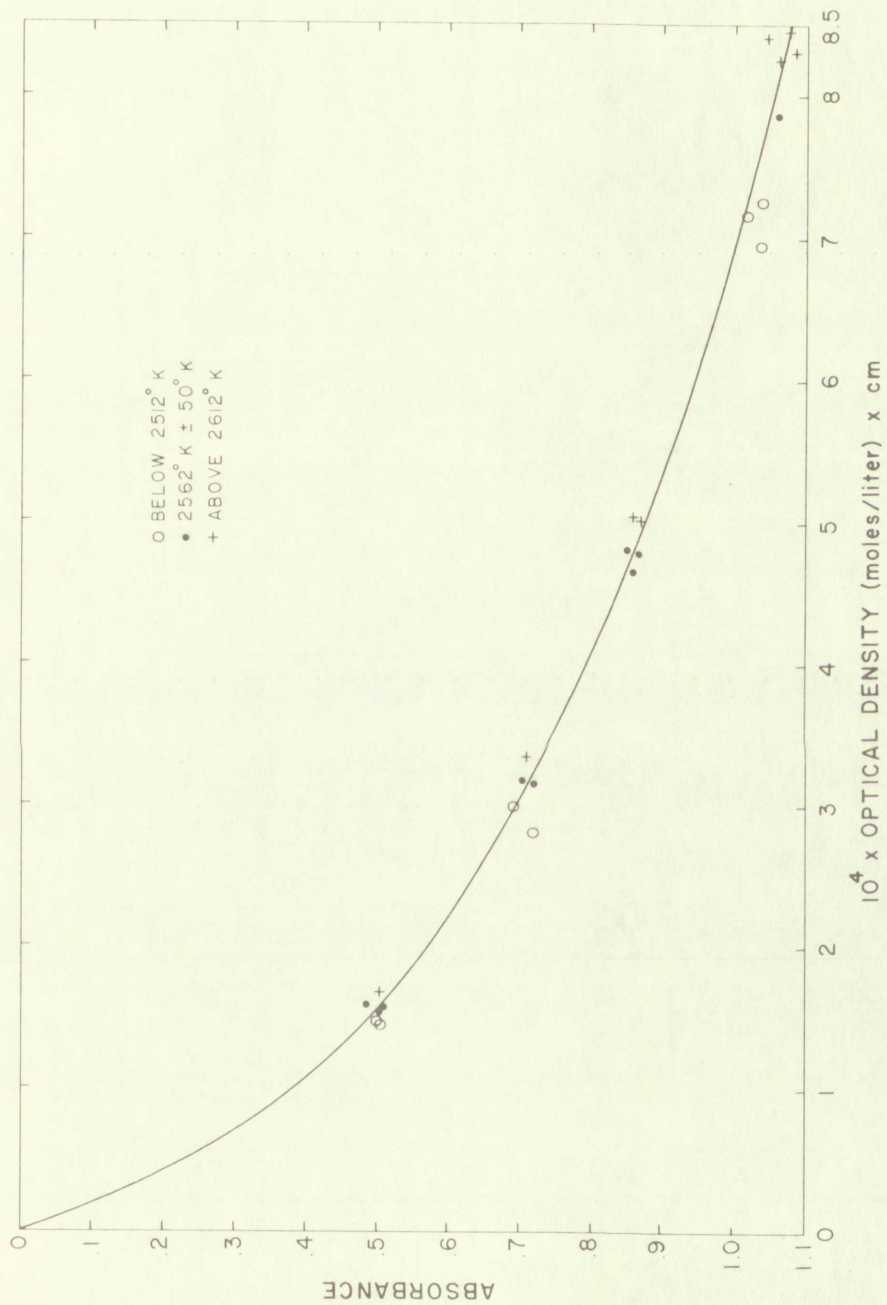
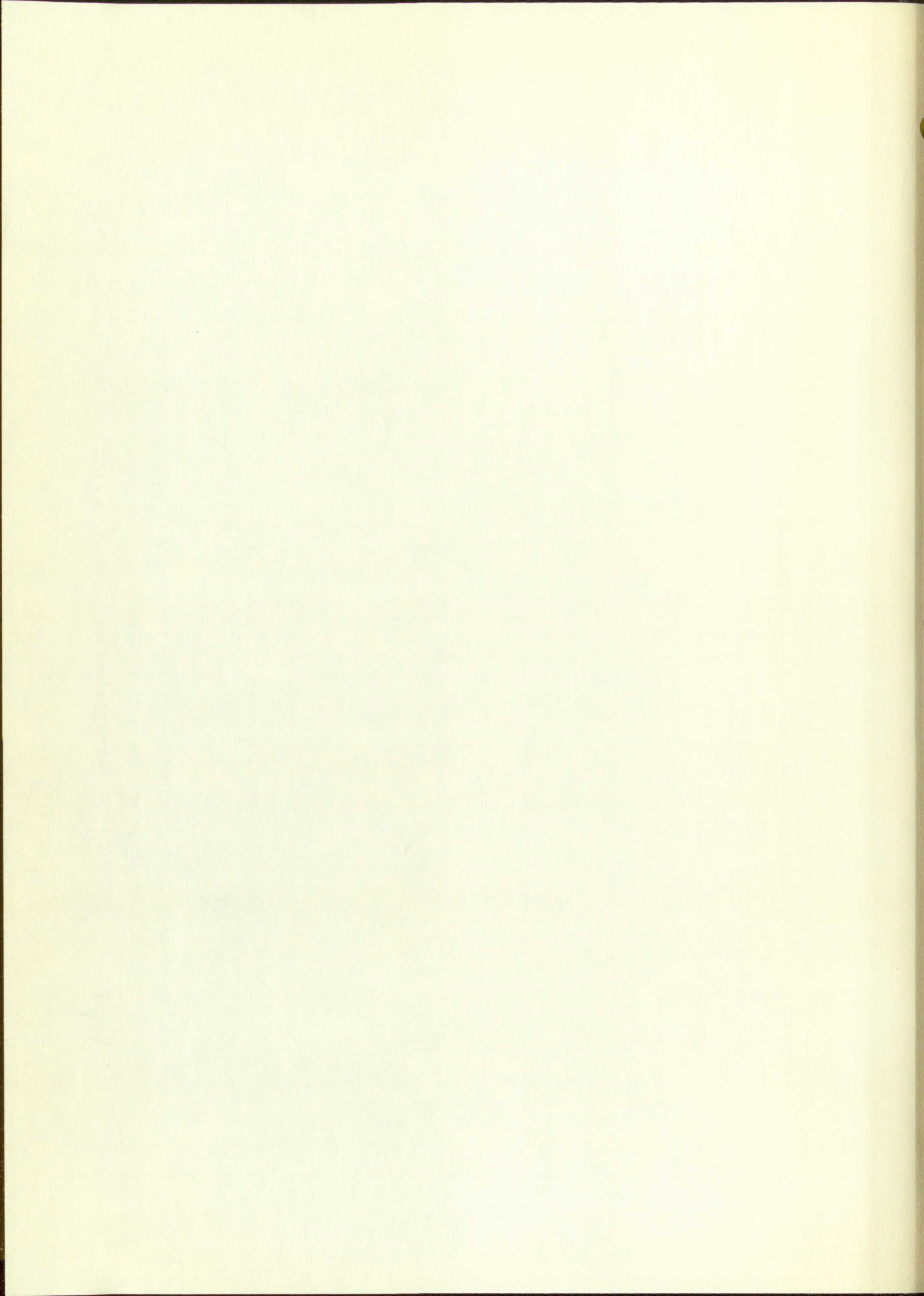


Fig. 16. Computed and measured absorbance for 2562°K. Incident radiation: 4400°K Doppler line shape and measured intensities. Absorption coefficient:  $\underline{a} = \frac{260p}{T}$ ;  $F = 2.57 \cdot 10^{-4}$ . The experimental pressure was used for  $\underline{a}$ .



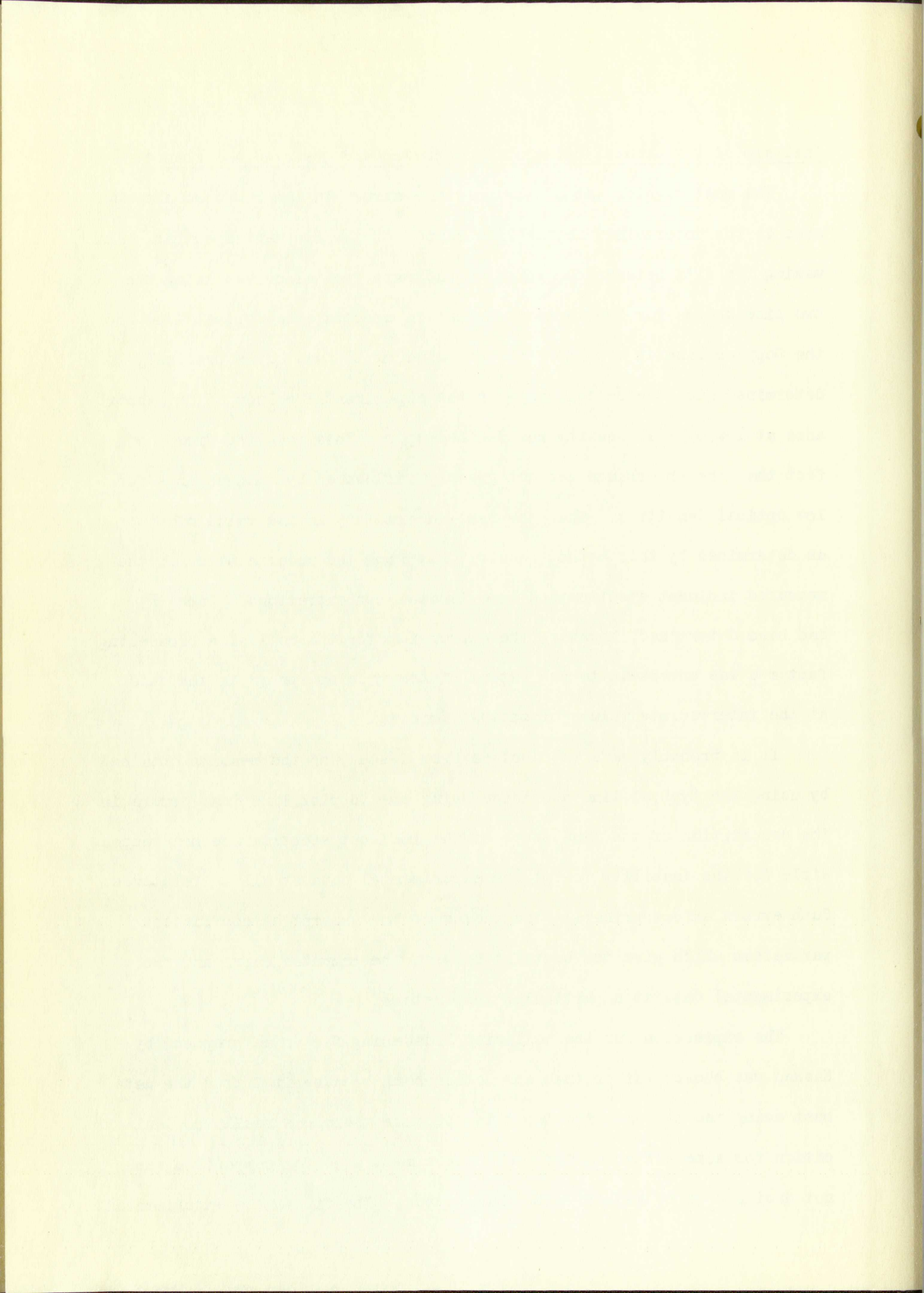


### Analysis of Differences Between the Computed and Observed Absorbance

The most significant of the possible errors in the computed absorbance is the uncertainty in the line shapes of the incident spectrum. In making the fits between the computed and experimental curves using the two line shapes for the incident radiation spectra, the typical line and the Doppler line at  $4400^{\circ}\text{K}$ , the best value of  $F$  was quite precisely determined once the best average of the experimental values of the absorbance at low optical density was decided upon. This resulted from the fact that the absorbance was not greatly influenced by changes in  $a$  for low optical densities. Thus the real uncertainty in the value of  $F$  as determined by this method results only from the uncertainties in the measured incident spectrum and experimental concentrations. Once  $F$  had been determined, however, the expression for the collision broadening factor  $a$  was uncertain to the extent of the greater spread in the data at the intermediate values of optical density.

It is probably safe to conclude from a study of the results obtained by using the typical line and those using the Doppler line that errors in the description of the line shape of the incident spectrum are not responsible for the inability to fit the experimental data at all temperatures. Such errors affect primarily the choice of the absorption coefficient parameters which give the best fit between the computed curve and the experimental data at a particular temperature.

The expression for the collision broadening factor as proposed by Kaskan was chosen rather than some other both because it fitted the data best using the typical line input and because there was really no indication for some better choice. The experiment used for comparison was not designed to be sensitive to this factor. The fit to the experimental





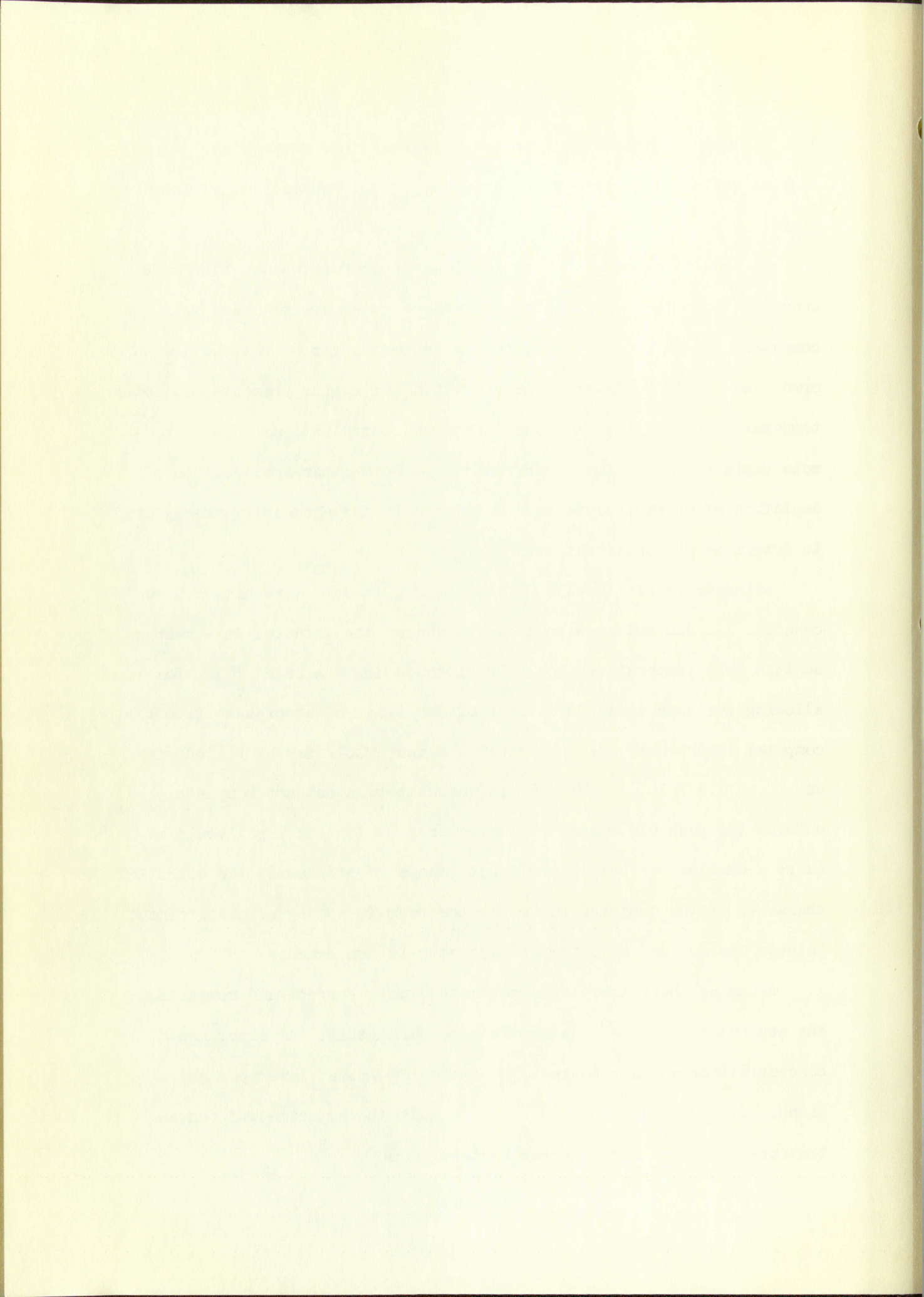
data was not significantly improved by using other expressions for  $a$ , such as making it inversely proportional to the square root of temperature.

It should be noted that at the lower temperatures and higher OH concentrations the experimental absorbance is apparently less than the computed. It is probable that the experimental concentrations are in error and should be lower. The conditions of higher pressure and lower temperature prevailing at these higher OH concentrations tend to promote rapid recombination of OH radical to form other species. Such depletion of OH radical is not considered in the elementary theory used to determine OH concentrations.

Attempts to fit the 1520°K and the 2000°K data were not very successful. It did not seem possible to change the  $a$  factor in a manner so that both temperatures could be fitted using the same  $F$ . But allowing for some small deviations of the measured absorbance from the computed absorbance, the data at 1520°K and 2000°K may be fitted with an  $F$  of  $4.2 \cdot 10^{-4}$ . This  $F$  is somewhat high but not completely outside the possible range.<sup>5</sup> A narrower line for the input would require a smaller  $F$  but it would not change significantly the essential character of the computed curves or the results as far as disagreement between the low and high temperature data is concerned.

Assuming these computed absorbances to be correct and computing the absorbance at 2562°K using the same parameters, the experimental concentrations at 2562°K are high by some 20-25% at lower concentrations. It is unreasonable to conclude that the experimental concentrations at 2562°K are in error by this amount.



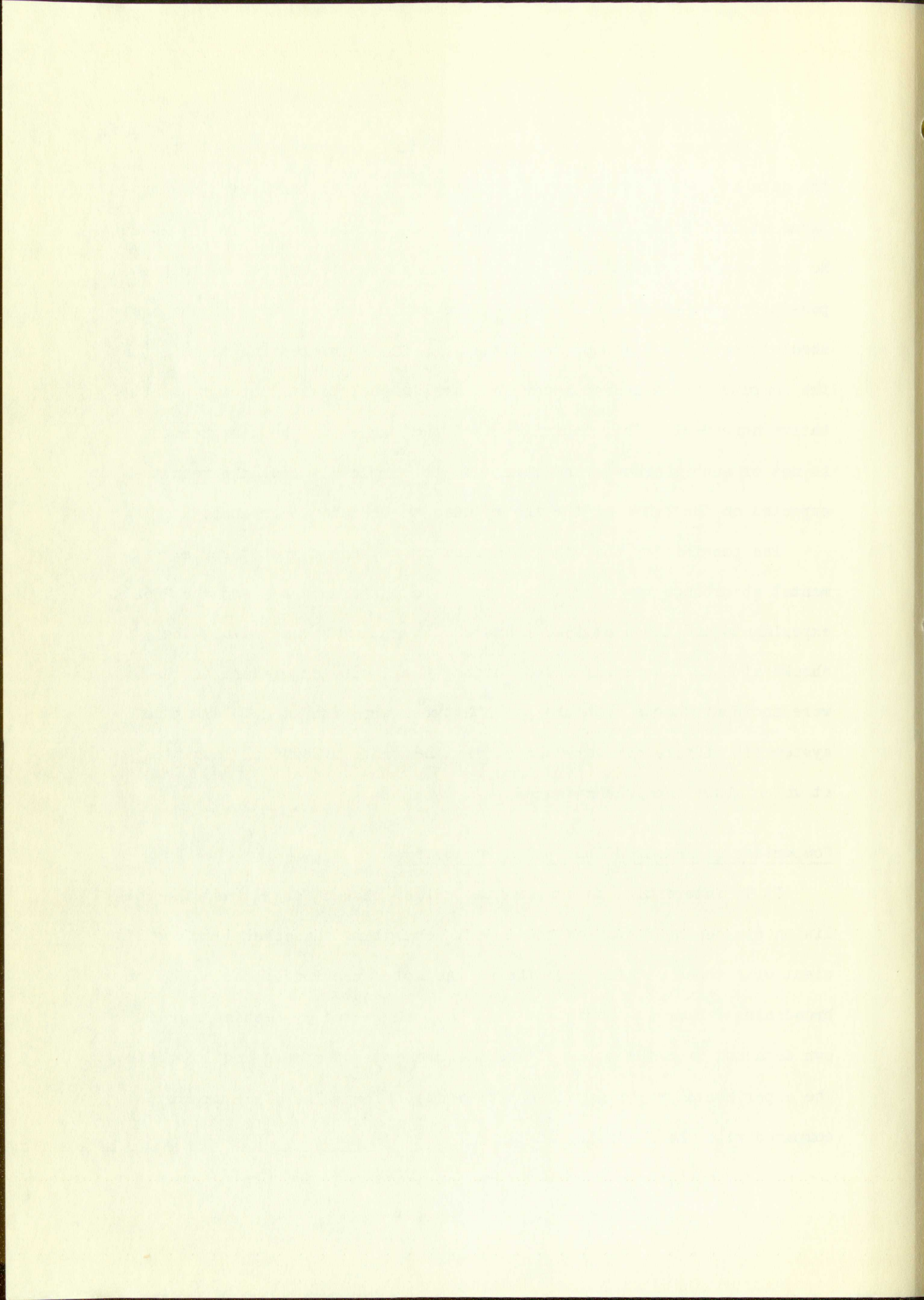


If the computed absorbance based on the parameters best fitting the data at 2562°K is correct, it must be concluded that the concentrations at 1500°K and 2000°K and lower optical densities are low by 20-25%. No reasonable explanation or logical comment can be offered on this possibility at present. However, disregarding the question of the best absolute representation of the situation, it is interesting to note that the computed and measured absorbance are in qualitative but not quantitative agreement. This indicates that the cause for the disagreement is not of such character and magnitude to completely mask the results expected on the basis of the theory used to compute absorbance.

The possibility that the disagreement between computed and experimental absorbance may be due to some basic difference between the 2562°K experiments and those at 1520°K and 2000°K cannot be excluded. The shocks at 2562°K were reflected shocks; the lower temperature shocks were incident shocks. Shocks of both types were run at 2000°K but no systematic differences were noted over the range of optical densities at which absorbance was measured.

#### Comparison of Measured Absorption Parameters

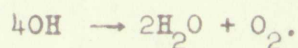
It is interesting to compare the values chosen for  $F$  and the collision broadening factor as those best describing the absorption coefficient with those obtained by others. As noted previously the collision broadening factor is consistent with that suggested by Kaskan from his own data and from the study of the measurements of others and is within the experimental error of all measurements. The value of  $F$  may be compared with the following list:





	<u><math>10^4 \cdot F</math></u>	<u>% error</u>
This work	3.32	--
Carrington <sup>6</sup>	3.24	30
Oldenberg and Rieke <sup>4</sup>	2.56	15
O & R with 10% correction as suggested by Kaskan <sup>28</sup>	2.82	--
Dyne <sup>5</sup> - curve of growth extrapolation	1.21 1.33	20 20
Lapp <sup>7</sup>	2.25	60

The published values of f-number given by O & R and Dyne are based on the measurement of Dwyer and Oldenberg<sup>4</sup> of  $\Delta H_{\text{O}}^{\circ} = -153.4$  kcal. for the reaction



The currently accepted value for this heat of reaction is -151.3 kcal. This calls for an increase in OH concentration of a factor of 1.2 and a corresponding decrease in F of the same factor. The figures in the above list have been corrected.

A value for F of  $1.33 \cdot 10^{-4}$  as found by Dyne does not agree with the experimental results of this investigation. The actual value of F probably lies between  $2.6 \cdot 10^{-4}$  and  $3.3 \cdot 10^{-4}$ . However, a higher value cannot be excluded.

Reaction	Rate constant, $k$	Order
1. $2\text{H}_2\text{O}_2 \rightarrow 2\text{H}_2\text{O} + \text{O}_2$	$1.1 \times 10^{-2} \text{ s}^{-1}$	1
2. $\text{H}_2\text{O}_2 + \text{I}^- \rightarrow \text{H}_2\text{O} + \text{IO}_3^-$	$1.1 \times 10^{-2} \text{ s}^{-1}$	2
3. $\text{H}_2\text{O}_2 + \text{Fe}^{2+} \rightarrow \text{H}_2\text{O} + \text{Fe}^{3+} + \text{OH}^-$	$1.1 \times 10^{-2} \text{ s}^{-1}$	2
4. $\text{H}_2\text{O}_2 + \text{Mn}^{2+} \rightarrow \text{H}_2\text{O} + \text{Mn}^{3+} + \text{OH}^-$	$1.1 \times 10^{-2} \text{ s}^{-1}$	2
5. $\text{H}_2\text{O}_2 + \text{Cu}^{2+} \rightarrow \text{H}_2\text{O} + \text{Cu}^{+} + \text{OH}^-$	$1.1 \times 10^{-2} \text{ s}^{-1}$	2

The following values of  $k$  were obtained from the measurements of  $\text{H}_2\text{O}_2$  and  $\text{O}_2$  concentrations in the reaction:

1.  $2\text{H}_2\text{O}_2 \rightarrow 2\text{H}_2\text{O} + \text{O}_2$  (catalyzed by  $\text{Fe}^{2+}$ )

2.  $\text{H}_2\text{O}_2 + \text{I}^- \rightarrow \text{H}_2\text{O} + \text{IO}_3^-$  (catalyzed by  $\text{Fe}^{2+}$ )

3.  $\text{H}_2\text{O}_2 + \text{Fe}^{2+} \rightarrow \text{H}_2\text{O} + \text{Fe}^{3+} + \text{OH}^-$  (catalyzed by  $\text{Fe}^{2+}$ )

4.  $\text{H}_2\text{O}_2 + \text{Mn}^{2+} \rightarrow \text{H}_2\text{O} + \text{Mn}^{3+} + \text{OH}^-$  (catalyzed by  $\text{Mn}^{2+}$ )

5.  $\text{H}_2\text{O}_2 + \text{Cu}^{2+} \rightarrow \text{H}_2\text{O} + \text{Cu}^{+} + \text{OH}^-$  (catalyzed by  $\text{Cu}^{2+}$ )

The values of  $k$  are independent of the concentration of  $\text{H}_2\text{O}_2$  and of the concentration of the catalyst. The figures in the table are the values of  $k$  for the reaction  $2\text{H}_2\text{O}_2 \rightarrow 2\text{H}_2\text{O} + \text{O}_2$  catalyzed by  $\text{Fe}^{2+}$ .

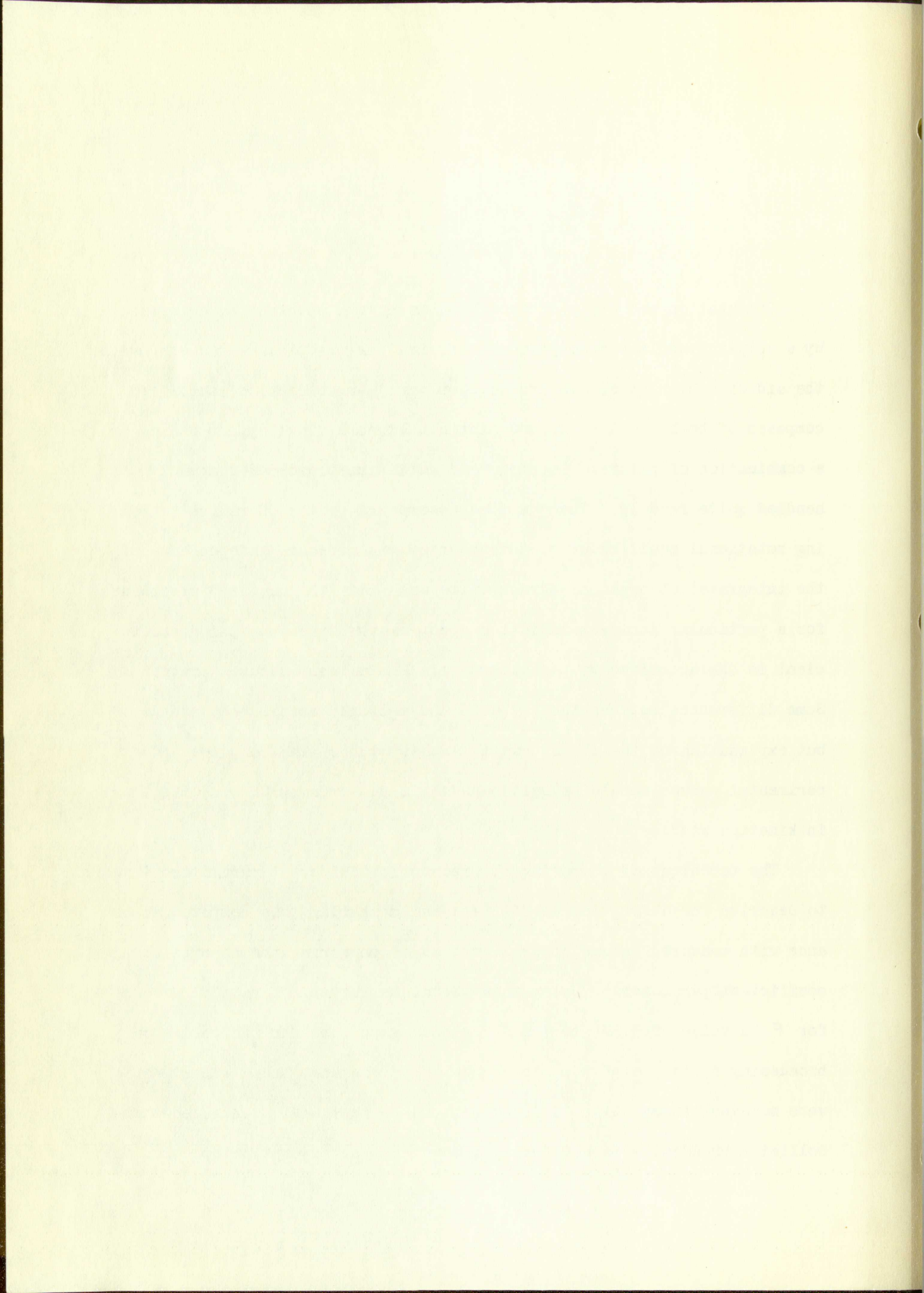


## CONCLUSIONS

Computation and study of the absorbance of a species characterized by a complicated line absorption coefficient is practical and useful with the aid of a high speed electronic computer. An absorption coefficient composed of both overlapping and distinct lines having Doppler shapes or a combination of natural, Doppler, and collision broadened shapes is handled quite readily. The computed absorbance of the OH radical assuming rotational equilibrium of the absorber and pressure independence of the integrated absorption, agrees quite well with the measured absorbance for a particular incident radiation spectrum when the absorption coefficient is characterized by parameters which have been measured previously. Some differences between the computed and measured absorbances are noted but explanation of these must await further study. The computed and experimental curves should be quite useful in determining OH concentrations in kinetics studies.

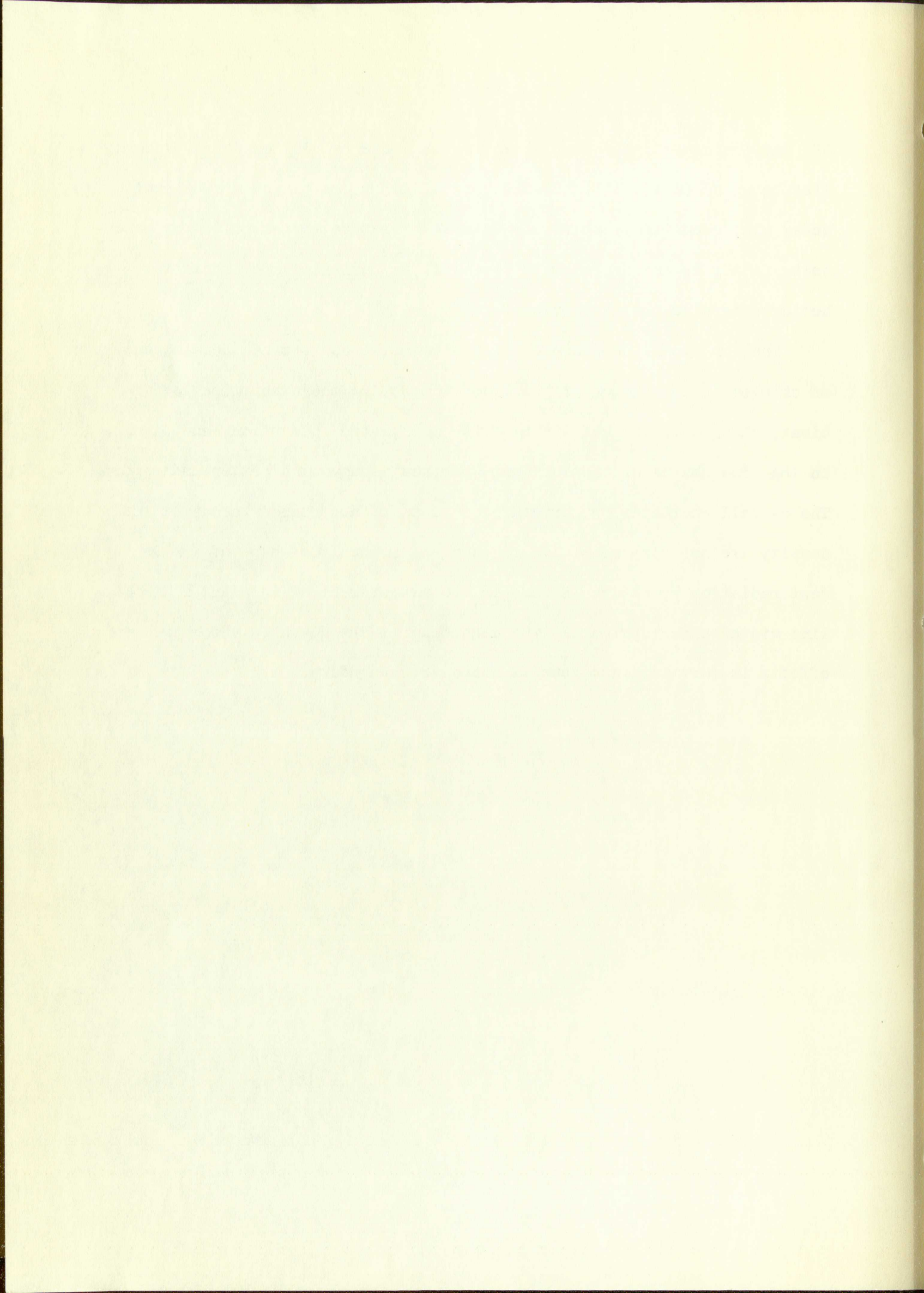
The technique of computing absorbance for different parameters assumed to describe the absorption coefficient and comparing this computed absorbance with measured values offers a method of measuring the absorption coefficient parameters. Using this technique for the OH radical gives for  $F$  a value of  $3.32 \cdot 10^{-4}$  and for the expression for the collision broadening factor,  $\underline{a} = \frac{450p}{T}$ , as suggested by Kaskan. These experiments were somewhat insensitive to  $\underline{a}$ , but it can be reasonably concluded that collision broadening is noticeably present in the absorption spectrum of





OH, and the numerical factor given in the above expression for  $\underline{a}$  probably lies between 260 and 450. Results of this work can be used to determine under what conditions absorbance is most sensitive to the collision broadening factor  $\underline{a}$ , and hence could be useful in devising experiments to better determine the expression for  $\underline{a}$ .

The functional dependence of absorbance versus optical density curves on changes in the shapes of the lines comprising the absorption coefficient, changes in the magnitude of the integrated absorption, and changes in the line shapes of the incident spectrum is now much better understood. The overall character or curvature of plots of absorbance versus optical density are not very sensitive to changes in the line shape of the incident radiation spectrum. Errors in the measurement of incident radiation line widths affect primarily the magnitude of the computed absorbance; effects in curvature and general shape are secondary.





## PROPOSALS FOR FURTHER STUDY

Additional work will be necessary to be able to state unequivocally that the absorbance as computed using currently available data and theory corresponds to the actual absorbance. Higher resolution spectrograms of the incident radiation spectrum are certainly needed. Experiments to better determine the collision broadening factor are necessary. Experiments to better establish dependence of  $\alpha$  on temperature are possible. Dependence of the integrated absorption on pressure might be checked. By using different lines in experiments of this type it is conceivable that any J-dependence of the integrated absorption might be determined.

Greater precision in the knowledge of the OH concentrations in the shock tube experiments must be acquired by further study of the chemistry of the  $H_2-O_2$  system. This will permit more accurate measurements of the parameters describing the spectral absorption coefficient of OH.

An additional refinement would be to improve the optical speed of the experimental apparatus so that fewer lines need be used and still retain the desired sensitivity and precision. This would reduce the errors due to uncertainties in the positions of lines in blends. A better determination of wavelengths, and hence energy levels, is suggested.

The first part of the paper is devoted to a discussion of the general principles of the theory of the structure of the atom. It is shown that the structure of the atom is determined by the laws of quantum mechanics, and that the structure of the atom is determined by the laws of quantum mechanics. The second part of the paper is devoted to a discussion of the structure of the atom, and the third part of the paper is devoted to a discussion of the structure of the atom.



## SUGGESTIONS FOR USE OF THESE TECHNIQUES BY OTHERS

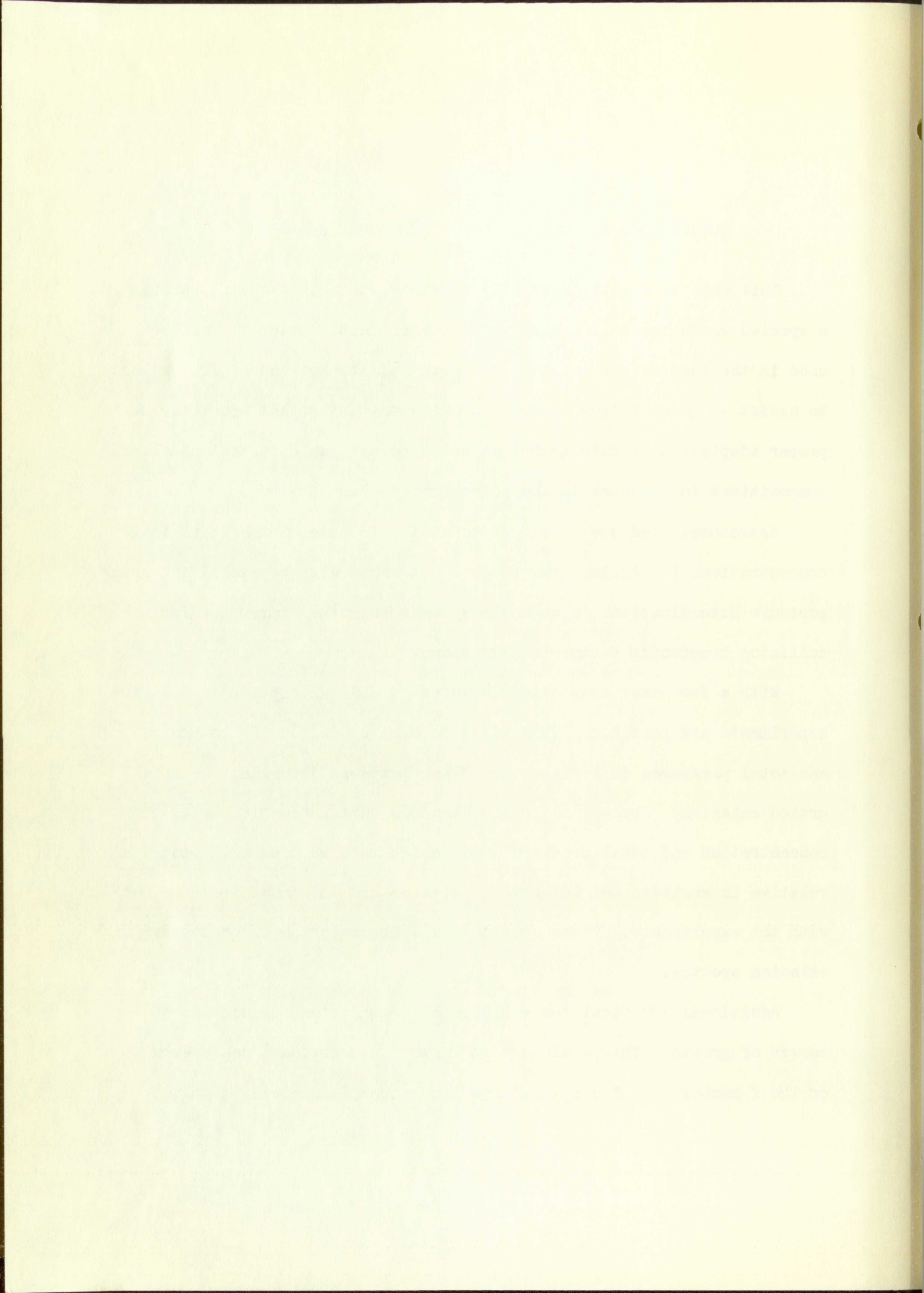
This code is readily adaptable to other chemical systems containing a species which has a line absorption coefficient. Hence it could be used in the same manner to study the spectral absorption coefficient and to assist in quantitative chemical studies involving such species. The proper adaptation of this technique would permit rapid control of flame compositions in furnaces in the petrochemical industry.

Astronomers can use this code to assist in determining OH radical concentrations in stellar atmospheres. It might also be useful in making pressure determinations in such atmospheres once the expression for the collision broadening factor is well known.

With a few minor adaptations studies of self-absorption in emission experiments are possible. This might be done by varying OH concentrations and total pressures in a flame or a flash lamp and observing the integrated emission. Spectra could be taken for certain conditions of OH concentration and total pressure. The code could be used to compute the relative intensities and integrated emission and this could be compared with the experiments. These studies could increase the understanding of emission spectra.

Additional modifications would permit simplified computation of curves of growth. This would assist in more conventional measurements of the f-number and line shapes of a line absorption coefficient.





### LIST OF REFERENCES

1. Bauer, Schott, and Duff, *J. Chem. Phys.* 28, 1089 (1958).
2. G. L. Schott and J. L. Kinsey, *J. Chem. Phys.* 29, 1177 (1958).
3. Garry L. Schott, *J. Chem. Phys.* 32, 710 (1960).
4. O. Oldenberg and F. F. Rieke, *J. Chem. Phys.* 6, 439 (1938);  
R. J. Dwyer and O. Oldenberg, *J. Chem. Phys.* 12, 351 (1944).
5. P. J. Dyne, *J. Chem. Phys.* 28, 999 (1958); Guggenheim Jet Propulsion  
Center Technical Report No. 12, Contract No. Nonr-220(03),  
NR 015 210, Pasadena (1954).
6. T. Carrington, *J. Chem. Phys.* 31, 1243 (1959).
7. M. Lapp, Guggenheim Jet Propulsion Center Technical Note No. 11,  
Contract AF 18(603)-2, Pasadena (1960).
8. S. S. Penner, Quantitative Molecular Spectroscopy and Gas  
Emissivities (Addison-Wesley Publishing Company, Inc., Reading,  
Mass., 1959), p. 62.
9. Ibid., p. 21.
10. A. C. G. Mitchell and M. W. Zemansky, Resonance Radiation and  
Excited Atoms (Cambridge University Press, Cambridge, England,  
1934), p. 96.
11. Ibid., p. 99.
12. F. Reiche, *Verh. d. D. Phys. Ges.* 15, 3 (1913).
13. G. Herzberg, Molecular Spectra and Molecular Structure, II.  
Infrared and Raman Spectra of Polyatomic Molecules (D. Van Nostrand  
Company, Inc., Princeton, N. J., 1945), pp. 519-521.
14. Values of physical constants were obtained from Cohen, DuMond,  
Layton and Rollett, *Rev. Mod. Phys.* 27, 363 (1955).
15. "Selected Values of Chemical Thermodynamic Properties", National  
Bureau of Standards, Washington, D. C., Series III, 1947, and  
supplements.

1. [Faint text]
2. [Faint text]
3. [Faint text]
4. [Faint text]
5. [Faint text]
6. [Faint text]
7. [Faint text]
8. [Faint text]
9. [Faint text]
10. [Faint text]
11. [Faint text]
12. [Faint text]
13. [Faint text]
14. [Faint text]
15. [Faint text]



16. Mitchell and Zemansky, p. 321.
17. W. Lash Miller and A. R. Gordon, *J. Phys. Chem.* 35, 2874 (1931).
18. L. N. G. Filon, *Proc. Royal Soc. (Edinburgh)* 49, 38 (1928-1929).
19. Mitchell and Zemansky, p. 329.
20. K. S. Gibson, "Spectrophotometry", National Bureau of Standards Circular No. 484, Washington, D. C., p. 8.
21. Grossman, Sawyer, and Vincent, *J. Opt. Soc. Am.* 33, 185 (1943).
22. G. H. Dieke and H. M. Crosswhite, "The Ultraviolet Bands of OH", Bumblebee Rpt. No. 86, The Johns Hopkins University, 1948.
23. S. S. Penner, *J. Chem. Phys.* 21, 31 (1953).
24. L. T. Earls, *Phys. Rev.* 48, 423 (1935).
25. E. Hill and J. H. Van Vleck, *Phys. Rev.* 32, 250 (1928).
26. W. E. Kaskan, *J. Chem. Phys.* 28, 729 (1958).
27. W. E. Kaskan, *J. Chem. Phys.* 29, 1420 (1958).
28. W. E. Kaskan, *Combustion and Flame* 3, 49 (1959).
29. W. E. Kaskan, *J. Chem. Phys.* 31, 944 (1959).
30. Mitchell and Zemansky, p. 170.

CONTENTS

vii	Introduction
1	1. The History of the ...
15	2. The ...
30	3. The ...
45	4. The ...
60	5. The ...
75	6. The ...
90	7. The ...
105	8. The ...
120	9. The ...
135	10. The ...
150	11. The ...
165	12. The ...
180	13. The ...
195	14. The ...
210	15. The ...
225	16. The ...
240	17. The ...
255	18. The ...
270	19. The ...
285	20. The ...
300	21. The ...
315	22. The ...
330	23. The ...
345	24. The ...
360	25. The ...
375	26. The ...
390	27. The ...
405	28. The ...
420	29. The ...
435	30. The ...
450	31. The ...
465	32. The ...
480	33. The ...
495	34. The ...
510	35. The ...
525	36. The ...
540	37. The ...
555	38. The ...
570	39. The ...
585	40. The ...
600	41. The ...
615	42. The ...
630	43. The ...
645	44. The ...
660	45. The ...
675	46. The ...
690	47. The ...
705	48. The ...
720	49. The ...
735	50. The ...
750	51. The ...
765	52. The ...
780	53. The ...
795	54. The ...
810	55. The ...
825	56. The ...
840	57. The ...
855	58. The ...
870	59. The ...
885	60. The ...
900	61. The ...
915	62. The ...
930	63. The ...
945	64. The ...
960	65. The ...
975	66. The ...
990	67. The ...
1005	68. The ...
1020	69. The ...
1035	70. The ...
1050	71. The ...
1065	72. The ...
1080	73. The ...
1095	74. The ...
1110	75. The ...
1125	76. The ...
1140	77. The ...
1155	78. The ...
1170	79. The ...
1185	80. The ...
1200	81. The ...
1215	82. The ...
1230	83. The ...
1245	84. The ...
1260	85. The ...
1275	86. The ...
1290	87. The ...
1305	88. The ...
1320	89. The ...
1335	90. The ...
1350	91. The ...
1365	92. The ...
1380	93. The ...
1395	94. The ...
1410	95. The ...
1425	96. The ...
1440	97. The ...
1455	98. The ...
1470	99. The ...
1485	100. The ...



BOSTON COLLEGE  
LEWIS  
MILERS PAINTS



COLLEGE COLLEGE  
EXERCISES  
MILITARY ARTS













